Schintgen, T. V., Förster, A., Förster, H.-J., Norden, B. (2015): Surface heat flow and lithosphere thermal structure of the Rhenohercynian Zone in the greater Luxembourg region. - *Geothermics*, *56*, p. 93-109.

DOI: http://doi.org/10.1016/j.geothermics.2015.03.007

Surface heat flow and lithosphere thermal structure of the Rhenohercynian Zone in the greater Luxembourg region

Tom Schintgen, Andrea Förster, Hans-Jürgen Förster, Ben Norden

Published in: Geothermics 56 (2015), 93–109.
http://dx.doi.org/10.1016/j.geothermics.2015.03.007

Supplementary data can be found in the Appendix.

Corrigendum to "Surface heat flow and lithosphere thermal structure of the Rhenohercynian Zone in the greater Luxembourg region"
http://dx.doi.org/10.1016/j.geothermics.2015.09.009

Abstract

Comprehensive knowledge of surface heat flow and subsurface temperature distribution is indispensable for the interpretation and quantification of crustal/mantle processes as well as for the evaluation of the geothermal potential of an area. In cases where subsurface temperature data are sparse, thermal modelling may be used as a tool for inferring the geothermal resource at depth but requires profound structural, geological, and petrophysical input data. The study area encompasses the Trier–Luxembourg Basin and the western realm of the Rhenish Massif, itself subdivided into the Ardennes region in the west as well as the Eifel and Hunsrück regions in the east. For the study area, 2-D steady-state and conductive thermal models were established based on geological models of lithosphere-scale which were parameterized using thermal rock properties including thermal conductivity, radiogenic heat production, and density. The thermal models are constrained by surface heat flow (q_s) and the geophysically-estimated depth of the lithosphere–asthenosphere boundary (LAB). A q_s of 75 ± 7 (2σ) mW m^{-2} was determined in the area. A LAB depth of 100 km, as seismically derived for the Ardennes, provides the best fit with the measured q_s. Modelled temperatures are in the range of 120–125 °C at 5 km depth and of 600–650 °C at the Moho, respectively. The mantle heat flow amounts to ~40 mW m^{-2}. Possible thermal consequences of the 10–20 Ma old Eifel plume, which caused elevation of the LAB to 50–60 km depth, were modelled in a steady-state thermal scenario resulting in a q_s of 91 mW m^{-2} in the Eifel region. Available q_s values (65–80 mW m^{-2}) are significantly lower and do indicate that the plume-related heating has not yet reached the surface in its entirety.

1 Introduction

Well-constrained thermal models help to evaluate the geothermal resources of a region. In general, structural data, representative thermal rock properties, and thermal boundary conditions represent the main input for the development of a thermal model. Logged subsurface temperature data are normally used for the calibration of a thermal model. For the greater Luxembourg region, only the Mersch borehole provides deep temperature data. In order to circumnavigate this fact, in-depth studies of the regional and local geology and of the thermal rock properties assigned to the geological units are required, providing reliable data for the parameterization of the geothermal model and for the definition of thermal boundaries. As a lower and upper boundary, the lithosphere-asthenosphere boundary (LAB) and the

surface heat flow (q_s), respectively, could be used. The geology of the study area is well known in the upper 15 km but is generalized in the lower segment down to the crust/mantle discontinuity. The rock types of the geological units in the model were assessed from surface and borehole observations and, for the deeper portions of the model, from geophysical surveys and from xenolith data of the adjoining volcanic field in the Eifel region (Germany). Thermal rock properties assigned to geological units relate to a large number of measured laboratory data on outcrop and drill core samples for the upper part of the crust and are complemented by literature data for the lower part of the lithosphere.

The focus of the paper is threefold: It assesses the thermal field by numerical modelling, provides new data on surface heat flow for verification of the thermal models, and delivers a database of measured thermal rock properties (thermal conductivity, radiogenic heat production and density), which all are essential for any type of thermal simulation. The models constitute the basis for the assessment of geothermal resources of Luxembourg and adjoining areas.

2 Regional geology

The local and regional geological setting of the study area is shown in Fig. 1. The bulk of the Earth's crust in the study area was shaped in response to the amalgamation of Western Europe during the Caledonian and Variscan orogenic cycles, which involved the deposition of thick sediment piles and their subsequent deformation (Pharaoh, 1999; Pharaoh et al., 2006). Since about 40 Ma, part of the study area is undergoing deformation due to the development and evolution of the ECRIS (European Cenozoic Rift System), which is expressed by uplift and volcanism in the Rhenish Massif (Bourgeois et al., 2007; Demoulin and Hallot, 2009; Schmincke, 2007; Ziegler and Dèzes, 2007; and references therein).

The subsurface geology is illustrated by three crustal cross sections (Fig. 2). Two of the sections (sections A and B) extend, perpendicular to the Variscan structures, from the Lower Palaeozoic Stavelot Massif in the Belgian Ardennes in the north to the Metz Fault/Hunsrück Boundary Fault in the south. The third section extends parallel to the Variscan structures approximately from the southwestern border of Luxembourg to the northeastern edge of the Mesozoic Trier–Luxembourg Basin (TLB) and the southwestern margin of the West Eifel Volcanic Field.

The TLB is the youngest sedimentary record of the pre-Tertiary evolution of the area (Schintgen and Förster, 2013). The basement of the TLB and the Ardennes (AD), as well as

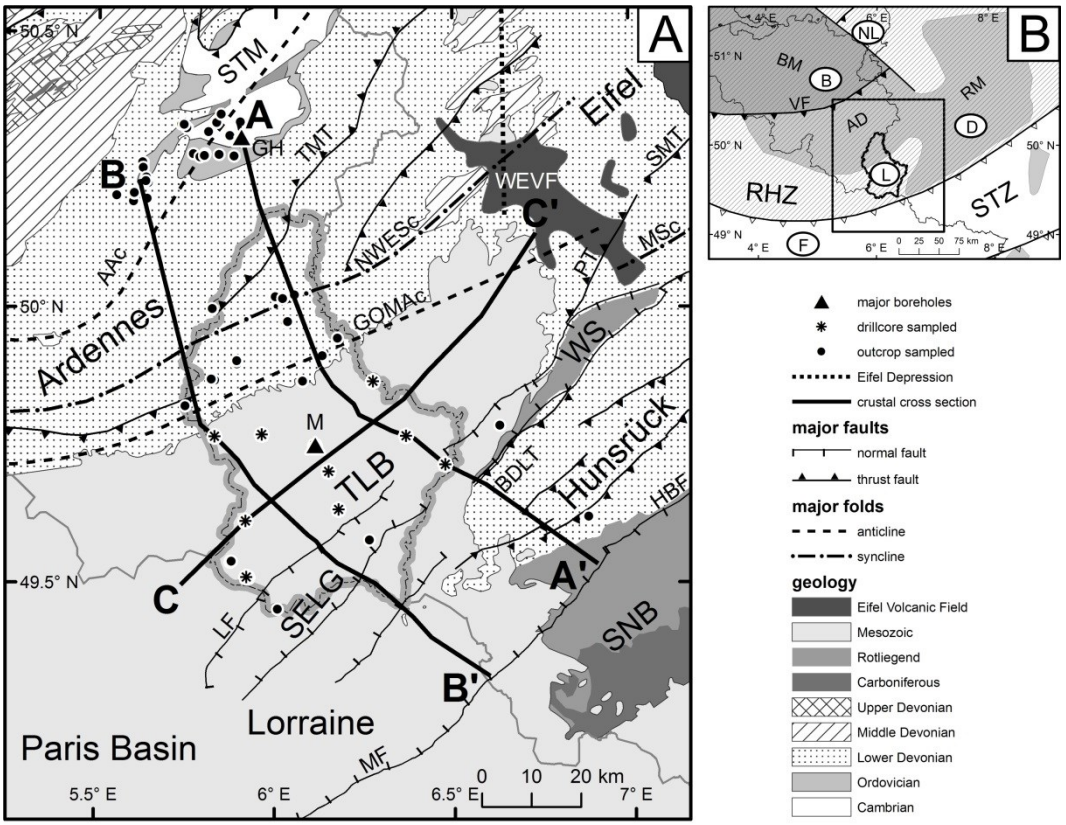

Fig. 1: (A) Regional geological map of the greater Luxembourg area (modified after Schintgen and Förster, 2013). Bold lines and letters indicate the three crustal cross sections shown in Fig. 2. Locations of the boreholes Grand-Halleux (GH) and Mersch (M) are indicated by triangles. Main structures: AAc = Ardennes Anticlinorium, NWESc = Neufchâteau–Wiltz–Eifel Synclinorium, GOMAc = Givonne–Oesling–Manderscheid Anticlinorium, MSc = Mosel Syncline, TMT = Troisvierges–Malsbenden Thrust, PT = Plein Thrust, SMT = Siegen Main Thrust, LF = Luxembourg Fault, SELG = SE-Luxembourg Graben, BDLT = Boppard–Dausenau–Longuich Thrust, MF = Metz Fault, HBF = Hunsrück Boundary Fault, STM = Stavelot Massif, TLB = Trier–Luxembourg Basin, WS = Wittlicher Senke and SNB = Saar–Nahe Basin; (B) Inset map: Basement tectonic map of Luxembourg and surroundings. B = Belgium, D = Germany, F = France, L = Luxembourg, NL = Netherlands. Terranes pertaining to Eastern Avalonia are hatched. Grey areas mark basins and platforms. AD = Ardennes, BM = Brabant Massif, RHZ = Rhenohercynian Zone, RM = Rhenish Massif, STZ = Saxothuringian Zone, VF = Variscan Front. Rectangle indicates location of geological map shown in the regional geological map.

the Eifel and the Hunsrück are part of the Rhenish Massif (RM). The latter belongs to the Variscan Rhenohercynian Zone (RHZ) (Fig. 1B). In the study area the RHZ is a generally northwest vergent fold-and-thrust belt, confined by the Variscan Front (VF) in the north (with its continuation at depth as the Eifel detachment) (Fig. 2) and the Saxothuringian Zone (STZ) in the south (Meyer, 1994; Meyer and Stets, 1980, 1996; Oncken et al., 1999). Large and persistent fold structures are typical for the Ardennes and Eifel regions (e.g., Meyer and Stets, 1996), whereas thrusts are characteristic for the Hunsrück area (e.g., Wildberger, 1992; Fig. 2, cross sections A and B). The orientation of the structures is dominantly WSW–ENE (N60–

70°E) in the Ardennes–Eifel region and SW–NE (N45°E) in the Hunsrück, but turns to the west in a W–E direction in the Belgian Ardennes.

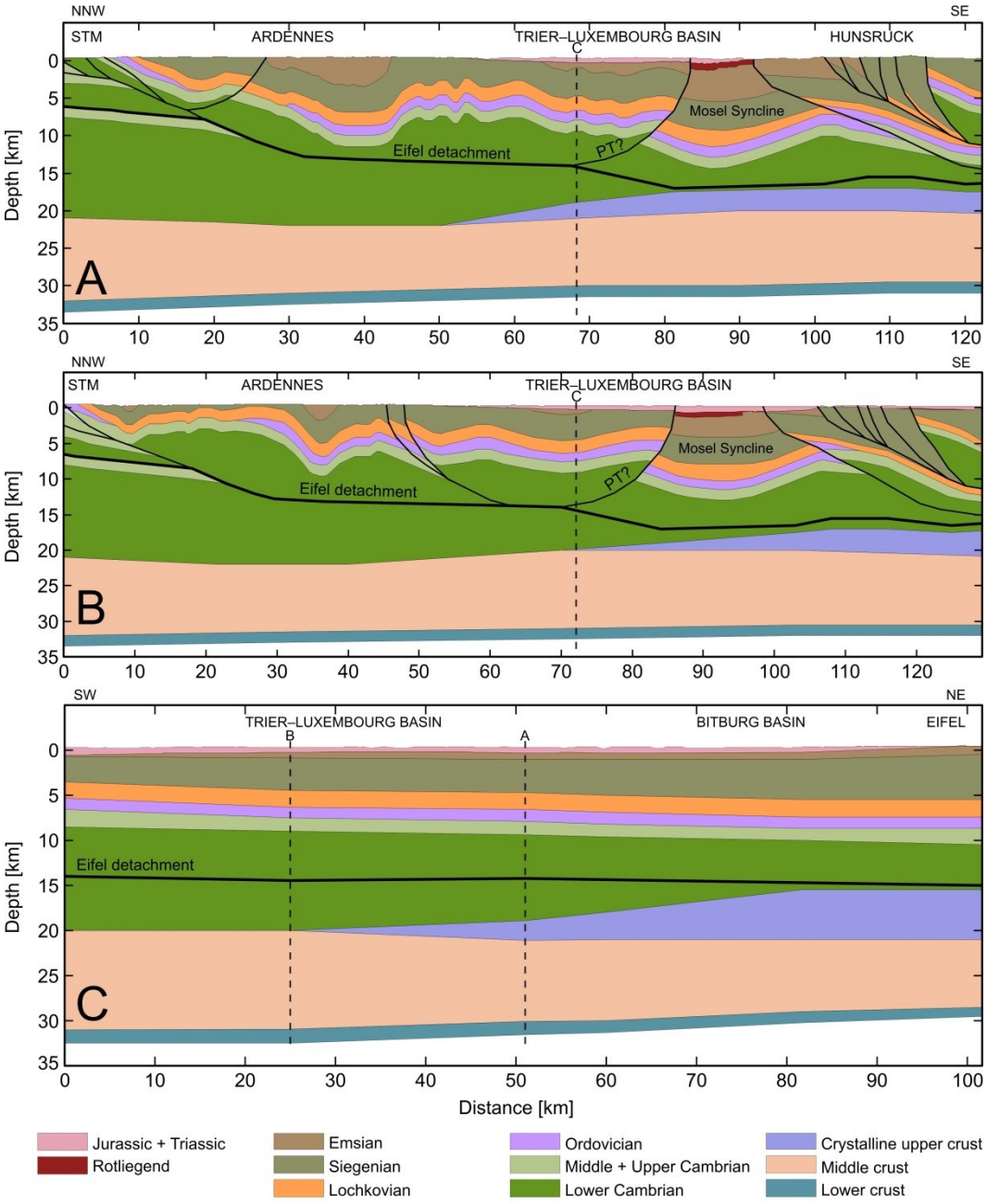

Fig. 2: Geological cross sections (for location see Fig. 1A) developed to the depth of crust–mantle transition. Vertical dashed lines indicate the intersection with the indicated cross section. STM = Stavelot Massif, PT = Plein Thrust. For details, see text.

Except for the Wittlicher Senke (Fig. 1A), which constitutes a remarkable intramontane Permian (Rotliegend) graben (Stets, 2004), the Variscan basement is largely composed of thick Lower Devonian (i.e., Lochkovian, Siegenian or Praguian and Emsian) syn-rift

sediments characterized by a generally homogeneous, shale-rich, clastic rock assemblage, which often displays a pervasive cleavage (Furtak, 1965; Konrad and Wachsmut, 1973; Lucius, 1950; Wildberger, 1992). The total thickness of the Lower Devonian sediments increases rapidly from the margin towards the centre of the Rhenohercynian basin, where maximum thicknesses of more than 10,000 m are reported (Meyer and Stets, 1996; Stets and Schäfer, 2002). An apparent facies change in the Hunsrück and the Mosel Syncline (Stets and Schäfer, 2002; Zitzmann and Grünig, 1987) explains the different lithostratigraphic classification in Belgium and Luxembourg (Dejonghe, 2008; Bultynck and Dejonghe, 2001; Lucius, 1950) and further used in Germany (LGB, 2005; Mittmeyer, 2008).

The Lower Devonian unconformably overlies Cambrian and Ordovician metamorphic rocks that are only known from outcrops in the Ardennes, notably in the Stavelot–Venn Massif (or Stavelot Massif; e.g., Bless et al., 1990; Fig. 1A). It is characterized by dominantly E–W oriented structures, strongly north-verging folds, and a southward dipping main cleavage (Verniers et al., 2002) associated with Variscan processes that have largely overprinted a weaker Caledonian metamorphism and deformation (Bless et al., 1990; Fielitz and Mansy, 1999). The subsurface Cambrian–Ordovician succession is suggested to be stratigraphically complete in the study area. A high background density in the Bouguer map (Schintgen and Förster, 2013) indicates relatively dense Ordovician rock at about 5 km depth, in accordance with the estimated position of the Lower Palaeozoic/Lower Devonian unconformity (Meyer and Stets, 1980, 1996; LGB, 2005). The N–S-oriented Eifel Depression (Eifeler-Nord-Süd Zone) is an important cross fold separating the Ardennes in the west from the Eifel in the east (Fig. 1A; Murawski et al., 1983). Beneath the Ardennes, seismic velocities (Mechie et al., 1983) infer that the Lower Cambrian rift sediments are particularly thick (Hollmann, 1997; Verniers et al., 2002; Sintubin and Everaerts, 2002) and may extend down to the top of the cratonic basement at about 19 km depth as shown in the adjoining Brabant Massif (BM) (Fig. 1B).

The deep geology of the RHZ above the basal Eifel detachment at about mid-crustal level (Fig. 2) is constrained from numerous seismic refraction (Mooney and Prodehl, 1978; Mechie et al., 1983; Meissner et al., 1983) and seismic reflection profiles farther east through the Eifel area (DEKORP Research Group, 1991; Oncken et al., 1999, 2000). These seismic surveys allow a structural and to some point compositional subdivision of the crust in an upper part, largely composed of Palaeozoic rocks (known from the surface), and a lower part, consisting of Precambrian rocks known from xenolith samples of the Eifel volcanic field (e.g., Downes, 1993; Mengel et al., 1991; Stosch et al., 1991; Voll, 1983, Wörner et al., 1982). Simplified

cross sections adapted to the geology of the study area (Wagner et al., 2012; Zitzmann and Grünig, 1987) were also considered. Still unresolved is the trace of the Plein thrust (Kölschbach, 1986), which appears to replace the Siegen Main Thrust, being an important thrust fault in the Rhenish Massif. Besides evidence from xenoliths, the small exposure of Wartenstein Gneiss of Neoproterozoic age (Meyer and Nagel, 2001) at the southern margin of the Hunsrück also shows the occurrence of Precambrian rock. In the Eifel region, xenoliths point towards large amounts of mica schists and paragneisses in between the Avalonian cratonic basement and the Cambrian rocks.

3 Analysis of thermal rock properties and surface heat flow

A sophisticated parameterization of a thermal model requires sample control for all major rock types. For the Mesozoic, drill core samples (66 samples) were obtained from 12 relatively shallow boreholes archived in the Geological Survey of Luxembourg. In addition, drill core (17 samples) from the Cambrian section of the 3225-m-deep Grand-Halleux borehole (GH in Fig. 1A; Graulich, 1980) was sampled in the archive of the Geological Survey of Belgium. To comprehensively characterize the major rock types of the Mesozoic–Palaeozoic and the Neoproterozoic geological formations on outcrop were also sampled (142 samples in the Palaeozoic and 9 in the Neoproterozoic; 12 samples in the Mesozoic; Fig. 1A). Table 1 provides the stratigraphic units and the sampled lithotypes. The Lower Devonian formations of the Mosel Syncline (Figs. 1A and 2), which is supposed to continue along strike underneath the Permian graben system (WS–SELG; Fig. 1A), and of the Hunsrück area are only exposed in Germany (e.g., LGB, 2005; Stets and Schäfer, 2002). Here, the Lower Devonian deposits differ with respect to their lithology and thus their stratigraphic subdivision from those in Belgium and Luxembourg (Dejonghe, 2008; Bultynck and Dejonghe, 2001; Lucius, 1950). As the formations in the Hunsrück were not sampled, they are characterized by a compilation of similar lithotypes sampled in the Ardennes. In the following, the methods applied for the determination of thermal conductivity and of radiogenic heat are described.

Table 1: Stratigraphic units and lithotypes sampled in different areas.

Sampling area	Stratigraphic unit	Lithotype	n
Stavelot Massif	Cambrian + Ordovician	Slate	25
		Silty slate	18
		Shale	1
		Siltstone	2
		Sandstone	9
		Quartzite	10
Ardennes	Lower Devonian	Slate	7
		Silty slate	5
		Shale	33
		Siltstone	18
		Sandstone	25
		Quartzite	3
Hunsrück	Lower Devonian	Slate	1
		Shale	1
		Quartzite	1
	Neoproterozoic	Gneiss	5
		Mica schist	2
		Quartzite	1
		Sandstone	1
Trier—Luxembourg Basin	Triassic + Jurassic	Claystone	4
		Siltstone	5
		Sandstone	22
		Marl/Marlstone	28
		Limestone	7
		Dolomite	8
		Anhydrite	1
		Gypsum + Anhydrite	1
		Conglomerate	2

n = number of samples

3.1 Thermal conductivity

Thermal-conductivity (TC) measurements were performed with the Thermal Conductivity Scanning (TCS) device (Lippmann and Rauen, GbR Schaufling, Germany). The measurement technique is based on high-resolution optical scanning with an inherent error of determination <3% (Popov et al., 1999). TC of samples was determined by comparison with standards (λ = 2.93 W m^{-1} K^{-1}). The method allows a TC sampling interval of 0.1 mm at a scanning speed of 5 mm s^{-1}. Sample sizes were 5–10 cm in length and a minimum of 2 cm in width. Samples were first oven-dried at 60 °C until constant mass was reached before TC was measured under ambient temperature and pressure conditions. Subsequently, samples were saturated under

vacuum in a desiccator for a minimum of 48 hours. The applied fluid-saturation with demineralized water allowed the determination of porosity and density using the Archimedes method (Tables 2 and 3, Table 4 for density).

Table 2: Porosity and transformation factor of thermal conductivity for different Palaeozoic lithotypes.

	Porosity [%]					Transformation factor			
Lithotype	Median	Mean	Min.	Max.	n_S	Median	Mean	1σ	n_m
Gneiss	4.5	4.5	2.8	6.2	2	1.19	1.20	0.05	6
Slate	2.6	3.1	1.8	6.5	7	1.24	1.23	0.11	14
Quartzite	6.0	6.4	0.5	12.7	3	1.37	1.38	0.09	6
Silty slate	2.6	2.5	1.1	3.8	8	1.16	1.19	0.08	16
Shale	2.7	3.3	1.4	8.0	10	1.17	1.19	0.11	20
Sandstone	2.3	2.3	0.4	3.5	7	1.15	1.17	0.10	14
Siltstone	1.8	2.9	1.3	8.1	6	1.13	1.17	0.10	12
All field samples	2.6	3.1	0.4	12.7					
Grand-Halleux slate	0.3	0.4	0.2	0.6	5	1.03	1.04	0.04	10
Grand-Halleux quartzite	0.1	0.2	0.1	0.3	3	1.10	1.12	0.06	6
All drill core samples	0.3	0.3	0.1	0.6					
Total					51				104

Min. = minimum, Max. = maximum, n_S = number of samples, σ = standard deviation, n_m = number of measurements.

For reduction of work load, not all the Palaeozoic samples were used for TC determination under saturated conditions. Only a subset was used as the Palaeozoic samples are characterized by low mean porosity values (<4%) in comparison to the Mesozoic samples (2–20%). Subsequently, transformation of dry-measured TC into water-saturated TC was accomplished by transformation factors derived from the measured subset (Table 2): First, ratios of saturated to dry TC were determined for every sample of the measured subset. Second, mean values of these ratios were calculated for single lithotypes and used as transformation factors. Application of simple transformation factors seemed justified due to similar mean values (1.17–1.23) and their relatively small standard deviations (Table 2) owing to low and similar porosities. Exceptions are the quartzites (1.38), showing the highest porosity values of the Palaeozoic rock samples, and the drill core samples from Grand-Halleux (quartzites and slates) showing lower transformation factors (1.12 and 1.04), characterized by the lowest porosity values.

Table 3: Porosity of the Mesozoic lithotypes.

	Porosity [%]				
Lithotype	Median	Mean	Min.	Max.	n
Dolomite	1.6	1.8	0.9	3.1	8
Limestone	8.2	12.7	3.8	28.1	7
Marl/Marlstone	9.3	10.6	2.4	20.6	28
Sandstone	13.5	14.7	2.5	30.1	22
Siltstone	18.4	16.3	7.5	26.9	5
Claystone	19.4	17.9	11.9	20.9	4

Min. = minimum, Max. = maximum, n = number of samples.

All Mesozoic samples were measured either water-saturated or isooctane-saturated. Isooctane saturation was applied to claystone and marlstone, to avoid clay swelling (Fuchs et al., 2013). TC measured under isooctane-saturation was converted to water-saturated TC using the geometric-mean model developed for a two component system of pores and matrix (e.g., Brigaud et al., 1990):

$$\lambda = \lambda_m^{1-\phi} \cdot \lambda_p^{\phi} \quad (1)$$

where λ is the TC of a sample (in W m^{-1} K^{-1}), λ_m is the TC of the rock matrix, λ_p is the TC of the pore fluid and ϕ is the porosity. The TC of saturating fluids (λ = 0.025 W m^{-1} K^{-1} for air, 0.095 W m^{-1} K^{-1} for isooctane and 0.604 W m^{-1} K^{-1} for water at room temperature) was taken according to Fuchs et al. (2013). The median, mean and range of TC for the different Palaeozoic and Mesozoic lithotypes are given in Table 4.

The anisotropy of TC ($A = \lambda_{\parallel}/\lambda_{\perp}$; e.g., Schön, 1996) was accounted for during sample preparation and orientation of the sample surfaces during the measurement, which allowed TC measurements parallel ($\lambda_{\parallel}$) and perpendicular ($\lambda_{\perp}$) to bedding (stratification; S_0) for layered sediments or schistosity (cleavage; S_1) for shale and slate (Table 4). Palaeozoic sandstone and quartzite, and shale are virtually isotropic. Siltstone commonly shows a minor anisotropy in the range of 1.0–1.3 (median 1.1). Silty slate ('quartzophyllade') is characterized by a range of 0.9–1.3 (median 1.2). Slate has the highest anisotropy, ranging from 0.9 to 2.0 (median 1.2). In the Mesozoic rocks, anisotropy is usually small in limestone, dolomite, siltstone and sandstone, but increases in fine-grained clastic rocks, notably claystone and marlstone showing anisotropies in the range 1.0–1.6 (median 1.1 and 1.3, respectively) (Table 4). Even though variation of TC as a function of anisotropy for lithotype classes was small in general, orientation-dependent formation TC was determined in addition

to mean formation TC values. Calculation of formation TCs was done by applying a weighted arithmetic mean based on the proportion of different lithotypes in each formation:

$$\lambda_{Fm} = \sum_{i}^{n} \left(X_i \cdot \lambda_i \right) \tag{2}$$

where λ_{Fm} is the formation TC (orientation-specific) calculated from a number i out of n different lithotypes representing volume proportions X_i of the formation and characterized by an orientation-dependent lithotype TC λ_i specified for each formation.

Table 4: Lithotype thermal conductivity under dry and water-saturated conditions, anisotropy of lithotype thermal conductivity and lithotype density.

Age	Lithology		λ_{dry}						λ_{sat}						A			ρ		
		n_S	Median	Mean	Min.	Q10	Q90	Max.	Median	Mean	Min.	Q10	Q90	Max.	Median	Min.	Max.	Median	Min.	Max.
			[W m^{-1} K^{-1}]						[W m^{-1} K^{-1}]									[10^3 kg m^{-3}]		
Paleozoic	Quartzite	13	4.7	4.8	3.7	4.1	5.6	5.6	6.1	6.1	5.1	5.4	6.9	7.7	1.0	1.0	1.1	2.64	2.35	2.71
	Sandstone	34	4.0	3.9	2.8	3.1	4.7	5.1	4.8	4.7	3.3	3.7	5.6	6.0	1.0	0.9	1.3	2.66	2.56	2.81
	Siltstone	20	2.7	2.8	1.8	2.3	3.3	3.7	3.2	3.3	2.1	2.7	3.9	4.3	1.1	1.0	1.3	2.69	2.43	2.80
	Slate	32	2.5	2.7	1.5	2.1	3.8	4.5	3.0	3.1	1.8	2.4	4.4	4.7	1.2	0.9	2.0	2.78	2.67	2.96
	Silty slate	23	2.5	2.5	1.7	2.0	3.2	3.8	2.9	3.0	2.0	2.3	3.8	4.5	1.2	0.9	1.3	2.75	2.64	2.94
	Shale	34	2.3	2.4	1.7	1.9	3.2	3.7	2.8	2.9	2.0	2.3	3.8	4.4	1.0	0.8	1.2	2.67	2.43	2.77
Mesozoic	Dolomite	8	3.8	3.8	3.2	3.4	4.3	4.5	3.8	3.9	3.4	3.4	4.4	4.6	1.0	0.9	1.1	2.78	2.66	2.82
	Limestone	7	2.0	1.9	1.1	1.3	2.3	2.7	2.3	2.3	2.0	2.1	2.6	2.9	1.0	1.0	1.1	2.51	1.97	2.62
	Marl/Marlstone	28	1.9	1.9	1.2	1.4	2.6	3.6	2.5	2.6	1.5	2.0	3.1	4.4	1.1	1.0	1.5	2.34	1.96	2.69
	Sandstone	22	2.2	2.2	0.9	1.5	3.0	3.8	3.2	3.3	1.9	2.7	3.9	5.0	1.0	0.8	1.2	2.29	1.85	2.60
	Siltstone	5	1.6	1.7	1.0	1.1	2.6	2.8	2.8	2.7	1.7	1.9	3.2	3.3	1.0	1.0	1.2	2.22	1.96	2.55
	Claystone	4	1.3	1.4	0.9	1.0	1.8	2.2	2.1	2.3	1.7	1.8	2.9	3.3	1.3	1.1	1.6	2.12	2.08	2.27

n_S = number of samples, λ_{dry} and λ_{sat} = thermal conductivity under dry and water-saturated conditions, respectively, A = anisotropy, ρ = density (dry state), Min. = minimum, Max. = maximum, Q10 = quantile 10, Q90 = quantile 90.

For the Lower Devonian formations, anisotropy is negligible and mean formation TC values calculated using the two orientation-dependent values are sufficient to characterize a formation. Exceptions are the Lower Palaeozoic (Cambrian and Ordovician) formations showing at least a weak anisotropy of 1.1, with the highest value of 1.4 in the slate-rich formations. Anisotropy in Mesozoic formations generally does not exceed 1.1 except in more clay- and marl-/marlstone-rich formations (commonly 1.2–1.3). Details on thermal conductivity, anisotropy of TC, transformation factors, porosity and formation TC error calculation are given in the Supplementary material (Appendix A).

3.2 Radiogenic heat production

Owing to the small thickness of the Mesozoic sedimentary succession (mostly 400–600 m increasing to about 1500 m only in the southwestern parts of the TLB in France) composed to 50–70% of marl/marlstone and claystone, the contribution of its radiogenic heat production (H) to surface heat flow is small (0.5–1 mW m^{-2}) and not considered. H of the thicker Rotliegend sediments is estimated from their lithological composition (Häfner et al., 2007) using lithotype-specific H values published by Vilà et al. (2010).

For the Palaeozoic basement rocks, H was determined based on geochemical data since they form the major part of the crust in the study area. Bulk-rock geochemical analyses included the measurement of U, Th and K concentrations (Table 5) by X-ray fluorescence spectrometry and inductively coupled plasma-mass spectrometry on 20 rock samples representative for the Cambrian, Ordovician and Lower Devonian basement. H was calculated according to the equation of Rybach (1976, 1988):

$$H = 10^{-5} \times \rho\left(9.52c_U + 2.56c_{Th} + 3.48c_K\right) \quad (3)$$

where H is the radiogenic heat production (in μW m^{-3}), ρ is rock density (in kg m^{-3}), c_U and c_{Th} are the concentrations of uranium and thorium (in ppm), respectively, and c_K is the concentration of potassium (in wt%). For the Palaeozoic rocks, lab-measured densities mostly range from 2.6 to 2.8 × 10^3 kg m^{-3} (Table 4). High density values between 2.8 and 2.96 × 10^3 kg m^{-3} refer to slate/silty slate samples from the Ordovician Salm Group.

The values of H are in the common range for the individual rock types (e.g., Schön, 1996; Vilà et al., 2010), with the lowest value for quartzite (0.6 μW m^{-3}) and the highest value for black slate (3.0 μW m^{-3}). For the Mesozoic–Palaeozoic upper crust, values of H for individual samples (Table 5) were then upscaled to formation H, ranging from 1.2 to 2.5 μW m^{-3} (median 1.9 μW m^{-3}) in the Cambrian to Ordovician formations, from 0.6 to 2.0 μW m^{-3} (median 1.8 and 1.6 μW m^{-3}, respectively) in the Ardennes and Hunsrück. The proportion of the different lithotypes in those formations was accounted for by applying a weighted arithmetic mean as done for the calculation of formation TC (Eq. (2)). The complete geochemical data and details on density and radiogenic heat production are given in the Supplementary material (Appendix A).

Table 5: U, Th, K concentrations and resulting radiogenic heat production (H) of representative rock samples.

Region	Ardennes										Stavelot Massif				SE Hunsrück			Grand-Halleux borehole			
Sample	E1b-07	E1a-04	E1a-09	E1a-11	Sg3-03	Sg1-03	Sg1-07	OlG-13	FEP-07	BIH-06	COL-05	PLA-01	SPA-02	SLW-10	War-01	War-03	GH350	GH2331	GH3128	GH3216
Lithotype	Stst	Sh	Sh	Sst	Sh	Sl	Sst	Sh	Sh	Ssl	Sl	Sl	Ssl	Sl	Gn	Gn	Q	Sl	Sl	Q
K_2O [wt.%]	1.88	3.82	3.90	0.31	3.62	3.16	0.89	3.40	2.88	3.38	3.63	3.17	3.90	6.76	2.82	3.36	0.39	5.26	4.47	0.68
Th [ppm]	11.0	13.6	14.3	7.6	13.6	13.2	9.0	15.3	12.5	16.5	16.9	14.7	14.6	20.1	7.0	9.9	4.2	14.2	17.1	8.4
U [ppm]	3.1	2.9	3.2	1.6	2.9	3.1	2.0	3.5	2.5	2.4	2.9	1.8	2.7	3.7	1.7	2.4	1.1	1.8	5.3	2.2
H [mW m^{-3}]	1.7	2.0	2.2	1.0	2.0	2.0	1.2	2.3	1.7	2.1	2.3	1.9	2.0	2.9	1.1	1.6	0.6	1.9	3.0	1.2

Stst = siltstone, Sh = shale, Sst = sandstone, Sl = Slate, Ssl = silty slate, Gn = gneiss, Q = quartzite.

3.3 Determination of surface heat flow

The terrestrial heat flow in Luxembourg was unknown prior to this study. To fill this gap in knowledge and to provide further input for the thermal modelling, heat flow was determined in the Mersch borehole, located in the Alzette river valley in the Trier–Luxembourg Basin (M in Fig. 1A). This borehole was drilled in 1968 as an exploration borehole to a final depth of 328 m and mostly encountered rocks of the Lower Middle Keuper, the Muschelkalk and the Buntsandstein (see Schintgen and Förster, 2013, their cross section B).

After completion, the borehole had been equipped with three piezometer tubes and the remaining open space cemented. The borehole was under thermal equilibrium when a continuous temperature (T) log could be obtained in 2011 by an analog, electric-line system with a 28-mm-diameter sensor. A downward logging speed of 2 m min^{-1} was applied in order to compensate for the buoyancy of the sensor and, thus, a loss in cable tension during descent in the narrow water-filled tube. The water level in the borehole corresponds to terrain level.

The T-log has a precision of 0.01°C and an accuracy of 0.1 °C. The recording interval was 0.1 m. The T-log was processed by applying a running average over 21 records (i.e., 2 m) for smoothing the data. T-gradients were calculated between consecutive temperature-depth points. As could be expected for a borehole in thermal equilibrium, the T-gradient plot well reflects the changes in lithology resembled by the gamma-ray log (Fig. 3).

For the determination of the surface heat flow (q_s), the interval method was applied (Powell et al., 1988). Five depth intervals are selected for the heat-flow determination (Fig. 3). The intervals correspond more or less to lithostratigraphic units composed of up to three major lithotypes. The lithological changes between the intervals are also reflected in changes of the interval T-gradient, which indicates that they are linked to changes in TC. Values of measured TC assigned to the intervals are from drill core samples of the Mersch borehole (interval A) and from cores of the same lithostratigraphy from nearby boreholes (intervals B–E).

Table 6 lists the lithotypes, TC values and T-gradients used in the heat-flow calculation. The T-gradient is the arithmetic mean of individual gradients of the recording intervals. The standard error α of the T-gradient was determined as follows:

$$\alpha = \sigma \cdot \sqrt{N-1} \qquad (4)$$

where σ is the standard deviation and N the number of T-gradient values of the interval. TC of lithotypes corresponds to laboratory measurements under water-saturated conditions, performed perpendicular to bedding honoring the geological situation. The lithotype TC is

pressure corrected (after Fuchs and Förster, 2014) and T-corrected (after Somerton, 1992) to resemble in-situ conditions (see Eqs. (10)–(12) in Section 4). However, the cumulative effect of both corrections on the interval TC in this shallow borehole is minor (cf. Table 6). The interval TC is calculated as a weighted mean:

$$\lambda_{\text{int}} = \frac{\sum_{i}^{n}(t_i \cdot \lambda_i)}{\sum_{i}^{n} t_i} \tag{5}$$

where λ_{int} is the interval TC, λ_i the TC of individual pressure and T-corrected lithotype TC values, t_i the volume fraction of the individual lithotypes, and n the number of lithotypes considered. The 1σ error of TC of interval A is estimated to be 5% compared to 10% in intervals B, C and D and 15% in the most heterogeneous interval E (Table 6). The estimated errors are a reflection of the small number of samples per lithotype and uncertainties in the geology.

The interval heat flow q_i (in mW m^{-2}) is obtained by the Fourier equation of heat conduction:

$$q = -\lambda \cdot \frac{dT}{dz} \tag{6}$$

where λ is the TC (in W m^{-1} K^{-1}) and dT/dz is the T-gradient of the interval (in K km^{-1}). The 1σ error (Table 6) is determined by error propagation:

$$\sigma_q = \sqrt{\left(\frac{\partial q}{\partial \lambda} \cdot \sigma_\lambda\right)^2 + \left(\frac{\partial q}{\partial gradT} \cdot \sigma_{gradT}\right)^2} = \sqrt{(gradT \cdot \sigma_\lambda)^2 + (\lambda \cdot \sigma_{gradT})^2} \tag{7}$$

where σ_q is the standard deviation (or error) of interval heat flow q, σ_λ and $\sigma_{grad\ T}$ are the respective standard deviations of interval TC λ and interval thermal gradient grad T. Interval heat-flow values range from 68 to77 mW m^{-2}. The resulting q_s (± 2σ) for the borehole site averages to 75 ± 7 mW m^{-2}. The uncertainty of q_s is calculated by error propagation:

$$\sigma_{q_S} = \frac{1}{n}\sqrt{\sum_i^n \sigma_{q_i}^{\ 2}} \tag{8}$$

where σ_{qs} is the error on q_s resulting from a number n of intervals i characterized each by an error σ_{qi} of interval heat flow q_i.

The consideration of depth intervals in the shallower part of the borehole seemed inappropriate for the following reasons. The overall T-gradient in the upper part of the borehole to a depth of 125 m is remarkably low compared to the lower part of the section (Fig. 3). The TC values determined for this borehole section cannot compensate for this T-gradient reduction in a thermal regime that is purely conductive. It is supposed that regional

water flow from a recharge area 10–15 km to the north is responsible for this situation. The first geological formation in which the heat transfer is apparently purely conductive is the marl/marlstone aquitard in the Middle Muschelkalk (heat-flow interval A). This assumption is underpinned by similar heat-flow values determined in intervals B–D. The somewhat lower heat flow in interval E compared to the upper intervals can be explained by a larger error/uncertainty in determining the true interval TC.

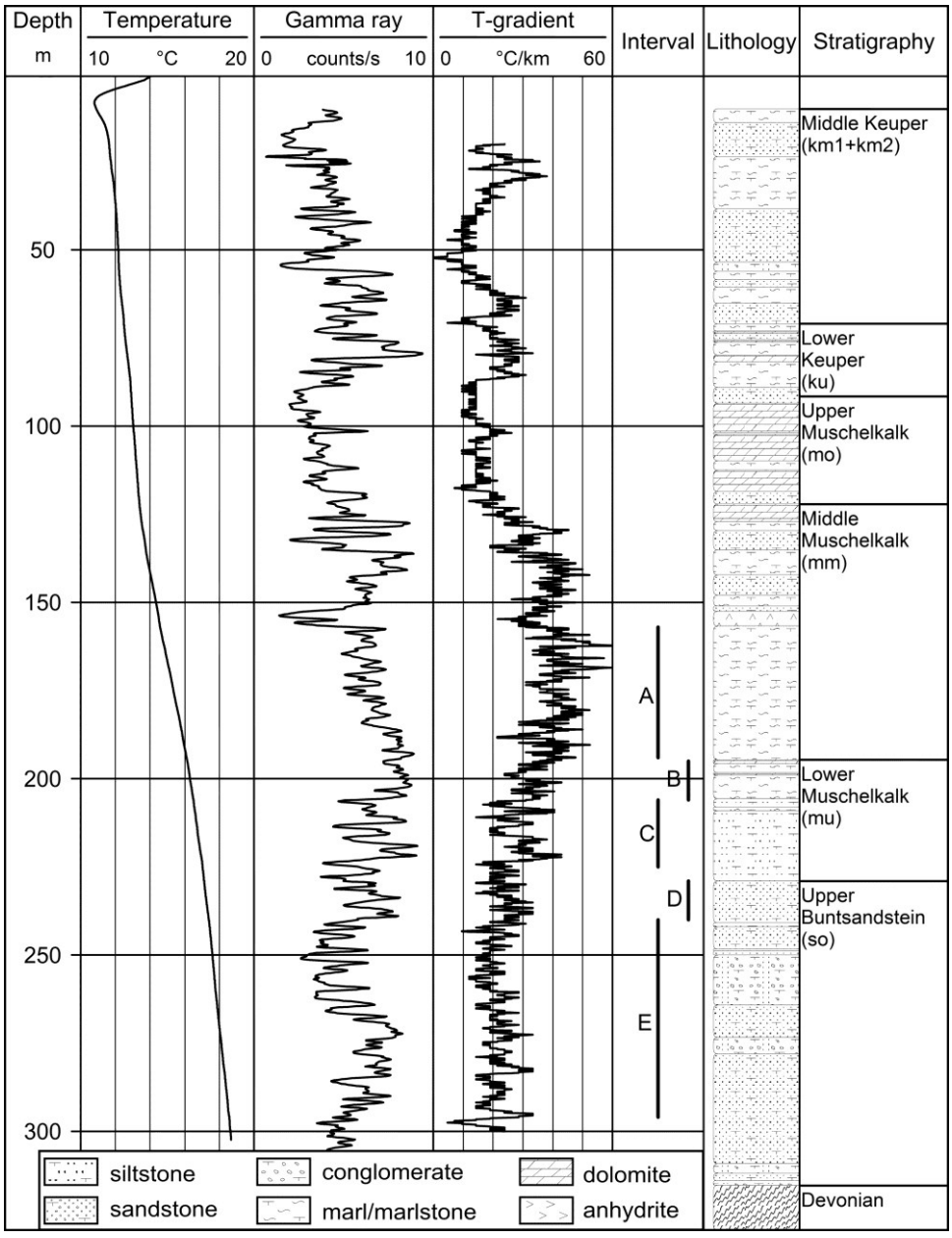

Fig. 3: Temperature, gamma ray, temperature gradient, simplified lithology, and stratigraphy of the Mersch borehole. Depth is given in meters below ground level. Black vertical bars mark the heat-flow intervals A–E (cf. Table 6).

The q_s of the Mersch borehole (75 ± 7 mW m^{-2}) is in accord with the bulk of data reported for

areas adjacent to Luxembourg. In the Eifel and the Saar–Nahe Basin, q_s values between 64 and 76 mW m^{-2} have been determined (Bram, 1979; Haenel, 1971; Haenel, 1983; Hückel and Kappelmeyer, 1966). The adjoining northeastern part of the Lorraine region may have a slightly higher q_s of 73–84 mW m^{-2} (Vasseur, 1980). The value of 59 mW m^{-2} (Vandenberghe, 2002) reported in the Cambrian section of the Grand-Halleux borehole in the Stavelot Massif in Belgium is exceptionally low. This value is suggested to underestimate the heat flow due to a disturbed temperature profile (see also Section 5).

Table 6: Thermal data of the Mersch borehole.

					Litho λ_{sat}	Interval T-gradient			Interval λ_{sat}				q_i		q_s		
ID	Depth int.	Strat.	Lithology	Vol.		AM	σ	α	Unc.	Corr.	σ	σ		σ	AM	1σ	2σ
	[m]			[%]	[W m^{-1} K^{-1}]	[K km^{-1}]			[W m^{-1} K^{-1}]		[%]	[W m^{-1} K^{-1}]	[mW m^{-2}]		[mW m^{-2}]		
A	157–194	mm1	Silty, gypsum-rich marl	99.8	1.85	41.2	6.3	0.3	1.85	1.87	5	0.09	77	4	75	3	7
			Dolomite	0.2	4.32												
B	195–206	mu2	Dolomitic, sandy marlstone	27.6	2.42	33.1	5.0	0.5	2.29	2.34	10	0.23	77	8			
			Dolomitic clay-/marlstone	70.2	2.22												
			Sandy siltstone	2.2	2.76												
C	206–225	mu1	Sandy siltstone	85.3	2.76	27.8	6.5	0.5	2.68	2.78	10	0.28	77	8			
			Dolomitic clay-/marlstone	14.7	2.22												
D	229–240	so2	Dolomitic sandstone	66.1	2.99	24.9	4.5	0.4	2.87	3.00	10	0.30	75	8			
			Marly sandstone	33.7	2.75												
			Clayey siltstone	0.2	2.38												
E	240–296	so1	Sandy, dolomitic conglomerate	39.9	3.42	21.0	4.5	0.2	3.10	3.26	15	0.49	68	10			
			Dolomitic sandstone	46.2	2.94												
			Marly sandstone	13.7	2.75												
			Clayey siltstone	0.2	2.38												

ID = interval label, Depth int. = depth interval, Strat. = stratigraphy, Vol. = volume fraction of lithotype, Litho λ_{sat} = arithmetic mean of the lithotype thermal conductivity in saturated state, AM = arithmetic mean, σ = standard deviation, α = standard error, Interval λ_{sat} = interval thermal conductivity in saturated state, Unc. and Corr. = values uncorrected and corrected for T and p, q_i = interval heat flow, q_s = surface heat flow. Formations: mm1 = Gipsmergel, mu2 = Orbicularisschichten, mu1 = Muschelsandstein, so2 = Voltziensandstein, so1 = Zwischenschichten (see also Fig. 3).

4 Lithosphere thermal modelling

Figs. 4 and 5 show the conceptual models simplified from the geological cross sections A, B and C (see Fig. 2; location in Fig. 1A) with the polygons considered in the thermal modelling. The cross sections encompass the lithosphere down to the thermal lithosphere–asthenosphere boundary (LAB). Temperatures are calculated numerically by solving the equation for two-dimensional steady-state heat conduction:

$$\frac{\partial}{\partial x}\left(\lambda\frac{\partial T}{\partial x}\right)+\frac{\partial}{\partial z}\left(\lambda\frac{\partial T}{\partial z}\right)=-H \qquad (9)$$

where H is the internal radiogenic heat production and the TC (λ) of the rock is assumed to be isotropic.

The temperature distribution T(x, z) within the lithosphere, x being the horizontal coordinate and z being the vertical coordinate, is determined based on temperature and pressure corrected TC λ(x, z), the distribution of radiogenic heat production H(x, z), and the appropriate thermal boundary conditions. Numerical calculations are based on a finite-element method using the MATLAB® R2010b software. For sedimentary rocks, the T-correction of ambient TC to in-situ conditions was performed separately for temperature and pressure (p). The combined correction equation is:

$$\lambda_{cor}=\lambda_{lab}+\Delta\lambda_T+\Delta\lambda_p \qquad (10) \quad \text{corrected}$$

where λ_{cor} is the in-situ TC (in W m^{-1} K^{-1}), and $\Delta\lambda_T$ and $\Delta\lambda_p$ are the temperature and pressure corrections after Somerton (1992) and Fuchs and Förster (2014), respectively. T-correction after Somerton (1992) is expressed as follows:

$$\Delta\lambda_T=-10^{-3}(T-293)\cdot(\lambda_{lab}-1.38)\cdot\left[\lambda_{lab}\left(1.8\cdot10^{-3}T\right)^{(-0.25\cdot\lambda_{lab})}+1.28\right]\cdot\lambda_{lab}^{-0.64} \qquad (11) \quad \text{corrected}$$

where $\Delta\lambda_T$ is the contribution of T-correction (in W m^{-1} K^{-1}), λ_{lab} is the TC measured in the laboratory (in W m^{-1} K^{-1}) and T is the temperature (in K = °C +273). Pressure correction after Fuchs and Förster (2014) is expressed as follows:

$$\Delta\lambda_p=\left(1.095\cdot\lambda_{lab}-0.172\right)\cdot p^{(0.0088\lambda_{lab}-0.0067)}-\lambda_{lab} \qquad (12) \quad \text{corrected}$$

Where $\Delta\lambda_p$ is the contribution of p-correction (in W m^{-1} K^{-1}), λ_{lab} is the TC measured in the laboratory (in W m^{-1} K^{-1}) and p is the assumed in-situ pressure (in MPa). For igneous and metamorphic rocks, lithotype-specific T- and p-corrections elaborated by Seipold (2001) were applied sequentially:

$$\lambda_T=\lambda_{lab}-a+\frac{1}{\left(b+c\cdot10^{-4}\cdot T\right)}+d\cdot10^{-9}\cdot T^3 \qquad (13)$$

and for peridotite:

$$\lambda_T = \lambda_{lab} - a + \frac{T}{\left(b + c \cdot 10^{-4} \cdot T\right)} + d \cdot 10^{-9} \cdot T^3 \qquad (14) \quad \text{added}$$

$$\lambda_{Tp} = \lambda_T \cdot \left(1 + \alpha \cdot 10^{-2} \cdot p\right) \qquad (15) \quad \text{corrected}$$

where λ_T is the T-corrected TC (in W m^{-1} K^{-1}), λ_{lab} is the TC measured in the laboratory (in W m^{-1} K^{-1}), T is the temperature (in K), and a, b, c and d are rock-specific coefficients (a = 2.2849, b = 0.344, c = 3.27, d = 0.445 for mafic granulite, a = 4.1241, b = –42.9, c = 3890, d = 0.072 for peridotite and a = 2.9169, b = 0.191, c = 5.25, d = 0.670 for gneiss). λ_{Tp} is the T- and p-corrected TC (in W m^{-1} K^{-1}), p is the assumed in-situ pressure (in kbar) and α is a rock-specific coefficient (α = 0.44 for mafic granulite, 1.52 for peridotite and 1.34 for gneiss).

In-situ pressure in the thermal models was estimated considering the density of the overburden. Density values of the Palaeozoic formations and model units (Table 7) resulted from stepwise calculating a weighted arithmetic mean based on the density of representative samples. For the density of the Precambrian crustal units, typical lithotype-specific values, further constrained by seismic velocities (Mechie et al., 1983), were compared and adapted to densities or density contrasts obtained by gravity modelling in adjacent regions (Jacoby et al., 1983; Edel and Schulmann, 2009). For the lithospheric mantle, a density of 3.3 × 10^3 kg m^{-3} was assumed (Kukkonen and Peltonen, 1999; Norden et al., 2008).

4.1 Thermal boundaries

The upper boundary condition for thermal modelling is the annual surface T that generally ranges from 7.5 to 8 °C in the Ardennes and from 8 to 8.5 °C in the Guttland (Haenel et al., 1980; www.asta.etat.lu) and in areas of the TLB. Average surface T is lowest on the plateau of the Ardennes (7 °C) and highest in the Mosel valley (11 °C). The surface T is influenced by the topography, which varies by about 500 m along the cross sections A and B.

For modelling, the conceptual cross sections (Figs. 4 and 5) were extended horizontally by 50 km in order to reduce boundary effects on the calculated temperatures. Heat flow through the lateral boundaries is set to zero, thereby excluding any horizontal heat transfer. The lower boundary of the models (the thermal LAB) is defined by the 1300 °C isotherm (McKenzie and Bickle, 1988; Turcotte and Schubert, 2002). Different, geophysically constrained depth scenarios for the thermal LAB (80 km, 100 km, 130 km) were tested for validation by comparing the modelled with the measured q_s at the Mersch borehole (see Section 5).

Table 7: Petrophysical parameters for the crust and the lithospheric mantle used in the lithosphere thermal modeling.

Polygons in section			Age	Description	Major rock type(s)	V_P	λ ± 1s	λ corr.		H	d
A	B	C				[km s^{-1}]	[W m^{-1} K^{-1}]	T	p	[µW m^{-3}]	[10^3 kg m^{-3}]
1	1, 2	1	Mesozoic	Jurassic – Triassic	Clay-/marlstone + limestone + sandstone + dolomite	/	2.5 ± 0.2	8	–	/	2.39
2	3		Permian	Rotliegend	Claystone + siltstone + sandstone + conglomerate	/	3.1	8	–	1.2	2.40
3, 4	4		Devonian (Eifel + Hunsrück)	Emsian – Upper Siegenian	Shale (+ slate) + siltstone + sandstone	2.6–5.6	3.4 ± 0.2	8	–	1.8	2.69
5	5, 6			Middle Siegenian	Sandstone (quartzite)		5.0 ± 0.5	8	–	0.6	2.66
6, 7	7, 8			Lower Siegenian – Lochkovian	Sandstone (quartzite) + siltstone + shale		3.9 ± 0.1	8	–	1.7	2.69
8	9	2	Devonian (Ardennes)	Emsian + Siegenian	Shale (+ slate) + sandstone		3.2 ± 0.2	8	–	1.8	2.68
9, 10	10, 11	3		Lochkovian	Sandstone + siltstone + shale		3.5 ± 0.1	8	–	1.7	2.64
11–15	12–15	4	Ordovician	Salm group	Slate/phyllite	6.1–6.35	3.1 ± 0.1	8	–	1.9	2.77
16–20	16–20	5	Upper + Middle Cambrian	Revin group	Slate/phyllite + quartzite		4.0 ± 0.1	8	–	2.0	2.73
21, 22	21, 22	6	Lower Cambrian	Deville group	Slate/phyllite + quartzite		4.3 ± 0.2	8	–	1.2	2.69
23	23	7	Neoproterozoic	Crystalline upper crust	Mica schist + gneiss	6.1–6.2	2.8	6	+	1.3	2.75
24	24	8		Middle crust	Tonalite + diorite + granodiorite	6.5–6.7	2.4	6	+	0.8	2.85
25	25	9		Lower crust	Hornblendite + pyroxenite	> 6.9	3.2	2	+	0.05	3.05
26	26	10		Lithospheric mantle	Lherzolite + harzburgite	8.0–8.5	4.2	4	+	0.02	3.30

Columns A, B and C refer to the corresponding cross sections with the polygon numbering as in Fig. 4 (A and B) and Fig. 5 (C). V_P = seismic velocity, λ = thermal conductivity at laboratory conditions (25 °C, atmospheric pressure), σ = standard deviation, λ corr. = correction of thermal conductivity for a temperature (T) and a pressure (p), H = radiogenic heat production, d = density. Numbers for T-correction (Eq. (13) and (14)) refer to specific categories by Seipold (2001) implemented in the used modeling algorithm: 2 mafic granulite, 4 peridotite and 6 gneiss. Category 8 refers to sediments to which a combination (Eq. (10)) of T-correction (Eq. (11)) after Somerton (1992) and p-correction (Eq. (12)) after Fuchs and Förster (2014) was applied. Pressure correction (Eq. (15)) was applied to the units marked by '+' according to Seipold (2001).

In addition to varying the LAB depth, the steady-state thermal effect of an uprised asthenospheric mantle, the Eifel plume (Budweg et al., 2006; Goes et al., 2000a; Seiberlich et al., 2013; Raikes, 1980; Raikes and Bonjer, 1983; Ritter, 2007), was modelled. Given the uncertainties with regard to the top of the plume, three scenarios were considered in the

thermal modelling for the easternmost part of cross section C: Top of plume at 60 km depth (e.g., Budweg et al., 2006), 50 km (Ritter, 2007; and references therein) or 40 km (Seiberlich et al., 2013). The transition from normal (100-km-thick) to thinned, plume-affected lithosphere apparently spans over 25–30 km and is located underneath northeastern Luxembourg and the eastern border of Belgium (Keyser et al., 2002; Walker et al., 2005).

4.2 Structure, composition and thermal properties of the lithosphere

Figs. 4 and 5 show the conceptual models with the polygons considered in the modelling. In Fig. 4, the models are shown with a cut-off at 35 km depth. In Fig. 5, the full extent of the model beyond the crust–mantle boundary to a maximum depth of LAB scenarios (130 km) is shown. The crustal thickness along the models varies slightly between 33.5 km in the north (beneath the Ardennes) and 29.5 km in the northeast (beneath the western part of the Eifel region) (Ziegler and Dèzes, 2006, 2007). These values are close to those reported by Budweg et al. (2006) who provide values of about 32 km for the Ardennes and of 28 km for the Eifel region.

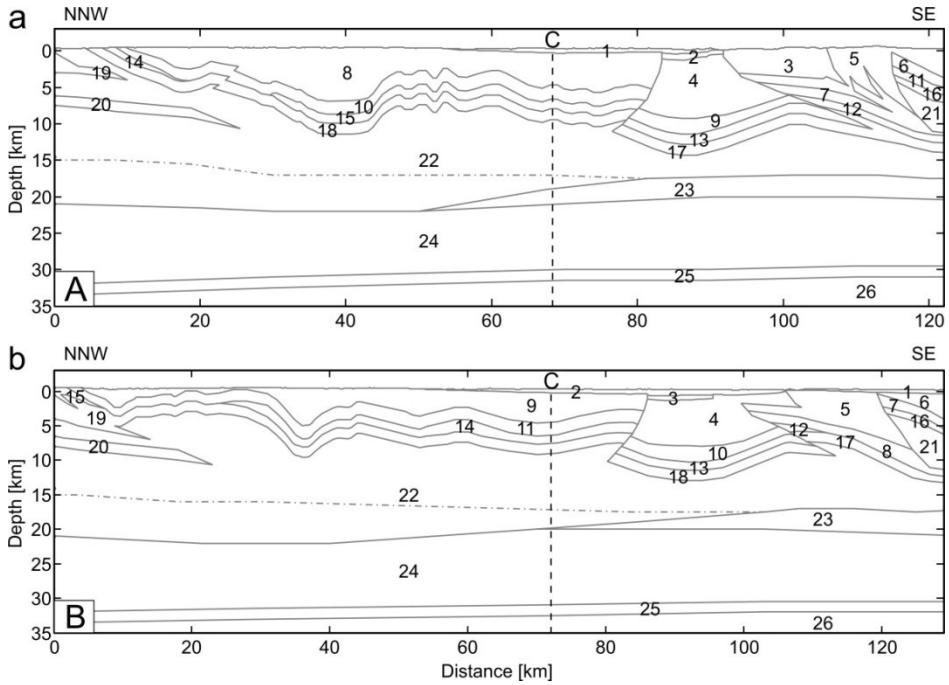

Fig. 4: Conceptual crustal models A and B (here cut off at 35 km depth) used in the thermal modelling. Vertical dashed lines indicate intersection with cross section C as shown in Fig. 2. Polygons marked with numbers denote units of different lithology and thermal properties (Table 7) extracted from the conceptual crustal cross sections shown in Fig. 2. The grey dash-dotted line marks a possible lateral extension of the gneiss in polygon 23.

The youngest unit of the crust is represented by the Mesozoic succession of the TLB (polygon 1, section A and C and polygons 1 and 2, section B, Figs. 4 and 5, Table 7). Modelling also considered a conceptual view according to which the central part of the TLB is underlain by a Permian graben (Schintgen and Förster, 2013), reflected in polygons 2 and 3 in sections A and B, respectively. The Lower Devonian succession is represented by polygons 3–10 (section A), 4–11 (section B) and polygon 2–3 (section C). Units of almost pure quartzite composition, even small, are delineated as single units owing to their exceptionally high TC values (polygon 5, section A, polygons 5 and 6, section B). The thick succession of parametamorphic Cambrian and Ordovician rocks (polygons 11–22, section A, 12–22, section B and 4–6, section C) has its base at about 22 km depth in the north, at 20 km in the southwest, at 17 km in the southeast, and at about 16 km in the northeast. In the latter two regions, i.e. underneath the Eifel and the Hunsrück, the succession is underlain by Proterozoic metasedimentary mica schist and gneiss (Mengel et al, 1991; attributed as crystalline upper crust in Table 7). The grey dash-dotted line within the crust (Figs. 4 and 5) indicates a possible lateral extension of the gneiss as a continuous and up to 6-km-thick layer. It replaces the lower part of Lower Cambrian metasediments below the dash-dotted line in Figs. 4 and 5 (extension of polygon 23, sections A and B and polygon 7, section C, respectively).

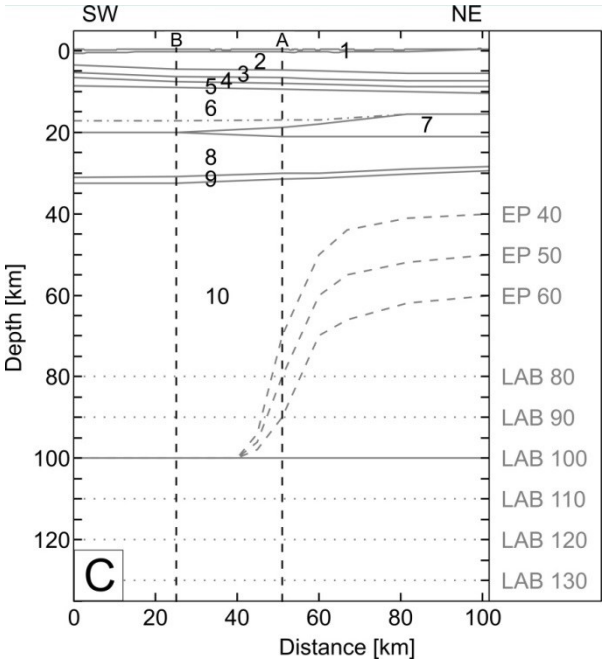

Fig. 5: Conceptual crustal model C used in the thermal modelling. Vertical dashed lines indicate intersection with cross sections A and B, respectively, as shown in Fig. 2. Polygons marked with numbers denote units of different lithology and thermal properties (Table 7). The dash-dotted line marks a possible lateral extension of the gneiss in polygon 7. Scenarios of variable LAB (lithosphere–asthenosphere boundary) depths are indicated as dotted lines. The location and variable depths of top of Eifel Plume (EP) are shown as dashed lines.

The middle crust (polygon 24, sections A and B and polygon 8, section C) encompasses the depth realm between approximately 19 and 30 km characterized by a seismic velocity of 6.5–6.7 km s^{-1} (Mechie et al., 1983). We interpret these velocities, which are typical of Palaeozoic middle crust, as representing metagranitoids (Rudnick and Fountain, 1995). Metaigneous gneiss xenoliths from the Eifel volcanic field support this assumption (Mengel et al., 1991; Stosch et al., 1991; and references therein). A relatively thin layer of pyroxenite and hornblendite (Voll, 1983; Mengel et al., 1991; Stosch et al., 1991) (polygon 25, sections A and B and polygon 9, section C) represents the lower crust. The present-day thin lower crust is the result of delamination in geological times, during which the crust lost more than 15 km of its original thickness (Wittenberg et al., 2000; Ziegler et al., 2004). The lithospheric mantle (polygon 26, sections A and B and polygon 10, section C) is likely made up of peridotite (spinel lherzolite and harzburgite) as indicated by xenoliths (Mengel et al., 1991; Shaw et al., 2005).

Thermal properties of the model units are compiled in Table 7. TC of the Mesozoic and Palaeozoic formations represents water-saturated conditions. The entire Mesozoic is represented by one TC value, which is the weighted average of TC measured perpendicular to bedding. For the isotropic Lower Devonian succession, mean TC values are assigned to model units. The TC values implemented for the Cambrian and Ordovician rocks refer to those measured perpendicular to cleavage. The TC of the crystalline upper crust, of the middle and lower crust, and of the lithospheric mantle was assigned based on literature TC data (Table 7; Norden et al., 2008; Schütz et al., 2014; and references therein). Details on thickness ranges of formations/stratigraphic units and error calculation used in the calculation of TC of model units are given in the Supplementary material (Appendix A).

Radiogenic heat production (H) data of Mesozoic and Palaeozoic rocks were implemented in the models as discussed in Section 3.2. Xenoliths data supported mica schist and gneiss as major constituents of the crystalline upper crust, the H of which averages to 1.3 μW m^{-3} (considering geochemical data of Stosch et al., 1991). This average is consistent with the H of the Wartenstein Gneiss determined in this study. Xenoliths of diverse types of metagranitoid (tonalite, diorite, granodiorite) studied by Stosch et al. (1991) suggest a value of 0.8 μW m^{-3} for the middle crust (Table 7). Data for the lower crust and lithospheric mantle were taken from different literature sources reporting consistently low H values (Förster and Förster, 2000; Förster et al., 2010; Furlong and Chapman, 2013; Hasterok and Chapman, 2011).

4.3 Modelling results

Fig. 6 shows heat-flow patterns resulting from the 2-D thermal modelling along the three cross sections. Values of q_s are retrieved from the model at 1 km depth, to omit topography-related heat-flow refraction at the surface. On average, the 1-km-depth value is only about 1.4–1.5 mW m^{-2} lower than the modelled mean q_s.

The uncertainty range of q_s determined at the Mersch borehole (75 ± 7 mW m^{-2}) did not permit to establish the LAB depth below Luxembourg with statistical significance (see Fig. 6). However, a LAB depth of ~100 km, compatible with the Mersch heat-flow mean, is coincident with the bulk of modern geophysical LAB-depth estimates (90–110 km) for the wider area of Luxembourg except for the adjoining Eifel region where the present-day lithosphere is considerably thinned (Geissler et al., 2010; Seiberlich et al., 2013; and references therein). The following discussion considers a 100 km LAB-depth as apparent best-fit scenario, but we are aware of the fact that the actual depth may as well be slightly shallower or greater.

Lithosphere scenarios without a mantle plume result in q_s patterns that are highly variable along cross sections A and B (Fig. 6a and b) and more gentle along section C (Fig. 6c). Particularly high values are implied for the Stavelot Massif in the NNW (80–85 mW m^{-2}) and the Hunsrück (90–92 mW m^{-2}) in the SE of the sections A and B. By contrast, the mantle heat flow (q_m) is largely homogeneous along all sections (~40 mW m^{-2}).

The thermal models predict isotherms for the crust that are more densely spaced in the middle and lower crust compared to the upper crust (the upper 20 km of the models) (Fig. 7a–c) reflecting different geothermal gradients caused by different values of TC. The central part of the study area appears slightly warmer in the upper 20 km compared to the northern and southern parts. Below 20 km, isotherms are evenly spaced and homogeneous. Moho temperatures along cross sections A and B range between 605–630 °C and 620–640 °C, respectively (Fig. 7a and b). Moho temperatures are inferred to decrease from ~650 °C to ~620 °C towards the northeast (Fig. 7c).

Modelling the conductive responses of a long-lived Eifel plume along cross section C would result in q_s values that are only slightly increased in the SW, but rise to ~90–110 mW m^{-2} in the NE depending on the different top Eifel plume scenarios considered (Fig. 6d). The corresponding q_m value would remain virtually unchanged in the SW but increase to ~55–77 mW m^{-2} in the NE. Plume-triggered steady-state Moho temperatures at assumed 60, 50 or 40 km plume depth would increase from 680 to 710 °C in the SW to 820–1070 °C at the

northeastern end of cross section C just above the plume (Fig. 7d).

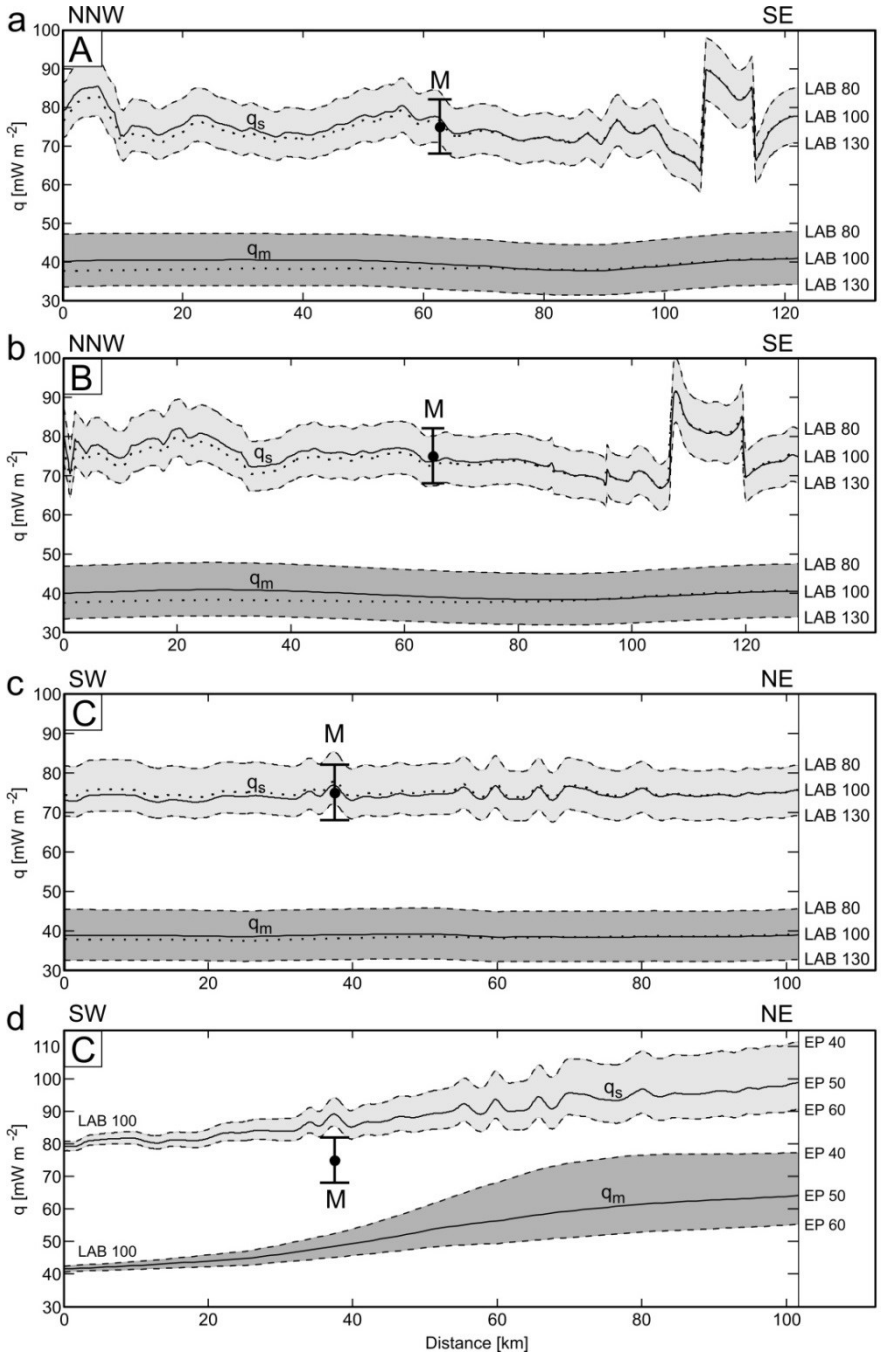

Fig. 6: (a–c) Modelled steady-state surface heat flow q_s (light grey zone) and mantle heat flow q_m (dark grey zone) according to three LAB-depth scenarios and (d) for the consideration of the Eifel plume (EP) at different depth. The q_s refers to 1 km depth below mean sea level to avoid heat refraction at the surface due to topography. This value is on average 1.4–1.5 mW m^{-2} lower than the q_s sensu stricto. The best-fit scenario of heat flow is indicated by a solid line. The dotted line in a–c shows the variation in q_s and q_m in case of a continuous gneiss layer (polygon 23 in cross sections A and B; polygon 7 in cross section C). The solid line (d) represents the scenario with the top of the Eifel plume at 50 km depth. Heat flow at the Mersch borehole location (denoted as M) with mean and standard deviation (2σ) is projected onto the sections.

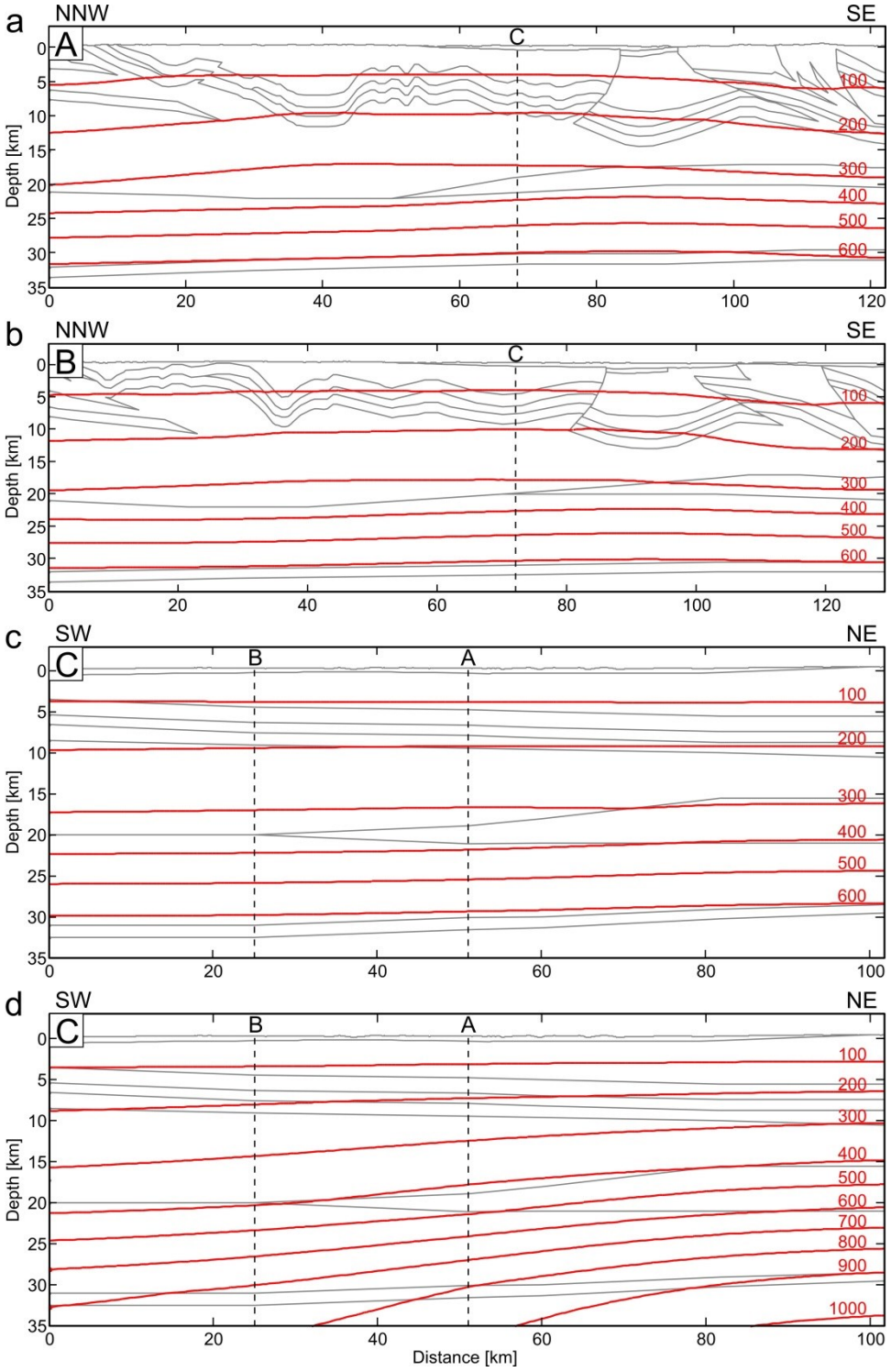

Fig. 7: (a–c) Modelled steady-state temperatures (in red and in °C) of sections A, B and C for the LAB-100-km-model; (d) Isotherms of cross section C for the top of the Eifel plume at 50 km depth.

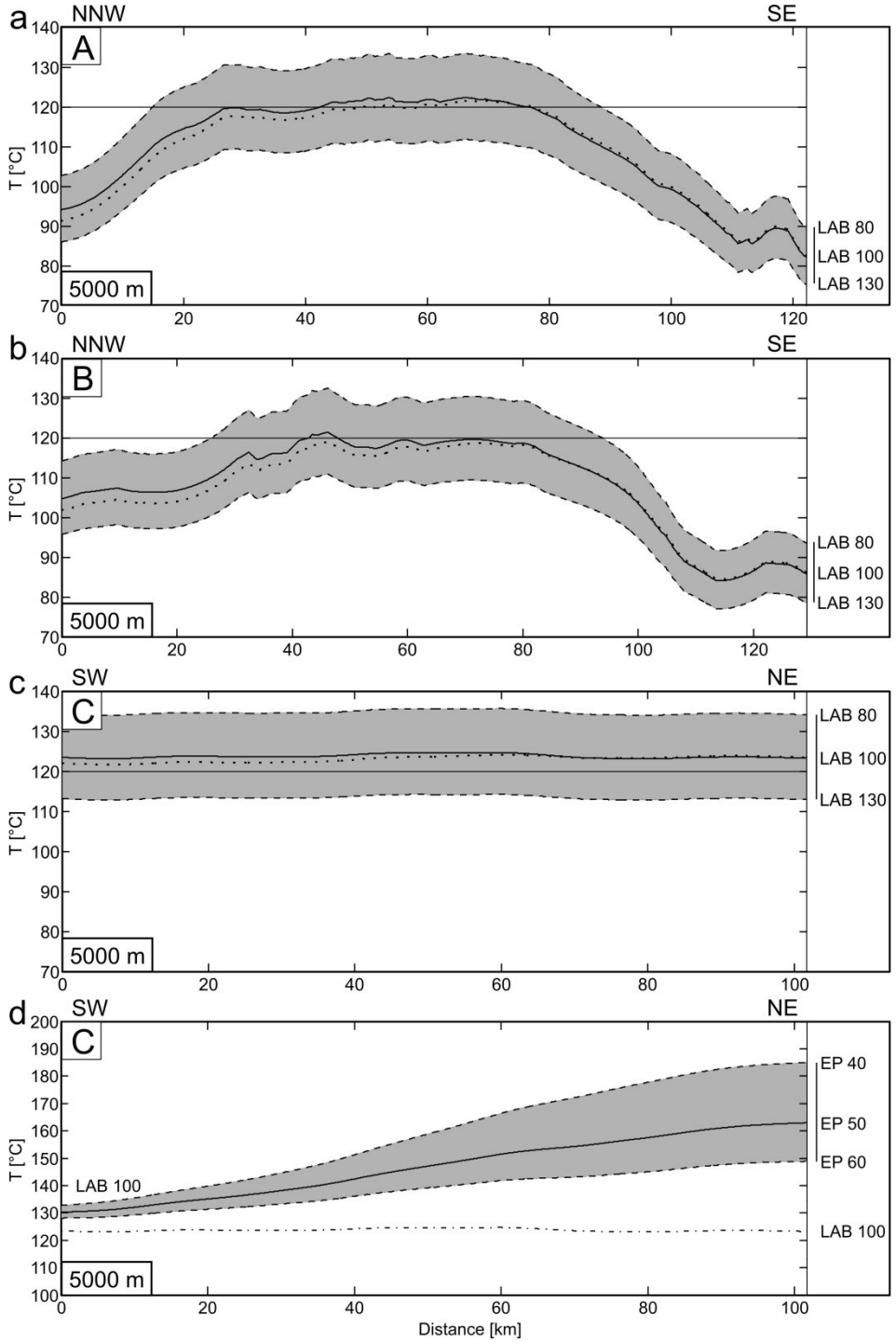

Fig. 8: (a–c) Modelled temperature at drillable depth of 5 km along cross sections A, B and C (dark grey zone) deduced from the LAB-100-km model (solid line) as well as from the LAB-80-km and LAB-130-km models (dashed lines). The 120 °C-isotherm is indicated by a solid line. The dotted line shows changes in T caused by a continuous gneiss layer (see Fig. 6). (d) Result for cross section C for a LAB at 100 km depth in the southwest and different Eifel plume (EP) scenarios at depths of 40, 50 and 60 km (see Fig. 5). A dash-dotted line is added for comparison with the LAB-100-km scenario in c.

For a borehole depth of 5 km, which may reflect a reasonable target depth for the development of deep geothermal energy applications, modelled temperatures are shown in Fig. 8a–c. In the central parts of cross section A (between 30 and 75 km; Fig. 8a) and B (between 40 and 85 km; Fig. 8b), the LAB-100-km-model predicts a temperature plateau with an average T of 120 °C, about 5 °C lower than predicted T in section C (Fig. 8c). The high temperatures result from the volume of shale-dominated Lower Devonian in the Ardennes (Emsian and Siegenian; $\lambda \approx 3.2$ W m^{-1} K^{-1}; Table 7) as well as in the Eifel and the Mosel Syncline (Emsian and Upper Siegenian; $\lambda \approx 3.4$ W m^{-1} K^{-1}; Table 7). Towards the Stavelot Massif in cross section A (0–30 km; Fig. 8a) and B (0–40 km; Fig. 8b) T is inferred to rapidly decrease to minimum values of 95–105 °C. These low temperatures are explained by a high TC of the quartzite-rich Cambrian rocks of the Stavelot Massif (Revin and Deville groups; λ >4 W m^{-1} K^{-1}; Table 7) in shallow position. Towards the Hunsrück region in cross section A (75–122 km; Fig. 8a) and B (85–127 km; Fig. 8b) T decreases to values of ~85 °C. Here, low temperatures are linked with the Middle Siegenian rocks (Taunusquarzit; $\lambda \approx 5$ W m^{-1} K^{-1}; Table 7) in shallow position. Compared to the LAB-100-km-model (Fig. 8a–c), variation of LAB depth (80 or 130 km) would result in temperatures that differ by only ~10 °C. In the steady-state Eifel-plume scenarios modelled in cross section C (Fig. 8d), T at 5 km would increase by about 40, 30 and 20 °C above the plume, resulting in absolute values of 165, 150 and 140 °C in the German–Luxembourgish border region (60 km).

5 Discussion

5.1 Surface heat flow and crustal temperature patterns

This paper presents the first subsurface T prognosis for the greater Luxembourg region based on steady-state 2-D thermal modelling. This prognosis benefitted from the determination of a reliable q_s value as well as from laboratory-measured TC and H data covering practically the entire Mesozoic–Palaeozoic succession.

The q_s value inferred from the Mersch borehole (75 ± 7 mW m^{-2}) and most values from neighbouring areas (64–85 mW m^{-2}) are higher than the average continental heat flow of 71 mW m^{-2} (Davies and Davies, 2010) and significantly exceed the average q_s value of 57–58 mW m^{-2} for Palaeozoic provinces (Jaupart and Mareschal, 2003). The q_s value of 75 ± 7 mW m^{-2} is consistent with a thermal model that shows the depth of the thermal LAB between 80 km and 130 km, with the mean value at the seismically favored 100 km depth (Geissler et al.,

2010; Jones et al., 2010). Given the properties of the crust and mantle in our conceptual models, the assumption of a lower q_s on the order of the Palaeozoic-province average (i.e., 60 mW m^{-2}) would require a LAB depth of 200 km, the upper end of lithospheric thickness range of Palaeozoic regions (150–200 km; Jaupart and Mareschal, 2003). Lithosphere thickness prior to Permo-Carboniferous delamination and thermal thinning is unknown but must have been higher than 100–120 km inferred for areas not affected by Cenozoic rifting (Ziegler et al., 2004; and references therein). Most of the granulitic base of the initially 45–60-km-thick crust is thought being removed shortly after the Variscan orogeny, which gave rise to the thin, extended crust imaged today (Christensen and Mooney, 1995; Wittenberg et al., 2000; Ziegler et al., 2004).

The variability of q_s modelled along the three cross sections (Fig. 6) is largely attributed to changes in the structure and composition of the crust in the uppermost 20 km. Thereby, changes in rock type, and therewith TC, exerted the major control on q_s, whereas the minor spread in H in the different model units imposed a negligible influence. The preferred LAB-100-km model results in q_m values of ~40 mW m^{-2} (Fig. 6), which coincide with values obtained for Palaeozoic extended crust in Europe (e.g., Balling, 1995; Norden et al., 2008). The crustal component of heat flow in our conceptual models is between 33 and 39 mW m^{-2} (Fig. 6a and b; cross sections A and B), with a mean of 36 mW m^{-2} (Fig. 6c; cross section C). These values, corresponding to an equivalent average crustal H of ~1.2 μW m^{-3}, are in the upper domain of bulk continental-crust averages (Rudnick et al., 1998).

As the deeper crustal structure and composition of the area are only incompletely known from geophysical surveys (e.g., seismics) and xenolith studies, it deemed valuable to test the sensitivity of the thermal models to slightly modified conceptual geological models. For example, the consideration of a continuous Precambrian gneiss layer (comparable H but λ = 2.8 instead of 4.3 W m^{-1} K^{-1}; Table 7) in cross section A (polygon 23; Fig. 4a) as an alternative to what is shown in Fig. 2 would negligibly affect the q_s and T patterns at 5 km depth (~–2.5 mW m^{-2} and –3 °C, respectively) and q_m (~–2.5 mW m^{-2}), but considerably affect the T pattern at the Moho (+40 °C). The same holds for varying the composition of the poorly known lowermost crust owing to the reduced thickness of this unit. In general, changes of parameters in the much less well known lower part of the crust (depth of ~15–30 km) have a relatively limited effect on the temperatures in the shallow subsurface (i.e., the upper 5 km).

Available borehole T-data as well as the modelled T from this study imply that the uppermost crust displays a rather normal T regime. Model temperatures between 120 °C and 125 °C at 5

km depth (Fig. 8) concur with T expectations resulting from large-scale extrapolation of T-data and published as subsurface temperature maps (Haenel et al., 1980; Hurter and Haenel, 2002). By comparison, model-T results of about 120 °C at 5 km depth are higher than temperatures of ~110 °C measured at similar depth in deep wells in the Ardennes in Belgium (Vandenberghe and Fock, 1989). Given the estimated uncertainty in our modelled T in the upper 5 km (<5 °C), the higher temperatures inferred for greater Luxembourg may be real and related to the larger thickness of thermally less conductive Lower Devonian shale/slate layers. The presence of these rock types also tends to hamper large-scale groundwater circulation and, therefore, provide shielding from the near-surface effects and a thermal blanketing. Temperature estimates as high as 150–155 °C at 5 km depth in the adjoining Lorraine region (Bonté et al., 2010) in the southern part of the study area are not supported by the results presented in this study (i.e., a maximum of 120–125 °C at 5 km depth; Fig. 8). In addition, borehole T-measurements in the Variscan Ardennes yielded temperatures of 110 °C at 5 km depth (Vandenberghe and Fock, 1987). The higher temperatures provided by Bonté et al. (2010) are obviously related to an extrapolation of the thermal gradient of about 30 °C km^{-1} from the Mesozoic sedimentary cover into the Variscan basement, for which borehole data are scarce. Our study suggests such a thermal gradient only in the 1000–1500-m-thick Mesozoic and for the Pre-Mesozoic basement a gradient of 20 °C km^{-1}, also supported by measured T in the Ardennes.

With regard to q_s, the large contrasts in TC, in particular in the shallow subsurface, triggered significant heat refraction, which is well demonstrated by regionally elevated q_s values, notably in the Stavelot Massif (~10 mW m^{-2}; Fig. 6a) and the Hunsrück (~10–15 mW m^{-2}; Fig. 6a and b). Our results strongly question the reliability of the low q_s value of 59 mW m^{-2}, reported by Vandenberghe (2002) for the Stavelot Massif, which was determined in the Cambrian section of the Grand-Halleux borehole. The low q_s inferred from this borehole could be readily explained by a disturbed T-profile, indicated by a high T of 22 °C at 25 m depth compared to a mean annual surface T of 7.5 °C (Legrand, 1975). The perturbation is in response to a long drilling process (>5 years) and a short shut-in time (47 h) when the borehole was T-logged. Because the well is not cased (Graulich, 1980), topography-driven groundwater flow in the fractured quartzitic rocks may have overprinted the heat flow. Those processes are common in elevated areas (Deming, 1994; Deming et al., 1992; Smith and Chapman, 1983) and, thus, also may apply for the Stavelot Massif. In order to validate the q_s value determined for Grand-Halleux, a 1-D temperature profile was calculated in a ‘top down’ approach by inversion of the Fourier equation of heat conduction. TC (2.6 W m^{-1} K^{-1} for slate

and 5.6 W m^{-1} K^{-1} for quartzite, this study) and H (1.94 μW m^{-3} for slate and 0.59 μW m^{-3} for quartzite) were measured on drill cores from the same borehole (this study). A mean annual surface T of 7.5 °C and an undisturbed T of 52.5 °C at 2250 m depth are assumed (Graulich, 1980). Using a detailed lithological profile and applying to the TC a T-correction after Somerton (1992) and a p-correction after Fuchs and Förster (2014), the q_s required to match the undisturbed T at depth and the surface T equals 79 mW m^{-2}. The inverted q_s supports the result of our 2-D thermal modelling for the Stavelot Massif (~80 mW m^{-2}).

5.2 Temperature impact of the Eifel plume

The occurrence of the active volcanic area in Western Europe and thus also the Eifel plume heating in the upper mantle is inferred from seismic anomalies (Goes et al., 1999, 2000a, 2000b; Goes and van der Lee, 2002; Cammarano et al., 2003; Hieronymus et al., 2007). The resultant temperature increase in the upper mantle under the Rhenish Massif is supposed being as high as 100–300 ± 100 °C (Goes et al., 2000b). In this paper, the top of the Eifel plume (supposedly between 60 and 50 km depth) is associated with an increase of mantle temperatures on the order of 325–400 °C, thus corroborating the results of seismological studies. The present-day lithosphere in the Eifel region is evidently in thermal disequilibrium. Veins containing hydrous minerals hosted by mantle xenoliths are characterized by minimum equilibration temperatures of 850–900 °C (Shaw et al., 2005). The minimum present-day T at the crust/mantle boundary underneath the Eifel region is ~850 °C, which would corroborate a thermal LAB depth slightly shallower than 60 km.

In a steady-state thermal scenario, the plume-top at 60 km depth would result in a q_s of 91 mW m^{-2} (this study) along the western margin of the Eifel (Fig. 6d), which is significantly higher than the range of measured q_s (65–80 mW m^{-2}). From this observation, it follows that the plume-related heat pulse has not yet reached (at least entirely) the surface. This is corroborated by a study of Goes et al. (2000b) showing that the time span of heat diffusion through the crust from a heated mantle at 50 km depth is about 20 Ma. If heating has started 10–20 Ma ago (Goes et al., 2000b), the heat flow in the near-surface parts of the crust would not yet be affected. A further verification of this open question of plume heating and heat diffusion cannot be made with the available data set of q_s values.

On the other hand, measured q_s may be afflicted with several problems which render the discussion above problematic. Available q_s values in the Eifel region were measured exclusively in shallow boreholes (<200 m) and lakes (<70 m) (Bram, 1979; Haenel, 1971,

1983) at a depth range where water movements in the Mesozoic aquifers and in the Lower Devonian succession may occur (e.g., Stober and Bucher, 2005), causing heat advection and eventually lowering of the conductive q_s value. As a consequence, the consideration and a quantification of possible advective processes (Manning and Ingebritsen, 1999; Smith and Chapman, 1983) cannot be made with the available data set of q_s values.

6 Conclusions

Numerical modelling of the thermal field strongly depends on the availability of reliable constraints and boundary conditions. The new surface heat flow of 75 ± 7 (2σ) mW m^{-2} determined for central Luxembourg represents a supplementary anchorpoint for verification of thermal models. A large database of measured thermal rock properties and values of thermal conductivity, radiogenic heat production and density are provided for virtually all geological formations exposed in the study area. These petrophysical properties represent substantial parameters for any type of thermal simulation. Our study underlines that surface heat flow determined in the shallow subsurface needs to be verified and corroborated by surface heat flow determined from high quality, continuous temperature logs in deep boreholes. Such recordings would shed light on the thermal regime as well as ongoing advective or convective processes linked to hydraulic conductivity in the Lower Devonian basement, in particular in the Eifel region. Considering the time lag of heat transfer of only several 10 Ma, another highly relevant but unresolved issue is the timing of the Eifel-plume emplacement relative to the onset of development of the ECRIS ~40 Ma ago. Our results show that the thermal effect caused by this heat pulse would be verifiable if already arrived at 5 km depth. The availability of suitable exploration data would lay the basis for quantification of various transient processes that may overprint purely steady-state conductive conditions.

Acknowledgements

This paper forms part of the doctoral thesis of TS entitled “The Geothermal Potential of Luxembourg”. The project is supported by the National Research Fund (Luxembourg) and the GFZ German Research Centre for Geosciences (Potsdam, Germany). The Geological Survey of Belgium is thanked for the possibility of sampling and measuring core material from the Grand-Halleux borehole. The Geological Survey of Luxembourg supported this work by granting access to their core-storage facility for sampling Mesozoic rock and by covering the costs for the geochemical analyses of whole-rock samples. The SEO (Société Electrique de l’Our) in Vianden (Luxembourg) and the “Amis de l’Ardoise” (Haut-Martelange, Luxembourg) are thanked for the opportunity of rock sampling in their premises. Constructive reviews by two anonymous reviewers helped to improve the manuscript and are gratefully acknowledged. H. Liep, M. Ospald and G. Arnold (GFZ) supported the sample preparation. C.-T. Rach, S. Kienast, C. Rudolph and M. Oldman (GFZ) are acknowledged for their assistance during TC measurements.

Appendix A. Supplementary data

Supplementary data associated with this article can be found, in the online version, at doi: 10.1016/j.geothermics.2015.03.007.

References

Balling, N. (1995). Heat flow and thermal structure of the lithosphere across the Baltic Shield and northern Tornquist Zone. Tectonophysics 244, 13–50.

Bless, M.J.M., Bouckaert, J., Camelbeeck, T., Dejonghe, L., Demoulin, A., Dupuis, C., Felder, P.J., Geukens, F., Gullentops, F., Hance, L., Jagt, J.W.M., Juvigné, E., Kramm, U., Ozer, A., Pissart, A., Robaszynski, F., Schumacker, R., Smolderen, A., Spaeth, G., Steemans, P, Streel, M., Vandenven, G., Vanguestaine, M., Walter, R., Wolf, M. (1990). The Stavelot Massif from Cambrian to Recent – a survey of the present state of knowledge. Ann. Soc. Géol. Belgique 113, 53–73.

Bonté, D., Guillou-Frottier, L., Garibaldi, C., Bourgine, B., Lopez, S., Bouchot, V., Lucazeau, F. (2010). Subsurface temperature maps in French sedimentary basins: new data compilation and interpolation. Bull. Soc. Géol. Fr. 181, 377–390.

Bourgeois, O., Ford, M., Diraison, M., Le Carlier de Veslud, C., Gerbault, M., Pik, R., Ruby, N., Bonnet, S. (2007). Separation of rifting and lithospheric folding signatures in the NW-Alpine foreland. Int. J. Earth Sci. 96, 1003–1031.

Bram, K. (1979). Heat flow measurements in the Federal Republic of Germany. In: Čermák, V., Rybach, L. (Eds.), Terrestrial Heat Flow in Europe. Springer, Berlin, Heidelberg, New York, NY, pp. 191–196.

Brigaud, F., Chapman, D.S., Le Douaran, S. (1990). Estimating thermal conductivity in sedimentary basins using lithological data and geophysical well logs. AAPG Bull. 74, 1459–1477.

Budweg, M., Bock, G., Weber, M. (2006). The Eifel Plume–imaged with converted seismic waves. Geophys. J. Int. 166, 579–589.

Bultynck, P., Dejonghe, L. (2001). Devonian lithostratigraphic units (Belgium). In: Bultynck, P., Dejonghe, L. (Eds.), Guide to a revised lithostratigraphic scale of Belgium. Geologica Belgica 4 (1–2). Brussels, pp. 39–69.

Cammarano, F., Goes, S., Vacher, P., Giardini, D. (2003). Inferring upper-mantle temperatures from seismic velocities. Phys. Earth Planet. Int. 138, 197–222.

Christensen, N.I., Mooney, W.D. (1995). Seismic velocity structure and composition of the continental crust: A global view. J. Geophys. Res. B100, 9761–9788.

Davies, J.H., Davies, D.R. (2010). Earth's surface heat flux. Solid Earth 1, 5–24.

Dejonghe, L. (2008). Carte géologique de Wallonie 1/25.000, feuille 55/5-6 Hotton–Dochamps. Notice explicative. Région Wallonne, Namur, 88 pp.

DEKORP Research Group (1991). Results of the DEKORP 1 (BELCORP-DEKORP) deep seismic reflection studies in the western part of the Rhenish Massif. Geophys. J. Int. 106, 203–227.

Deming, D. (1994). Fluid flow and heat transport in the upper continental crust. In: Parnell, J. (Ed.), Geofluids: Origin, Migration and Evolution of Fluids in Sedimentary Basins, Spec. Publ. 78. Geol. Soc., London, pp. 27–42.

Deming, D., Sass, J.H., Lachenbruch, A.H., De Rito, R.F. (1992). Heat flow and subsurface temperature as evidence for basin-scale ground-water flow, North Slope of Alaska. Geol. Soc. Am. Bull. 104, 528–542.

Demoulin, A., Hallot, E. (2009). Shape and amount of the Quaternary uplift of the western Rhenish shield and the Ardennes (western Europe). Tectonophysics 474, 696–708.

Downes, H. (1993). The nature of the lower continental crust of Europe: petrological and geochemical evidence from xenoliths. Phys. Earth Planet. Int. 79, 195–218.

Edel, J.-B., Schulmann, K (2009). Geophysical constraints and model of the „Saxothuringian and Rhenohercynian subductions – magmatic arc system" in NE France and SW Germany. Bull. Soc. Géol. Fr. 180, 545–558.

Fielitz, W., Mansy, J.-L. (1999). Pre- and synorogenic burial metamorphism in the Ardenne and neighbouring areas (Rhenohercynian zone, central European Variscides). Tectonophysics 309, 227–256.

Förster, A., Förster, H.-J. (2000). Crustal composition and mantle heat flow: Implications from surface heat flow and radiogenic heat production in the Variscan Erzgebirge (Germany). J. Geophys. Res. B 105, 27917–27938.

Förster, H.-J., Förster, A., Oberhänsli, R., Stromeyer, D. (2010). Lithospheric composition and thermal structure of the Arabian Shield in Jordan. Tectonophysics 481, 29–37.

Fuchs, S., Förster, A. (2014). Well-log based prediction of thermal conductivity of sedimentary successions: a case study from the North German Basin. Geophys. J. Int., 196, 291–311.

Fuchs, S., Schütz, F., Förster, H.-J., Förster, A. (2013). Evaluation of common mixing models for calculating bulk thermal conductivity of sedimentary rocks: Correction charts and new conversion equations. Geothermics 47, 40–52.

Furlong, K.P., Chapman, D.S. (2013). Heat flow, heat generation, and the thermal state of the lithosphere. Ann. Rev. Earth Planet. Sci. 41, 385–410.

Furtak, H., 1965. Die Tektonik der underdevonischen Gesteinsfolge im deutsch–belgisch–luxemburgischen Grenzgebiet. Geol. Mitt. 4, 273–332.

Geissler, W.H., Sodoudi, F., Kind, R. (2010). Thickness of the central and eastern European lithosphere as seen by S receiver functions. Geophys. J. Int. 181, 604–634.

Goes, S., van der Lee, S. (2002). Thermal structure of the North American uppermost mantle inferred from seismic tomography. J. Geophys. Res. B 107, 2050, http://dx.doi.org/10.1029/2000JB000049.

Goes, S., Spakman, W., Bijwaard, H. (1999). A lower mantle source for central European Volcanism. Science 286, 1928, http://dx.doi.org/10.1126/science.286.5446.1928.

Goes, S., Govers, R., Vacher, P. (2000a). Shallow mantle temperatures under Europe from P and S wave tomography. J. Geophys. Res. B105, 11153–11169.

Goes, S., Loohuis, J.J.P., Wortel, M.J.R., Govers, R. (2000b). The effect of plate stresses and shallow mantle temperatures on tectonics of northwestern Europe. Global Planet. Change 27, 23–38.

Graulich, J. M. (1980). Le sondage de Grand-Halleux. In: Professional Paper 175, Administration des Mines. Service géologique de Belgique, Brussels, 78 pp.

Hasterok, D., Chapman, D.S (2011). Heat production and geotherms for the continental lithosphere. Earth Planet. Sci. Lett. 307, 59–70.

Haenel, R. (1971). Heat flow measurements and a first heat flow map of Germany. Z. Geophys. 37, 975–992.

Haenel, R. (1983). Geothermal investigations in the Rhenish Massif. In: Fuchs, K., von Gehlen, K., Mälzer, H., Murawski, H., Semmel, A. (Eds.), Plateau Uplift: The Rhenish Shield – A Case History. Springer, Berlin, Heidelberg, New York, Tokyo, pp. 228–246.

Haenel, R., Legrand, R., Balling, N., Saxov, S., Bram, K., Gable, R., Meunier, J., Fanelli, M., Rossi, A., Salomone, M., Taffi, L., Prins, S., Burley, A.J., Edmunds, W.M., Oxburgh, E.R., Richardson, S.W., Wheildon, J. (1980), Atlas of Subsurface Temperatures in the European Community. Publ. No. EUR 6578 EN of the Commission of the European Communities, Directorate-General Telecommunication, Information Industries and Innovation, Luxembourg, 36 pp.

Häfner, F., Kött, A., Spindeldreher, J., Rein, B., Grubert, A. (2007). Nutzung von oberflächennaher Erdwärme für die Gebäudeheizung in Rheinland-Pfalz. Landesamt für Geologie und Bergbau Rheinland-Pfalz, Mainz, 97 pp., unpublished report.

Hieronymus, C.F., Shomali, Z.H., Pedersen, L.B. (2007). A dynamical model for generating sharp seismic velocity contrasts underneath continents: Application to the Sorgenfrei–Tornquist Zone. Earth Planet. Sci. Lett. 262, 77–91.

Hollmann, E.G. (1997). Der variszische Vorlandüberschiebungsgürtel der Ostbelgischen Ardennen – Ein bilanziertes Modell. Aachener Geowiss. Beitr. 25, 235 pp.

Hückel, B., Kappelmeyer, O. (1966). Geothermische Untersuchungen im Saarkarbon. Z. Dt. Geol. Ges. 117 (1), 280–311.

Hurter, S., Haenel (2002). Atlas of Geothermal Resources in Europe. Publ. No. EUR 17811 of the European Commission, Office for Official Publ. of the European Communities, Luxembourg, 91 pp.

Jacoby, W.R., Joachimi, H, Gerstenecker, C (1983). The gravity field in the Rhenish Massif, in: Fuchs, K., von Gehlen, K., Mälzer, H., Murawski, H., Semmel, A. (Eds.), Plateau Uplift: The Rhenish Shield – A case history. Springer, Berlin, Heidelberg, New York, Tokyo, pp. 247–258.

Jaupart, C., Mareschal, J.-C. (2003). Constraints on crustal heat production from heat flow data. Treatise on Geochem. 3, 65–84.

Jones, A.G., Plomerova, J., Korja, T., Sodoudi, F., Spakman, W. (2010). Europe from the bottom up: A statistical examination of the central and northern European lithosphere-asthenosphere boundary from comparing seismological and electromagnetic observations. Lithos 120, 14–29.

Keyser, M., Ritter, J.R.R., Jordan, M. (2002). 3D shear-wave velocity structure of the Eifel plume, Germany. Earth Planet. Sci. Lett. 203, 59–82.

Kölschbach, K.-H. (1986). Eine nach SE gerichtete Aufschiebung auf der NW-Flanke der Moselmulde (Liesertal, SW-Eifel). N. Jb. Geol. Paläont., Mh., 671–680.

Konrad, H.J., Wachsmut, W. (1973). Zur Lithologie und Tektonik des Unterdevons im südlichen Oesling Luxemburgs. Publ. Serv. Géol. Luxemb. 5, 1–20.

Kukkonen, I.T., Peltonen, P. (1999). Xenolith-controlled geotherm for the central Fennoscandian Shield: implications for lithosphere–asthenosphere relations. Tectonophysics 304, 301–315.

Legrand, R. (1975). Jalons géothermiques. Mém. Expl. Cartes Géol. et Minières de la Belgique, vol. 16. Service géologique de Belgique, Brussels, 46 pp.

LGB (Landesamt für Geologie und Bergbau Rheinland-Pfalz) (Ed.) (2005). Geologie von Rheinland-Pfalz. Schweizerbart, Stuttgart, 400 pp.

Lucius, M. (1950). Das Oesling – Erläuterungen zu der geologischen Spezialkarte Luxemburgs. Publ. Serv. Géol. Luxemb., vol. 6. Luxembourg, 174 pp.

Manning, C.E., Ingebritsen, S.E. (1999). Permeability of the continental crust: Implications of geothermal data and metamorphic systems. Rev. Geophys. 37, 127–150.

McKenzie, D., Bickle, M.J. (1988). The volume and composition of melt generated by extension of the lithosphere. J. Petrol. 29, 625–679.

Mechie, J., Prodehl, C., Fuchs, K. (1983). The Long-Range Seismic Refraction Experiment in the Rhenish Massif. In: Fuchs, K., von Gehlen, K., Mälzer, H., Murawski, H., Semmel, A. (Eds.), Plateau Uplift: The Rhenish Shield – A Case History. Springer, Berlin, Heidelberg, New York, Tokyo, pp. 260–275.

Meissner, R., Springer, M., Murawski, H, Bartelsen, H., Flüh, E.R., Dürschner, H. (1983). Combined seismic reflection-refraction investigations in the Rhenish Massif and their relation to recent tectonic movements. In: Fuchs, K., von Gehlen, K., Mälzer, H., Murawski, H., Semmel, A. (Eds.), Plateau Uplift: The Rhenish Shield – A Case History. Springer, Berlin, Heidelberg, New York, Tokyo, pp. 276–287.

Mengel, K., Sachs, P.M., Stosch, H.G., Wörner, G., Loock, G. (1991). Crustal xenoliths from Cenozoic volcanic fields of West Germany: Implications for structure and composition of the continental crust. Tectonophysics 195, 271–289.

Meyer, D.E., Nagel J. (2001). 4.20.3 Proterozoikum. In: Hoth, K., Leonhardt, D. (Eds.), Stratigraphie von Deutschland II – Ordovizium, Kambrium, Vendium, Riphäikum – Teil II: Baden-Württemberg, Bayern, Hessen, Rheinland-Pfalz, Nordthüringen, Sachsen-Anhalt, Brandenburg., vol. 234. Cour. Forsch.-Inst. Senckenberg, Frankfurt a.M, pp. 119–120 (Deutsche Stratigraphische Kommission).

Meyer, W. (1994). Geologie der Eifel, third edition. Schweizerbart (Nägele und Obermiller), Stuttgart, 618 pp.

Meyer, W., Stets, J. (1980). Zur Paläogeographie von Unter- und Mitteldevon im westlichen und zentralen Rheinischen Schiefergebirge. Z. Dt. Geol. Ges. 131, 725–751.

Meyer, W., Stets, J. (1996). Das Rheintal zwischen Bingen und Bonn. In: Sammlung geol. Führer 89. Borntraeger, Berlin, Stuttgart, 386 pp.

Mittmeyer, H.G. (2008). Unterdevon der Mittelrheinischen und Eifeler Typ-Gebiete (Teile von Eifel, Westerwald, Hunsrück und Taunus). In: Stratigraphie von Deutschland VIII,

Devon. Schriftenreihe Dt. Ges. Geowiss., vol. 52. Deutsche Stratigraphische Kommission, Hannover, pp. 139–203.

Mooney, W.D., Prodehl, C. (1978). Crustal structure of the Rhenish Massif and adjacent areas; a reinterpretation of existing seismic-refraction data. J. Geophys. 44, 573–601.

Murawski, H., Albers, H.J., Bender, P., Berners, H.-P., Dürr, St., Huckriede, R., Kauffmann, G., Kowalczyk, G., Meiburg, P., Müller, R., Muller, A., Ritzkowski, S., Schwab, K., Semmel, A., Stapf, K., Walter, R., Winter, K.-P., Zankl, H. (1983). Regional tectonic setting and geological structure of the Rhenish Massif. In: Fuchs, K., von Gehlen, K., Mälzer, H., Murawski, H., Semmel, A. (Eds.), Plateau Uplift: The Rhenish Shield – A Case History. Springer, Berlin, Heidelberg, New York, Tokyo, pp. 9–38.

Norden, B., Förster, A., Balling, N. (2008). Heat flow and lithospheric thermal regime in the Northeast German Basin. Tectonophysics 460, 215–229.

Oncken, O., von Winterfeld, C., Dittmar, U. (1999). Accretion of a rifted passive margin: The Late Palaeozoic Rhenohercynian fold and thrust belt (Middle European Variscides). Tectonics 18, 75–91.

Oncken, O., Plesch, A., Weber, J., Ricken, W., Schrader, S. (2000). Passive margin detachment during arc-continent collision (Central European Variscides). In: Franke, W., Haak, V., Oncken, O., Tanner, D. (Eds.), Orogenic processes: Quantification and Modelling in the Variscan Belt. Spec. Publ. 179, Geol. Soc., London, pp. 199–216.

Pharaoh, T.C. (1999). Palaeozoic terranes and their lithospheric boundaries within the Trans-European Suture Zone (TESZ): a review. Tectonophysics 314, 17–41.

Pharaoh, T.C., Winchester, J.A., Verniers, J., Lassen, A., Seghedi, A. (2006). The western accretionary margin of the East European Craton: an overview. In: Gee, D.G., Stephenson, R.A. (Eds.), European Lithosphere Dynamics, vol. 32. Mem. Geol. Soc. London, 291–311.

Popov, Y.A., Pribnow, D.F.C., Sass, J.H., Williams, C.F., Burkhardt, H. (1999). Characterization of rock thermal conductivity by high-resolution optical scanning. Geothermics 28, 253–276.

Powell, W.G., Chapman, D.S., Balling, N., Beck, A.E. (1988). Continental heat flow density. In: R. Haenel, L. Rybach, L. Stegena (Eds.), Handbook of Terrestrial Heat-Flow Density Determination. Kluwer Academic Press, Dordrecht, pp. 167–222.

Raikes, S. (1980). Teleseismic evidence for velocity heterogeneity beneath the Rhenish Massif. J. Geophys. 48, 80–83.

Raikes, S., Bonjer, K.-P. (1983). Large-scale mantle heterogeneity beneath the Rhenish Massif and its vicinity from teleseismic P-residuals measurements. In: Fuchs, K., von Gehlen, K., Mälzer, H., Murawski, H., Semmel, A. (Eds.), Plateau Uplift: The Rhenish Shield – A Case History. Springer, Berlin, Heidelberg, New York, Tokyo, pp. 315–331.

Ritter, J.R.R. (2007). The seismic signature of the Eifel Plume. In: Ritter, J.R.R., Christensen, U.R. (Eds.), Mantle Plumes. A Multidisciplinary Approach. Springer, Berlin, Heidelberg, pp. 379–404.

Rudnick, R.L., Fountain, D.M. (1995). Nature and composition of the continental crust: a lower crustal perspective. Rev. Geophys. 33, 267–309.

Rudnick, R.L., McDonough, W.F., O'Connell, R.J. (1998). Thermal structure, thickness and composition of continental lithosphere. Chem. Geol. 145, 395–411.

Rybach, L. (1976). Radioactive heat production; a physical property determined by the chemistry of rocks. In: Strens, R.G.J. (Ed.), The Physics and Chemistry of Minerals and Rocks. J. Wiley and Sons, London, New York, Sydney, pp. 309–318.

Rybach, L. (1988). Determination of heat production rate. In: R. Haenel, L. Rybach, L. Stegena (Eds.), Handbook of Terrestrial Heat-Flow Density Determination. Kluwer Academic Press, Dordrecht, pp. 125–142.

Schintgen, T., Förster, A. (2013). Geology and basin structure of the Trier–Luxembourg Basin – implications for the existence of a buried Rotliegend graben. Z. Dt. Ges. Geowiss. 164 (4), 615–637.

Schmincke, H.-J. (2007). The Quaternary volcanic fields of the east and west Eifel (Germany). In: Ritter, J.R.R., Christensen, U.R. (Eds.), Mantle Plumes. A Multidisciplinary Approach. Springer, Berlin, Heidelberg, pp. 241–322.

Schön, J.H. (1996). Physical properties of rocks: fundamentals and principles of petrophysics. In: Helbig, K., Teitel, S. (Eds.), Handbook of Geophysical Exploration, Section 8, Thermal Properties of Rocks. Pergamon, Oxford, UK, pp. 323–373.

Schütz, F., Förster, H.-J., Förster, A. (2014). Thermal conditions of the central Sinai Microplate inferred from new surface heat-flow values and continuous borehole temperature logging in central and southern Israel. J. Geodyn. 76, 8–24.

Seiberlich, C.K.A., Ritter, J.R.R., Wawerzinek, B. (2013). Topography of the lithosphere–asthenosphere boundary below the Upper Rhine Graben Rift and the volcanic Eifel region, Central Europe. Tectonophysics 603, 222–236.

Seipold, U. (2001). Der Wärmetransport in kristallinen Gesteinen unter den Bedingungen der kontinentalen Kruste. In: Scientific Technical Report STR 01/13. GeoForschungsZentrum Potsdam, Potsdam, 148 pp.

Shaw, C.S.J., Eyzaguirre, J., Fryer, B., Gagnon, J. (2005). Regional variations in the mineralogy of metasomatic assemblages in mantle xenoliths from the West Eifel Volcanic Field, Germany. J. Petrol. 46, 945–972.

Sintubin, M., Everaerts, M. (2002). A compressional wedge model for the lower Palaeozoic Anglo-Brabant Belt (Belgium) based on potential field data. In: Winchester, J.A., Pharaoh, T.C., Verniers, J. (Eds.), Palaeozoic Amalgamation of Central Europe, vol. 201. Geol. Soc., London, pp. 327–343.

Smith, L., Chapman, D.S. (1983). On the thermal effects of groundwater flow. J. Geophys. Res. B88, 593–608.

Somerton, W.H. (1992). Thermal Properties and Temperature Related Behaviour of Rock/Fluid Systems. In: Developments in Petroleum Sciences 37. Elsevier, Amsterdam, 256 pp.

Stets, J. (2004). Geologische Karte der Wittlicher Rotliegend-Senke 1:50000 mit Erläuterungen. Landesamt für Geologie und Bergbau Rheinland-Pfalz, Mainz, 82 pp.

Stets, J., Schäfer, A. (2002). Depositional environments in the Lower Devonian siliciclastics of the Rhenohercynian Basin (Rheinisches Schiefergebirge, W-Germany) – Case studies and a model. Contr. Sed. Geol. 22, 77 pp.

Stober, I., Bucher, K. (2005). The upper continental crust, an aquifer and its fluid: hydraulic and chemical data from 4 km depth in fractured crystalline basement rocks at the KTB test site. Geofluids 5, 8–19.

Stosch, H.-G., Schmucker, A., Reys, C. (1991). The nature and geological history of the deep crust under the Eifel, Germany. Terra Nova 4, 53–62.

Turcotte, D.L., Schubert, G. (2002). Geodynamics, second ed. Cambridge University Press, Cambridge, 456 pp.

Vandenberghe, N., Fock, W. (1989). Temperature data in the subsurface of Belgium. In: Čermák, V., Rybach, L., Decker, E.R. (Eds.), Heat Flow and Lithosphere Structure, vol. 164. Tectonophysics, pp 237–250.

Vandenberghe, N. (2002). Belgium. In: Hurter, S., Haenel, R., 2002 (Eds.), Atlas of Geothermal Resources in Europe. Publ. No. EUR 17811 of the European Commission, Office for Official Publ. of the European Communities, Luxembourg, pp. 23–24.

Vasseur, G. (1980). Some aspects of heat flow in France. In: Strub, A.S., Ungemach, P. (Eds.), Advances in European Geothermal Research, Second International Seminar on the Results of EC Geothermal Energy Research. Reidel Publ. Co., Dordrecht, pp. 170–175.

Verniers, J., Pharaoh, T., André, L., Debacker, T.N., De Vos, W., Everaerts, M., Herbosch, A., Samuelsson, J., Sintubin, M., Vecoli, M. (2002). The Cambrian to mid Devonian basin development and deformation history of Eastern Avalonia, east of the Midlands Microcraton: new data and a review. In: Winchester, J.A., Pharaoh, T.C., Verniers, J. 2002 (Eds.), Palaeozoic Amalgamation of Central Europe, Spec. Publ. 201. Geol. Soc., London, pp. 47–93.

Vilà, M., Fernández, M., Jiménez-Munt, I. (2010). Radiogenic heat production variability of some common lithological groups and its significance to lithospheric thermal modelling. Tectonophysics 490, 152–164.

Voll, G. (1983). Crustal xenoliths and their evidence for crustal structure underneath the Eifel volcanic district. In: Fuchs, K., von Gehlen, K., Mälzer, H., Murawski, H., Semmel, A. (Eds.), Plateau Uplift: The Rhenish Shield – A Case History. Springer, Berlin, Heidelberg, New York, Tokyo, pp. 336–342.

Wagner, H.W., Kremb-Wagner, F., Koziol, M., Negendank, J.F.W (2012). Trier und Umgebung, third edition. Gebr. Bornträger, Stuttgart, 396 pp.

Walker, K.T., Bokelmann, G.H.R., Klemperer, S.L., Bock, G. (2005). Shear-wave splitting around the Eifel hotspot: evidence for a mantle upwelling. Geophys. J. Int. 163, 962–980.

Wildberger, J. (1992). Zur tektonischen Entwicklung des südwestlichen Hunsrücks (SW-Deutschland). Mitt. Pollichia 79, 5–119.

Wittenberg, A., Vellmer, C., Kern, H., Mengel, K. (2000). The Variscan lower continental crust: evidence for crustal delamination from geochemical and petrophysical investigations. In: Franke, W., Haak, V., Oncken, O., Tanner, D. (Eds.), Orogenic Processes: Quantification and Modelling in the Variscan Belt, Spec. Publ. 179. Geol. Soc., London, pp. 401–414.

Wörner, G., Schminke, H.-U., Schreyer, W. (1982). Crustal xenoliths from the Quaternary Wehr volcano (East Eifel). Neues Jahrb. Miner. Abh. 144, 29–55.

Ziegler, P.A., Dèzes, P. (2006). Crustal evolution of Western and Central Europe. In: Gee, D.G., Stephenson, R.A. (Eds.), European Lithosphere Dynamics, vol. 32. Geol. Soc., London, Mem., pp. 43–56.

Ziegler, P.A., Dèzes, P. (2007). Cenozoic uplift of Variscan Massifs in the Alpine foreland: Timing and controlling mechanisms. Global Planet. Change 58, 237–269.

Ziegler, P.A., Schumacher, M.E., Dèzes, P., Van Wees, J.-D., Cloetingh, S. (2004). Post-Variscan evolution of the lithosphere in the Rhine Graben area: constraints from subsidence modelling. In: Wilson, M., Neumann, E.-R., Davies, G.R., Timmerman, M.J., Heeremans, M., Larsen, B.T. (Eds.), Permo-Carboniferous Magmatism and Rifting in Europe, Spec. Publ. 223. Geol. Soc., London, pp. 289–317.

Zitzmann, A., Grünig, S. (with contributions by Meyer, W., Stets, J., Mittmeyer, H.-G., Konrad, H.J., Ribbert, K.-H., Fuchs, G.) (1987). Geologische Übersichtskarte 1:200000, Blatt CC 6302 Trier. BGR (Bundesanstalt für Geowissenschaften und Rohstoffe), Hannover.

Supplementary material

Upscaling of thermal rock properties to geological formations

Thermal conductivity (TC) of samples was used to calculate TC of lithotypes. These TC values were transformed to formation TC by applying a weighted arithmetic mean based on the proportion of different lithotypes in each formation (Eq. (2); Section 3.1; Schintgen et al.; Tables A.9–A.13 detailed in Tables A.4–A.8). Subsequently, the formation TC values were upscaled to thermal-model units (see Section 4.2; Table 7) by applying a weighted arithmetic mean similar to Eq. (2) (see Section 3.1), but accounting for the proportion/thickness of each formation within the model unit.

For the Mesozoic series, formation TC is characterized by anisotropy related to stratification. Due to the subhorizontal bedding in the Mesozoic succession, the orientation of anisotropy is constant. Therefore, anisotropy was accounted for throughout the upscaling procedure from sample TC, lithotype TC, formation TC to the TC of the model unit. The resulting anisotropy is relatively small. The uncertainty of TC of each geological unit is addressed by an error estimate (1σ) in the range of 5–15% for the basin facies (Table A.12) and 15–20% for the margin facies (Table A.13). The uncertainty/error is based on the quality of the borehole data, the lateral and vertical geological heterogeneity and the contrast in thermal conductivity of the lithotypes. The limited number of samples used per formation precluded the calculation of standard deviations. In addition, the bulk density of each formation was calculated using the corresponding values for the samples used for formation TC determination (Tables A.9–A.13 detailed in Tables A.4–A.6, A.2 and A.3). Similarly, for the Mesozoic, the bulk-formation porosity was determined without uncertainty indication (Tables A.2 and A.3).

In addition to anisotropy, for the Mesozoic sedimentary formations, two distinct facies types were discriminated (Schintgen and Förster, 2013): (1) for a basin facies and (2) for a margin facies. However, lateral variations and, thus, the geological complexity are difficult to adequately account for. The proportion of the different lithotypes in the formations was evaluated using relevant borehole sections if available (generally the case in the TLB). The resulting TC perpendicular to bedding for the entire Jurassic is 2.3 ± 0.1 W m^{-1} K^{-1}. The result for the Triassic is 2.7 ± 0.2 W m^{-1} K^{-1} for the basin and 2.8 ± 0.2 W m^{-1} K^{-1} for the margin facies, respectively. The resulting TC parallel to bedding for the entire Jurassic is 2.6 ± 0.1 W m^{-1} K^{-1}. The result for the Triassic is 3.0 ± 0.2 W m^{-1} K^{-1} and identical for both the basin and margin facies. TC of the margin facies in the Triassic succession is only insignificantly higher and an important observation is the fact that water saturation generally

lowers the contrasts in TC resulting from a large porosity range and, thus, reduces the impact of laterally heterogeneous geology on the overall TC.

For the thick and lithologically more homogeneous but intensively structured (folded/thrust) Lower Palaeozoic and Lower Devonian succession, estimations of the lithological composition are based on geological maps and bulk descriptions from field studies (Bultynck and Dejonghe, 2001; Dejonghe, 2008; Häfner et al., 2007, unpublished report; LGB, 2005; Lucius, 1950; Verniers et al., 2001). It is assumed that the proportions of lithotypes in the individual formations remain relatively constant, which is acceptable according to recent knowledge but, most importantly, a necessary assumption and simplification for the thermal model. A summary of the bulk TC values of the various Palaeozoic formations (in part subdivided into formation members) is reported in Tables A.9–A.11.

The anisotropy of TC has been considered in the calculation of formation TC. For the Palaeozoic series, variation of formation TC as a function of orientation due to anisotropy generally is small. For orientation-dependent variations of TC related to bedding for lithotypes such as Palaeozoic sandstone, quartzite, siltstone and silty slate mean lithotype TC was calculated. The reason is that, despite a higher anisotropy of siltstone and silty slate, the orientation/bedding of those rocks in the folded Palaeozoic basement cannot be assessed. By contrast, cleavage is more constant (e.g., Lucius, 1950; Graulich, 1980). Therefore, for orientation-dependent variations of TC related to cleavage for lithotypes such as shale and slate, TC parallel and perpendicular to cleavage was considered separately. The resulting TC (Eq. (2)) of the Lower Devonian formations in the Ardennes (Table A.10) as well as in the Eifel and Mosel Syncline/Hunsrück (Table A.11) is largely isotropic. This observation also was made by Häfner et al. (2007). In fact, slate presenting a relatively high anisotropy is a minor lithotype in the Lower Devonian, and shale is virtually isotropic. For these formations, mean formation TC values calculated using the two orientation-dependent values are sufficient to characterize a formation. Exceptions are the Lower Palaeozoic formations showing at least a weak anisotropy of 1.1, with the highest value of 1.4 in the slate-rich formations (Table A.9). Anisotropy in the Cambrian and Ordovician (Table A.9) is due to cleavage, which is practically horizontal at depth as described in the Lower Cambrian section of the 3,225-m-deep Grand-Halleux borehole (Graulich, 1980; Hollmann, 1997).

Values of formation thickness considered for the calculation of weighted arithmetic mean TC are variable (Tables A.9–A.13). Thickness estimates for the Belgian Ardennes (Bultynck and Dejonghe, 2001; Dejonghe, 2008; Verniers et al., 2001) are, in general, lower than those known for the central parts of the Rhenohercynian basin in the Eifel region and the Mosel

Syncline (e.g., Meyer and Stets, 1996; Stets and Schäfer, 2002). Especially for the buried and barely explored Lower Devonian units in the Luxembourgish Ardennes and the adjoining Eifel region, the available thickness values constitute rough estimates. This also pertains to the structurally complex thrust sheets of the Hunsrück, for which correct thickness values are difficult to obtain and associated with large lateral variations (e.g., LGB, 2005; Wildberger, 1992). The values preferred in this study (Tables A.9–A.11) are the most conservative, minimum thickness estimates published in literature, considering that the sum of the individual estimates honors the bulk thickness estimates for the Lochkovian, Siegenian and Emsian (LGB, 2005; Meyer and Stets, 1980, 1996) and the total estimated thickness of the Lower Devonian (10,000 m; Stets and Schäfer, 2002). In addition, the extremely high local thicknesses reported in literature for the Gladbach-Schichten, Kaub-Schichten (Hunsrückschiefer) and Taunusquarzit were reduced to values adaptable to the region of Luxembourg. Relative thickness variations within the sediment pile barely influence the calculated weighted average.

Estimation of the uncertainty of formation TC is based on error propagation:

$$\sigma_{\lambda_{Fm}} = \lambda_{Fm} \sqrt{\sum_i^n \left(X_i \cdot \frac{\sigma_{\lambda_i}}{\lambda_i} \right)^2} \qquad \text{(a1)}$$

Where $\sigma_{\lambda_{Fm}}$ is the uncertainty of formation TC (in W m^{-1} K^{-1}), λ_{Fm} is the mean formation TC, X_i is the proportion of the different lithotypes within a formation and σ_{λ_i} is the standard deviation of TC λ_i of the different lithotypes. Uncertainties of formation TC were estimated by considering the standard deviations calculated for Palaeozoic formation TC. These uncertainties/errors frequently amount to 10–15% (Tables A.9–A.11) and depend on the homogeneity of the formation. Applying an error propagation law similar to Eq. (a1), the uncertainty (1σ) for a set of several formations generally is much smaller (i.e., 2–4%).

Appendix A. Supplementary data

Table A.1: Supplement to Table 2. Details on calculation of the relationship between measured thermal conductivities of dry and saturated Paleozoic samples.

Sample	Litho	O	λ_{dry}				λ_{sat}				$\lambda_{sat}/\lambda_{dry}$			TF			A		ϕ		
			⊥	//	a	b	AM	⊥	//	a	b	AM	⊥	//	a	b	$\mu_{1/2}$	AM	σ	Dry	Sat	[%]	$\mu_{1/2}$	AM
			[W m^{-1} K^{-1}]					[W m^{-1} K^{-1}]																
War-01	Gn	L		3.17	2.92	2.81	2.97		3.67	3.58	3.34	3.53		1.16	1.23	1.19	1.19	1.20	0.05	1.1	1.1	2.8	4.5	4.5
War-04	Gs	L	2.02		2.91	2.10	2.34	2.41		3.30	2.70	2.80	1.19		1.13	1.28				1.4	1.4	6.2		
Sg3a-2	Sl	S_1	2.37	2.68				2.57	2.88				1.08	1.07			1.24	1.23	0.11	1.1	1.1	2.5	2.6	3.1
Sg1-003	Sl	S_1	2.42	2.69				2.72	3.11				1.12	1.16						1.1	1.1	1.8		
COL-02	Sl	S_1	2.44	2.60				3.04	3.39				1.25	1.30						1.1	1.1	1.8		
PLA-01	Sl	S_1	2.26	2.67				2.86	3.28				1.26	1.23						1.2	1.1	2.6		
PLA-06	Sl	S_1	2.01	2.41				2.78	3.13				1.38	1.30						1.2	1.1	6.5		
VEN-04	Sl	S_1	1.97	2.60				2.28	2.97				1.16	1.14						1.3	1.3	2.9		
BEL-03	Sl	S_1	2.42	2.74				3.34	3.81				1.38	1.39						1.1	1.1	3.4		
Sg1-007	Ssl	S_0	3.20	3.40				4.19	4.34				1.31	1.28			1.16	1.19	0.08	1.1	1.0	3.8	2.7	2.7
BIH-04	Ssl	S_0	2.10	2.48				2.67	2.82				1.27	1.14						1.2	1.1	3.0		
BIH-06	Ssl	S_0	1.96	2.47				2.41	2.91				1.23	1.18						1.3	1.2	2.4		
MEU-03	Ssl	S_0	2.60	2.88				2.80	3.31				1.07	1.15						1.1	1.2	2.8		
LIE-04	Ssl	S_0	2.17	2.23				2.60	3.06				1.20	1.37						1.0	1.2	3.7		
SPA-02	Ssl	S_0	2.41	3.12				2.66	3.58				1.11	1.15						1.3	1.3	1.1		
GLE-03	Ssl	S_0	2.76	2.42				3.20	2.80				1.16	1.16						0.9	0.9	2.6		
WAN-08	Ssl	S_0	2.21	2.68				2.54	3.12				1.15	1.16						1.2	1.2	1.8		
E3-001	Sh	S_1	2.28	1.94				2.43	2.43				1.07	1.25			1.17	1.19	0.11	0.9	1.0	2.8	2.7	3.3
E1a-003	Sh	S_1	2.11	2.39				2.42	2.61				1.14	1.10						1.1	1.1	2.0		
E1a-004	Sh	S_1	2.52	2.53				2.73	2.69				1.08	1.06						1.0	1.0	2.1		
E1a-010	Sh	S_1	2.50	3.05				2.59	3.24				1.03	1.06						1.2	1.3	1.4		
Sg3-003	Sh	S_1	2.52	2.45				2.98	2.84				1.18	1.16						1.0	1.0	3.4		
Sg3-011	Sh	S_1	2.52	2.30				2.75	2.61				1.09	1.13						0.9	1.0	4.3		
VIL-05	Sh	S_1	2.05	2.28				2.63	3.15				1.28	1.38						1.1	1.2	8.0		
OIG-13	Sh	S_1	2.48	2.38				3.16	3.26				1.27	1.37						1.0	1.0	2.6		
FEP-07	Sh	S_1	2.42	2.60				3.11	3.28				1.29	1.26						1.1	1.1	3.4		
gd-02	Sh	S_1	3.16	3.29				4.08	4.23				1.29	1.28						1.0	1.0	2.6		

Litho – lithotype, Gn – Gneiss, Gs – mica schist, Sl – slate, Ssl – sandy slate, Sh – shale, Stst – siltstone, Sst – sandstone, Q – quartzite, O – sample orientation, L – foliation, S_1 – cleavage, S_0 – bedding, λ_{dry} and λ_{sat} – thermal conductivity in dry and saturated states, respectively, TF – transformation factor, A – anisotropy of thermal conductivity, ϕ – porosity, ⊥ and // – perpendicular and parallel to orientation, a and b – other oblique orientations, AM – arithmetic mean, $\mu_{1/2}$ – median value, σ – standard deviation.

Table A.1 continued

Sample	Litho	O	λ_{dry}					λ_{sat}					$\lambda_{sat}/\lambda_{dry}$				TF			A		ϕ		
			⊥	//	a	b	AM	⊥	//	a	b	AM	⊥	//	a	b	$\mu_{1/2}$	AM	σ	Dry	Sat		$\mu_{1/2}$	AM
			[W m^{-1} K^{-1}]					[W m^{-1} K^{-1}]														[%]		
E2-002	Stst	S_0	2.35	2.34				2.64	2.73				1.12	1.17			1.13	1.17	0.10	1.0	1.0	2.1	1.8	2.9
E2-007	Stst	S_0	2.84	3.15				3.49	3.45				1.23	1.10						1.1	1.0	1.6		
E1b-012	Stst	S_0	2.50	2.63				2.88	2.98				1.15	1.13						1.1	1.0	2.9		
STH-04	Stst	S_0	2.90	3.30				3.26	3.69				1.12	1.12						1.1	1.1	1.3		
OIG-01	Stst	S_0	2.64	2.75				3.54	3.85				1.34	1.40						1.0	1.1	8.1		
MEU-08	Stst	S_0	2.83	3.22				2.99	3.65				1.06	1.13						1.1	1.2	1.5		
E1b-008	Sst	S_0	3.19	3.47				3.78	3.95				1.19	1.14			1.15	1.17	0.10	1.1	1.0	2.0	2.0	2.1
E1a-011	Sst	S_0	4.08	4.39				4.61	5.28				1.13	1.20						1.1	1.1	0.4		
VIL-08	Sst	S_0	3.18	3.39				4.10	3.76				1.29	1.11						1.1	0.9	3.5		
STH-09	Sst	S_0	4.92	5.08				6.55	6.78				1.33	1.34						1.0	1.0	1.3		
FEP-02	Sst	S_0	4.59	4.77				5.57	5.25				1.21	1.10						1.0	0.9	1.6		
SPA-06	Sst	S_0	3.86	4.09				3.94	4.14				1.02	1.01						1.1	1.1	2.6		
SLW-08	Sst	S_0	3.69	3.98				4.27	4.59				1.16	1.15						1.1	1.1	3.1		
q-001	Q	S_0	3.73	3.99				5.62	5.38				1.50	1.35			1.37	1.38	0.09	1.1	1.0	12.7	6.0	6.4
WAN-06	Q	S_0	4.40	4.32				5.74	5.52				1.30	1.28						1.0	1.0	0.5		
HUR-12	Q	S_0	4.41	4.44				6.09	6.42				1.38	1.45						1.0	1.1	6.0		
GH835	Sl	S_1	2.49	2.51				2.56	2.55				1.03	1.01			1.03	1.04	0.04	1.0	1.0	0.6	0.3	0.4
GH2008	Sl	S_1	2.35	2.62				2.37	2.67				1.01	1.02						1.1	1.1	0.4		
GH2331	Sl	S_1	2.51	3.87				2.73	4.03				1.09	1.04						1.5	1.5	0.3		
GH2386	Sl	S_1	2.56	4.24				2.48	4.55				0.97	1.07						1.7	1.8	0.2		
GH2728	Sl	S_1	2.31	4.47				2.51	4.63				1.09	1.04						1.9	1.8	0.3		
GH350	Q	S_0	5.57	5.60				6.11	6.21				1.10	1.11			1.10	1.12	0.06	1.0	1.0	0.1	0.1	0.2
GH2021	Q	S_0	4.87	4.69				5.28	4.89				1.08	1.04						1.0	0.9	0.3		
GH2600	Q	S_0	5.06	5.15				6.01	6.10				1.19	1.18						1.0	1.0	0.1		

Litho – lithotype, Gn – Gneiss, Gs – mica schist, Sl – slate, Ssl – sandy slate, Sh – shale, Stst – siltstone, Sst – sandstone, Q – quartzite, O – sample orientation, L – foliation, S_1 – cleavage, S_0 – bedding, λ_{dry} and λ_{sat} – thermal conductivity in dry and saturated states, respectively, TF – transformation factor, A – anisotropy of thermal conductivity, ϕ – porosity, ⊥ and // – perpendicular and parallel to orientation, a and b – other oblique orientations, AM – arithmetic mean, $\mu_{1/2}$ – median value, σ – standard deviation.

Table A.2: Details on samples used to compose the density and porosity of the Mesozoic geological formations (basin facies) of the Trier–Luxembourg Basin.

						Density						Porosity		
						Sample		Litho.		Unit		Sample	Litho.	Unit
Strat. unit	Lithology	Vol.	Sample	Unit	Lithotype	Dry	Sat	Dry	Sat	Dry	Sat			
		[%]				[10^3 kg m^{-3}]						[%]		
dom4b	Sandy marlstone	100	Ru2	dom4b	Calcareous marlstone	2.35	2.48	2.35	2.48	2.35	2.48	13.4	13.4	13.4
dom4a	Limestone	80	Ru6	dom4a	Limestone	1.98	2.24	1.98	2.24	2.09	2.31	26.7	26.7	22.4
	Reef limestone (corals)	20	Ru4	dom4a	Limestone	2.55	2.60	2.55	2.60			5.3	5.3	
dom3	Sandy limestone	100	M9	dom3	Limestone	2.51	2.59	2.51	2.59	2.51	2.59	8.2	8.2	8.2
dom2	Limestone	70	M9	dom3	Limestone	2.51	2.59	2.51	2.59	2.50	2.59	8.2	8.2	8.4
	Marlstone	30	M8	dom1	Calcareous marlstone	2.47	2.60	2.47	2.60			8.9	8.9	
dom1	Marlstone	10	M8	dom1	Calcareous marlstone	2.47	2.60	2.47	2.60	2.10	2.26	8.9	8.9	15.7
	Marl	90	Bv4	lo4	Silty marl	2.06	2.22	2.06	2.22			16.5	16.5	
lo6-7 + dou	Iron-rich limestone + calcareous sandstone	50	M3	dou	Limestone	2.48	2.60	2.53	2.62	2.25	2.43	11.9	8.4	18.2
			M6	dou	Limestone	2.58	2.63					4.8		
	Iron-rich + marly sst.	50	M5	dou	Iron-rich limestone	1.97	2.25	1.97	2.25			28.1	28.1	
lo5	Marl	100	Bv4	lo4	Silty marl	2.06	2.22	2.06	2.22	2.06	2.22	16.5	16.5	16.5
lo4	Sandstone	50	Bv2	lo4	Marly siltstone	1.96	2.23	1.96	2.23	2.01	2.23	26.9	26.9	21.7
	Sandy marl	50	Bv4	lo4	Silty marl	2.06	2.22	2.06	2.22			16.5	16.5	
lo3	Marl	83	Bv11	lo3	Claystone	2.08	2.29	2.08	2.29	2.06	2.27	20.8	20.8	20.8
	Sandy marl	17	Bv12	lo3	Silty marl	1.96	2.17	1.96	2.17			20.6	20.6	
lo2	Marly claystone	100	Bv14	lo2	Claystone	2.11	2.32	2.12	2.31	2.12	2.31	20.9	19.5	19.5
			Bv16	lo1	Claystone	2.12	2.30					18.0		
lo1	Marly claystone	100	Bv14	lo2	Claystone	2.11	2.32	2.12	2.31	2.12	2.31	20.9	19.5	19.5
			Bv16	lo1	Claystone	2.12	2.30					18.0		
lm3b	Marly sandstone	19	Rb34	lm3a	Silty sandstone	2.45	2.55	2.45	2.55	2.09	2.27	9.7	9.7	16.7
	Sandy claystone	81	Rb40	lm3b	Clayey siltstone	2.01	2.20	2.01	2.20			18.4	18.4	
lm3a	Clayey sandstone	2	Rb34	lm3a	Silty sandstone	2.45	2.55	2.45	2.55	2.16	2.35	9.7	9.7	19.2
	Silty marl	98	Rb35	lm2	Marl	2.16	2.34	2.16	2.35			18.8	19.4	
			Rb36	lm2	Marl	2.15	2.35					19.9		

Strat. unit – stratigraphic unit, Vol. – volume fraction, Dry and Sat – dry and saturated conditions, respectively, Litho. – lithotype, sst. – sandstone, marlst. – marlstone, calc. – calcareous, fibr. – fibrous. Composition of individual units is estimated from different borehole sections located in the basin facies of the Trier–Luxembourg Basin.

Table A.2 continued

Strat. unit	Lithology	Vol. [%]	Sample	Unit	Lithotype	Density Sample Dry [10^3 kg m^{-3}]	Density Sample Sat [10^3 kg m^{-3}]	Density Litho. Dry [10^3 kg m^{-3}]	Density Litho. Sat [10^3 kg m^{-3}]	Density Unit Dry [10^3 kg m^{-3}]	Density Unit Sat [10^3 kg m^{-3}]	Porosity Sample [%]	Porosity Litho. [%]	Porosity Unit [%]
lm3	Clayey sandstone	11	Rb34	lm3a	Silty sandstone	2.45	2.55	2.45	2.55	2.14	2.32	9.7	9.7	18.0
	Silty marl	89	Rb35	lm2	Marl	2.16	2.34	2.11	2.30			18.8	19.0	
			Rb36	lm2	Marl	2.15	2.35					19.9		
			Rb40	lm3b	Clayey siltstone	2.01	2.20					18.4		
lm2	Clayey marl	100	Rb35	lm2	Marl	2.16	2.34	2.16	2.35	2.16	2.35	18.8	19.4	19.4
			Rb36	lm2	Marl	2.15	2.35					19.9		
lm1	Limestone	23	Rb39	li3	Marly limestone	2.62	2.66	2.62	2.66	2.26	2.42	3.8	3.8	15.8
	Marl	77	Rb35	lm2	Marl	2.16	2.34	2.16	2.35			18.8	19.4	
			Rb36	lm2	Marl	2.15	2.35					19.9		
li4	Clayey, silty marl	87	Rb38	li4	Marly siltstone	2.25	2.35	2.25	2.35	2.30	2.39	9.9	9.9	9.1
	Limestone	13	Rb39	li3	Marly limestone	2.62	2.66	2.62	2.66			3.8	3.8	
li3	Marlstone	59	Rw13	li1	Marlstone	2.31	2.38	2.31	2.38	2.44	2.49	6.7	6.7	5.5
	Limestone	41	Rb39	li3	Marly limestone	2.62	2.66	2.62	2.66			3.8	3.8	
li2	Sandstone	45	Rw10	li2	Sandstone	1.94	2.21	1.94	2.21	2.21	2.38	26.3	26.3	16.9
	Calcareous sandstone	55	Kb2	li2	Calcareous sandstone	2.43	2.53	2.43	2.52			9.5	9.2	
			Rw2	li2	Marly, calc. sandstone	2.42	2.51					8.9		
li1	Marlstone	46	Rw13	li1	Marlstone	2.31	2.38	2.31	2.38	2.35	2.43	6.7	6.7	7.5
	Sandy marlstone	30	Gr6	li1	Sandy marlstone	2.21	2.33	2.21	2.33			11.8	11.8	
	Limestone	24	Rb39	li3	Marly limestone	2.62	2.66	2.62	2.66			3.8	3.8	
ko	Clayey marl	25	Rb5	km3	Clayey marl	2.44	2.50	2.38	2.46	2.30	2.40	6.5	8.1	9.3
			Rb9	km2	Marl	2.32	2.42					9.6		
	Sandstone + conglomerate	33	Gr7	ko1	Marly sandstone	2.23	2.37	2.23	2.37			13.6	13.6	
	Claystone	42	Rw13	li1	Marlstone	2.31	2.38	2.31	2.38			6.7	6.7	
km3	Dolomitic marlstone	45	Gr11	km3	Dolomitic marlstone	2.29	2.41	2.29	2.41	2.39	2.47	11.5	11.5	7.9
	Marl	39	Rb5	km3	Clayey marl	2.44	2.50	2.44	2.50			6.5	6.5	
	Anhydrite + gypsum	11	Rb16	km3	Anhydrite + fibr. gypsum	2.41	2.41	2.41	2.41			0.8	0.8	
	Dolomite	5	Rb17	km1	Dolomite	2.82	2.83	2.82	2.83			1.1	1.1	

Table A.2 continued

Strat. unit	Lithology	Vol. [%]	Sample	Unit	Lithotype	Density Sample Dry [10^3 kg m^{-3}]	Density Sample Sat [10^3 kg m^{-3}]	Density Litho. Dry [10^3 kg m^{-3}]	Density Litho. Sat [10^3 kg m^{-3}]	Density Unit Dry [10^3 kg m^{-3}]	Density Unit Sat [10^3 kg m^{-3}]	Porosity Sample [%]	Porosity Litho. [%]	Porosity Unit [%]
km2	Clayey marl	89	Rb9	km2	Marl	2.32	2.42	2.32	2.42	2.34	2.43	9.6	9.6	8.8
	Gypsum	0	Rb16	km3	Anhydrite + fibr. gypsum	2.41	2.41	2.41	2.41			0.8	0.8	
	Sandstone	11	Rb8	km2	Dolomitic sandstone	2.52	2.55	2.52	2.55			2.5	2.5	
km2S	Sandstone	90	Ki5	km2S	Silty, micaceous sst.	1.85	2.15	1.85	2.15	1.90	2.18	30.1	30.1	28.1
	Claystone	10	Rb9	km2	Marl	2.32	2.42	2.32	2.42			9.6	9.6	
km1	Clayey marl	4	Wb1	km1	Clayey marl	2.15	2.32	2.15	2.32	2.32	2.43	16.8	16.8	10.9
	Marl	30	Rb13	km1	Silty marl	2.27	2.39	2.27	2.39			12.3	12.3	
	Sandstone	6	Rb10	km1	Dolomitic sandstone	2.42	2.50	2.42	2.50			8.5	8.5	
	Dolomitic marlstone	60	Wb7	ku	Silty, dolomitic marlstone	2.35	2.45	2.35	2.45			10.0	10.0	
ku	Dolomite	7	Rb17	km1	Dolomite	2.82	2.83	2.82	2.83	2.30	2.43	1.1	1.1	12.0
	Marl	39	Wb1	km1	Clayey marl	2.15	2.32	2.15	2.32			16.8	16.8	
	Marlstone	54	Wb7	ku	Silty, dolomitic marlstone	2.35	2.45	2.35	2.45			10.0	10.0	
mos	Dolomitic sandstone	100	Id1	mos	Dolomitic sandstone	2.60	2.66	2.60	2.66	2.60	2.66	6.4	6.4	6.4
mo2	Marlstone	5	Wb15	mm1	Marlstone	2.53	2.55	2.53	2.55	2.74	2.77	2.4	2.4	2.3
	Dolomite	23	Wb8	mo1	Dolomite	2.81	2.82	2.81	2.82			1.0	1.0	
			Wb12	mo1	Dolomite	2.81	2.81					0.9		
	Dolomitic siltstone/marlstone	13	Wb9	mo1	Dolomitic siltstone	2.55	2.63	2.62	2.68			7.5	5.9	
			Wb10	mo1	Dolomitic marlstone	2.69	2.73					4.3		
	Marly dolomite	59	Wb11	mo1	Marly dolomite	2.77	2.79	2.77	2.79			2.2	2.1	
			Wb13	mo1	Marly dolomite	2.76	2.78					2.0		
mo1	Marlstone	0	Wb15	mm1	Marlstone	2.53	2.55	2.53	2.55	2.78	2.80	2.4	2.4	1.6
	Dolomite	52	Wb8	mo1	Dolomite	2.81	2.82	2.81	2.82			1.0	1.0	
			Wb12	mo1	Dolomite	2.81	2.81					0.9		
	Dolomitic siltstone/marlstone	3	Wb9	mo1	Dolomitic siltstone	2.55	2.63	2.62	2.68			7.5	5.9	
			Wb10	mo1	Dolomitic marlstone	2.69	2.73					4.3		
	Marly dolomite	45	Wb11	mo1	Marly dolomite	2.77	2.79	2.77	2.79			2.2	2.1	
			Wb13	mo1	Marly dolomite	2.76	2.78					2.0		

Table A.2 continued

						Density						Porosity		
						Sample		Litho.		Unit		Sample	Litho.	Unit
Strat. unit	Lithology	Vol. [%]	Sample	Unit	Lithotype	Dry	Sat	Dry	Sat	Dry	Sat			
						[10^3 kg m^{-3}]						[%]		
mm2	Marlstone	67	Wb15	mm1	Marlstone	2.53	2.55	2.44	2.48	2.56	2.59	2.4	4.7	3.5
			Me2	mm1	Silty, dolomitic marlstone	2.39	2.45					5.7		
			Me6	mm1	Dolomitic marlstone	2.39	2.45					6.1		
	Dolomite	33	Wb8	mo1	Dolomite	2.81	2.82	2.81	2.82			1.0	1.0	
			Wb12	mo1	Dolomite	2.81	2.81					0.9		
mm1	Marl (gypsum-rich)	45	Me12	mm1	Silty marl	2.22	2.27	2.30	2.37	2.43	2.48	5.2	7.1	5.3
			Me13	mm1	Silty marl	2.36	2.44					7.9		
			Me14	mm1	Silty marl	2.39	2.47					8.6		
			Me15	mm1	Silty marl	2.24	2.31					6.7		
	Dolomitic marlstone	27	Me2	mm1	Silty, dolomitic marlstone	2.39	2.45	2.44	2.48			5.7	4.7	
			Me6	mm1	Dolomitic marlstone	2.39	2.45					6.1		
			Wb15	mm1	Marlstone	2.53	2.55					2.4		
	Dolomite	3	Wb8	mo1	Dolomite	2.81	2.82	2.81	2.82			1.0	1.0	
			Wb12	mo1	Dolomite	2.81	2.81					0.9		
	Sandstone	13	Me7	mm1	Silty sandstone	2.47	2.53	2.47	2.53			5.8	5.8	
	Anhydrite	12	Me8	mm1	Anhydrite	2.74	2.74	2.74	2.74			0.1	0.1	
mu2	Dolomite	20	Rd18	mu	Marly dolomite	2.66	2.69	2.66	2.69	2.46	2.54	3.1	3.1	7.6
	Marlstone	55	Rd17	mu	Dolomitic marlstone	2.43	2.51	2.43	2.51			7.3	7.3	
	Sandy marlstone	25	Rd14	mu	Dolomitic, sandy marlstone	2.37	2.49	2.37	2.49			11.7	11.7	
mu1	Dolomite	2	Rd18	mu	Marly dolomite	2.66	2.69	2.66	2.69	2.39	2.50	3.1	3.1	10.2
	Marlstone	31	Rd17	mu	Dolomitic marlstone	2.43	2.51	2.43	2.51			7.3	7.3	
	Sandy marlstone	67	Rd14	mu	Dolomitic, sandy marlst.	2.37	2.49	2.37	2.49			11.7	11.7	
so2	Sandstone	46	Rd1	so1	Dolomitic sandstone	2.20	2.38	2.18	2.36	2.23	2.38	17.9	18.7	15.0
			Rd4	so1	Dolomitic sandstone	2.15	2.34					19.5		
	Claystone	54	Rd12	so1	Silty claystone	2.27	2.39	2.27	2.39			11.9	11.9	
so1	Dolomitic sandstone	71	Rd1	so1	Dolomitic sandstone	2.20	2.38	2.18	2.36	2.20	2.37	17.9	18.7	16.7
			Rd4	so1	Dolomitic sandstone	2.15	2.34					19.5		
	Clayey sst./sandy claystone	29	Rd12	so1	Silty claystone	2.27	2.39	2.27	2.39			11.9	11.9	

Table A.2 continued

Strat. unit	Lithology	Vol.	Sample	Unit	Lithotype	Density						Porosity		
						Sample		Litho.		Unit		Sample	Litho.	Unit
						Dry	Sat	Dry	Sat	Dry	Sat			
		[%]				[10^3 kg m^{-3}]						[%]		
sm (+ su)	Sandstone	81	Bi2	sm	Sandstone (soft)	2.05	2.27	2.05	2.27	2.08	2.29	21.9	21.9	20.6
	Sandstone (conglomeratic)	12	Bi5	sm	Sandstone (coarse, gravel)	2.20	2.36	2.20	2.36			16.6	16.6	
	Claystone	7	Rd12	so1	Silty claystone	2.27	2.39	2.27	2.39			11.9	11.9	

Table A.3: Details on samples used to compose the density and porosity of Mesozoic geological formations (margin facies) of the Trier-Luxembourg Basin.

						Density						Porosity		
						Sample		Litho.		Unit		Sample	Litho.	Unit
Strat. unit	Lithology	Vol.	Sample	Unit	Lithotype	Dry	Sat	Dry	Sat	Dry	Sat			
		[%]				[10^3 kg m^{-3}]						[%]		
km2	Sandy marlstone	47	Rb12	km1	Sandy marlstone	2.38	2.45	2.34	2.43	2.34	2.43	6.7	9.7	9.8
+ km2S			Rb11	km1	Marly sandstone	2.35	2.41					6.3		
			El3	km1	Clayey sandstone	2.35	2.48					13.3		
	Sandy marl	35	Rb13	km1	Silty marl	2.27	2.39	2.27	2.39			12.3	12.3	
	Dolomitic sandstone	18	Rb10	km1	Dolomitic sandstone	2.42	2.50	2.47	2.53			8.5	5.5	
			Rb8	km2	Dolomitic sandstone	2.52	2.55					2.5		
km1	Sandy marlstone	51	Rb12	km1	Sandy marlstone	2.38	2.45	2.36	2.45	2.40	2.48	6.7	8.8	8.3
			Rb11	km1	Marly sandstone	2.35	2.41					6.3		
			El3	km1	Clayey sandstone	2.35	2.48					13.3		
	Conglomeratic dolomite	2	Rb17	km1	Dolomite (marly)	2.82	2.83	2.82	2.83			1.1	1.1	
	Dolomitic + sandy congl.	14	Rb19	km1	Sandy, dolomitic congl.	2.52	2.57	2.52	2.57			5.0	5.0	
	Marly sandstone	24	Rb10	km1	Dolomitic sandstone	2.42	2.50	2.42	2.50			8.5	8.5	
	Marl	9	Rb13	km1	Silty marl	2.27	2.39	2.27	2.39			12.3	12.3	
ku	Siltstone	21	Rb21	ku	Silty marlstone	2.44	2.51	2.44	2.51	2.39	2.49	7.3	7.3	9.7
	Marl + claystone	23	Ev1	ku	Sandy, dolomitic marlst.	2.30	2.45	2.26	2.43			14.9	16.9	
			Ev3	ku	Sandy, dolomitic marl	2.22	2.41					18.8		
	Sandstone	48	Rb12	km1	Sandy marlstone	2.38	2.45	2.36	2.45			6.7	8.8	
			Rb11	km1	Marly sandstone	2.35	2.41					6.3		
			El3	km1	Clayey sandstone	2.35	2.48					13.3		
	Sandy dolomite	8	Rb17	km1	Dolomite (marly)	2.82	2.83	2.82	2.83			1.1	1.1	

Strat. unit – stratigraphic unit, Vol. – volume fraction, Dry and Sat – dry and saturated conditions, respectively, Litho. – lithotype, congl. – conglomerate, marlst. – marlstone. Composition of individual units is estimated from different borehole sections located in the margin facies of the Trier–Luxembourg Basin.

Table A.3 continued

						Density						Porosity		
						Sample		Litho.		Unit		Sample	Litho.	Unit
Strat. unit	Lithology	Vol. [%]	Sample	Unit	Lithotype	Dry	Sat	Dry	Sat	Dry	Sat			
						[10^3 kg m^{-3}]						[%]		
mo(s)	Marly, sandy dolomite	24	Rb24	mo	Marly dolomite	2.69	2.72	2.69	2.72	2.50	2.59	3.1	3.1	9.4
(Rebierg +		15	Rb25	mo	Marly, sandy dolomite	2.79	2.80	2.79	2.80			1.0	1.0	
Everlange)	Dolomitic sandstone	23	Ev5	mo	Dolomitic sandstone	2.40	2.53	2.40	2.53			13.4	13.4	
		11	Id1	mos	Dolomitic sandstone	2.60	2.66	2.60	2.66			6.4	6.4	
	Sandstone + siltstone	11	Ev9	mg	Sandstone	1.98	2.24	1.98	2.24			26.9	26.9	
		6	Ev11	mg	Sandy siltstone	2.22	2.41	2.22	2.41			18.6	18.6	
		10	Me11	mm1	Silty sandstone	2.49	2.56	2.49	2.56			6.9	6.9	
mo(s)	Dolomitic sandstone	11	Id1	mos	Dolomitic sandstone	2.60	2.66	2.60	2.66	2.67	2.71	6.4	6.4	4.4
(Bissen +	Marlstone	5	Wb15	mm1	Marlstone	2.53	2.55	2.53	2.55			2.4	2.4	
Mersch)	Dolomite	19	Wb8	mo1	Dolomite	2.81	2.82	2.81	2.82			1.0	1.0	
			Wb12	mo1	Dolomite	2.81	2.81					0.9		
	Dolomitic siltstone/marlstone	54	Wb9	mo1	Dolomitic siltstone	2.55	2.63	2.62	2.68			7.5	5.9	
			Wb10	mo1	Dolomitic marlstone	2.69	2.73					4.3		
	Marly dolomite	11	Wb11	mo1	Marly dolomite	2.77	2.79	2.765	2.79			2.2	2.1	
			Wb13	mo1	Marly dolomite	2.76	2.78					2.0		
mg	Sandstone/conglomerate	27	Ev9	mg	Sandstone	1.98	2.24	1.98	2.24	2.24	2.38	26.9	26.9	13.5
(Rebierg +	Siltstone	11	Ev11	mg	Sandy siltstone	2.22	2.41	2.22	2.41			18.6	18.6	
Everlange)		12	Me11	mm1	Silty sandstone	2.49	2.56	2.49	2.56			6.9	6.9	
	Dolomite	4	Rd18	mu	Marly dolomite	2.66	2.69	2.66	2.69			3.1	3.1	
	Clay-/marlstone	46	Me12	mm1	Silty marl	2.22	2.27	2.30	2.37			5.2	7.1	
			Me13	mm1	Silty marl	2.36	2.44					7.9		
			Me14	mm1	Silty marl	2.39	2.47					8.6		
			Me15	mm1	Silty marl	2.24	2.31					6.7		

Table A.3 continued

Strat. unit	Lithology	Vol. [%]	Sample	Unit	Lithotype	Density Sample Dry [10^3 kg m^{-3}]	Density Sample Sat [10^3 kg m^{-3}]	Density Litho. Dry [10^3 kg m^{-3}]	Density Litho. Sat [10^3 kg m^{-3}]	Density Unit Dry [10^3 kg m^{-3}]	Density Unit Sat [10^3 kg m^{-3}]	Porosity Sample [%]	Porosity Litho. [%]	Porosity Unit [%]
mm	Marl (gypsum-rich)	70	Me12	mm1	Silty marl	2.22	2.27	2.30	2.37	2.37	2.43	5.2	7.1	6.3
(Mersch)			Me13	mm1	Silty marl	2.36	2.44					7.9		
			Me14	mm1	Silty marl	2.39	2.47					8.6		
			Me15	mm1	Silty marl	2.24	2.31					6.7		
	Dolomite	5	Wb8	mo1	Dolomite	2.81	2.82	2.81	2.82			1.0	1.0	
			Wb12	mo1	Dolomite	2.81	2.81					0.9		
	Dolomitic marlstone	21	Me2	mm1	Silty, dolomitic marlstone	2.39	2.45	2.42	2.48			5.7	5.9	
			Me6	mm1	Dolomitic marlstone	2.39	2.45					6.1		
			Me7	mm1	Silty sandstone	2.47	2.53					5.8		
	Anhydrite	4	Me8	mm1	Anhydrite	2.74	2.74	2.74	2.74			0.1	0.1	
mu	Sandy/marly dolomite	3	Rd18	mu	Marly dolomite	2.66	2.69	2.66	2.69	2.28	2.42	3.1	3.1	13.3
	Sandstone	6	Ev13	mu	Dolomitic sandstone	2.19	2.39	2.19	2.39			19.4	19.4	
	Sandy marlstone	3	Rd14	mu	Dolomitic, sandy marlst.	2.37	2.49	2.37	2.49			11.7	11.7	
	Dolomitic marlstone	11	Rd17	mu	Dolomitic marlstone	2.43	2.51	2.43	2.51			7.3	7.3	
	Claystone	51	Rd12	so1	Silty claystone	2.27	2.39	2.27	2.39			11.9	11.9	
	Siltstone	26	Ev11	mg	Sandy siltstone	2.22	2.41	2.22	2.41			18.6	18.6	
so2	Dolomitic sandstone	22	Rd1	so1	Dolomitic sandstone	2.20	2.38	2.18	2.36	2.22	2.36	17.9	18.7	14.5
			Rd4	so1	Dolomitic sandstone	2.15	2.34					19.5		
	Sandstone	24	Ev19	so	Marly sandstone	2.13	2.30	2.13	2.30			16.4	16.4	
	Claystone + (sandy) siltstone	54	Rd12	so1	Silty claystone	2.27	2.39	2.27	2.39			11.9	11.9	
so1	Conglomerate	25	Ev25	so	Sandy, dolomitic congl.	2.42	2.50	2.42	2.50	2.23	2.38	8.4	8.4	15.3
	Conglomeratic sandstone	43	Ev24	so	Sandstone (conglomeratic)	2.08	2.32	2.14	2.35			23.0	20.1	
			Rd1	so1	Sandstone (dolomitic)	2.20	2.38					17.9		
			Rd4	so1	Sandstone (dolomitic)	2.15	2.34					19.5		
	Marly sandstone	17	Ev19	so	Marly sandstone	2.13	2.30	2.13	2.30			16.4	16.4	
	Claystone + siltstone	15	Rd12	so1	Silty claystone	2.27	2.39	2.27	2.39			11.9	11.9	

Table A.4: Details on samples used to compose the petrophysical properties of the Cambrian and Ordovician groups, geological formations and their members in the Lower Paleozoic Stavelot Massif.

							λ_{dry}			Litho. λ_{dry}				Fm. λ_{dry}			TF	λ_{sat} calc.		Litho. λ_{sat}			Fm. λ_{sat}			Density		
Group	Fm.	Mbr.	Lithology	Vol.	Sample	Lithotype	O	⊥	//	⊥	//	AM	A	⊥	//	AM		⊥	//	⊥	//	AM	⊥	//	AM	Sample	Litho.	Fm.
				[%]				[W m^{-1}K^{-1}]																		[10^3 kg m^{-3}]		
SALM	BIH		Silty slate (includes slate 65% and minor sandstone 15 %)	100	BIH-01	Silty slate	S_0	1.88	2.34	2.0	2.4	2.2	1.2	2.0	2.4	2.2	1.18	2.22	2.76	2.3	2.8	2.6	2.3	2.8	2.6	2.78	2.78	2.78
					BIH-02	Silty slate	S_0	2.22	2.37								1.18	2.62	2.80							2.79		
					BIH-03	Silty slate	S_0	1.73	2.26								1.18	2.04	2.66							2.77		
					BIH-04	Silty slate	S_0	2.10	2.48								1.18	2.48	2.93							2.75		
					BIH-05	Silty slate	S_0	1.92	2.42								1.18	2.27	2.86							2.80		
					BIH-06	Silty slate	S_0	1.96	2.47								1.18	2.31	2.91							2.79		
	OTT	COL	Slate	100	COL-01	Slate	S_1	1.85	2.62	2.2	2.6	2.4	1.2	2.2	2.6	2.4	1.23	2.28	3.22	2.7	3.2	3.0	2.7	3.2	3.0	2.79	2.87	2.87
					COL-02	Slate	S_1	2.44	2.60								1.23	3.00	3.20							2.92		
					COL-04	Slate	S_1	2.41	2.88								1.23	2.96	3.54							2.90		
					COL-05	Slate	S_1	2.23	2.37								1.23	2.75	2.92							2.88		
		PLA	Slate	100	PLA-01	Slate	S_1	2.26	2.67	1.9	2.7	2.3	1.4	1.9	2.7	2.3	1.23	2.78	3.29	2.4	3.3	2.8	2.4	3.3	2.8	2.96	2.89	2.89
					PLA-02	Slate	S_1	2.04	3.67								1.23	2.51	4.51							2.90		
					PLA-06	Slate	S_1	2.01	2.41								1.23	2.47	2.96							2.86		
					PLA-07	Slate	S_1	1.48	1.85								1.23	1.82	2.28							2.84		
		MEU	Silty slate	90	MEU-01	Silty slate	S_0	2.00	2.46	2.4	2.8	2.6	1.2	2.4	2.9	2.6	1.18	2.36	2.90	2.8	3.4	3.1	2.9	3.4	3.1	2.94	2.92	2.91
					MEU-02	Silty slate	S_0	2.46	3.20								1.18	2.90	3.77							2.90		
					MEU-03	Silty slate	S_0	2.60	2.88								1.18	3.07	3.40							2.92		
			Sandstone	10	MEU-06	Sandstone	S_0	3.59	3.41	3.0	3.1	3.0	1.0				1.19	4.27	4.05	3.5	3.6	3.6				2.81	2.80	
					MEU-07	Siltstone	S_0	2.55	2.57								1.17	2.98	3.01							2.80		
					MEU-08	Siltstone	S_0	2.83	3.22								1.17	3.31	3.77							2.80		

Fm. – formation, Mbr. – Member, Vol. – volume fraction, λ_{dry} and λ_{sat} – thermal conductivity under dry and saturated conditions, respectively, Litho. – lithotype, O – orientation, S_0 and S_1 – bedding and cleavage, respectively, ⊥ and // – thermal conductivity perpendicular and parallel to orientation, AM – arithmetic mean, A – anisotropy, TF – transformation factor, sst. – sandstone. Lithological composition estimated after Geukens (2008) and Verniers et al. (2001).

Table A.4 continued

Group	Fm.	Mbr.	Lithology	Vol. [%]	Sample	Lithotype	λ_{dry} O	λ_{dry} ⊥ [W m^{-1}K^{-1}]	λ_{dry} // [W m^{-1}K^{-1}]	Litho. λ_{dry} ⊥ [W m^{-1}K^{-1}]	Litho. λ_{dry} // [W m^{-1}K^{-1}]	Litho. λ_{dry} AM [W m^{-1}K^{-1}]	Litho. λ_{dry} A [W m^{-1}K^{-1}]	Fm. λ_{dry} ⊥ [W m^{-1}K^{-1}]	Fm. λ_{dry} // [W m^{-1}K^{-1}]	Fm. λ_{dry} AM [W m^{-1}K^{-1}]	TF	λ_{sat} calc. ⊥ [W m^{-1}K^{-1}]	λ_{sat} calc. // [W m^{-1}K^{-1}]	Litho. λ_{sat} ⊥ [W m^{-1}K^{-1}]	Litho. λ_{sat} // [W m^{-1}K^{-1}]	Litho. λ_{sat} AM [W m^{-1}K^{-1}]	Fm. λ_{sat} ⊥ [W m^{-1}K^{-1}]	Fm. λ_{sat} // [W m^{-1}K^{-1}]	Fm. λ_{sat} AM [W m^{-1}K^{-1}]	Density Sample [10^3 kg m^{-3}]	Density Litho. [10^3 kg m^{-3}]	Density Fm. [10^3 kg m^{-3}]
	JAL	LIE	Silty slate	80	LIE-03	Silty slate	S_0	1.97	2.31	2.1	2.3	2.2	1.1	2.6	2.8	2.7	1.18	2.33	2.72	2.4	2.7	2.6	3.1	3.3	3.2	2.69	2.70	2.69
					LIE-04	Silty slate	S_0	2.17	2.23								1.18	2.56	2.63							2.70		
			Sandstone	20	LIE-01	Sandstone	S_0	4.68	4.79	4.7	4.8	4.7	1.0				1.19	5.57	5.70	5.6	5.7	5.6				2.68	2.68	
		SPA	Silty slate	40	SPA-01	Silty slate	S_0	2.76	2.98	2.6	3.1	2.8	1.2	3.3	3.5	3.4	1.18	3.25	3.52	3.0	3.6	3.3	3.9	4.1	4.0	2.74	2.75	2.69
					SPA-02	Silty slate	S_0	2.41	3.12								1.18	2.84	3.68							2.75		
			Quartzitic sst.	60	SPA-06	Quartzitic sst.	S_0	3.86	4.09	3.6	3.8	3.7	1.1				1.19	4.60	4.87	4.3	4.6	4.4				2.65	2.66	
					SPA-07	Quartzitic sst.	S_0	3.36	3.57								1.19	3.99	4.24							2.67		
		SLW	Slate	20	GH2386	Slate	S_1	2.56	4.24	2.4	4.4	3.4	1.9	3.2	3.7	3.4	1.04	2.67	4.41	2.5	4.6	3.5	3.7	4.2	3.9	2.78	2.78	2.72
					GH2585	Slate	S_1	2.36	4.52								1.04	2.46	4.70							2.78		
					GH2728	Slate	S_1	2.31	4.47								1.04	2.40	4.65							2.80		
					GH3072	Slate	S_1	2.27	4.52								1.04	2.36	4.70							2.76		
					GH3128	Slate	S_1	2.29	4.28								1.04	2.38	4.45							2.76		
			Silty slate	50	SPA-01	Silty slate	S_0	2.76	2.98	3.0	3.2	3.1	1.1				1.18	3.25	3.52	3.5	3.7	3.6				2.74	2.73	
					SPA-02	Silty slate	S_0	2.41	3.12								1.18	2.84	3.68							2.75		
					SLW-02	Silty slate	S_0	3.78	3.42								1.18	4.46	4.03							2.71		
			Quartzite	30	SLW-03	Quartzitic sst.	S_0	3.63	4.67	3.7	4.3	4.0	1.2				1.19	4.32	5.56	4.4	5.2	4.8				2.69	2.68	
					SLW-08	Sandstone	S_0	3.69	3.98								1.19	4.40	4.74							2.66		

Table A.4 continued

Group	Fm.	Mbr.	Lithology	Vol. [%]	Sample	Lithotype	λ_{dry} O	λ_{dry} ⊥ [W m^{-1}K^{-1}]	λ_{dry} // [W m^{-1}K^{-1}]	Litho. λ_{dry} ⊥ [W m^{-1}K^{-1}]	Litho. λ_{dry} // [W m^{-1}K^{-1}]	Litho. λ_{dry} AM [W m^{-1}K^{-1}]	Litho. λ_{dry} A [W m^{-1}K^{-1}]	Fm. λ_{dry} ⊥ [W m^{-1}K^{-1}]	Fm. λ_{dry} // [W m^{-1}K^{-1}]	Fm. λ_{dry} AM [W m^{-1}K^{-1}]	TF	λ_{sat} calc. ⊥ [W m^{-1}K^{-1}]	λ_{sat} calc. // [W m^{-1}K^{-1}]	Litho. λ_{sat} ⊥ [W m^{-1}K^{-1}]	Litho. λ_{sat} // [W m^{-1}K^{-1}]	Litho. λ_{sat} AM [W m^{-1}K^{-1}]	Fm. λ_{sat} ⊥ [W m^{-1}K^{-1}]	Fm. λ_{sat} // [W m^{-1}K^{-1}]	Fm. λ_{sat} AM [W m^{-1}K^{-1}]	Density Sample [10^3 kg m^{-3}]	Density Litho. [10^3 kg m^{-3}]	Density Fm. [10^3 kg m^{-3}]
REVIN	GLE	Rv5	Slate	50	GH2386	Slate	S_1	2.56	4.24	2.4	4.4	3.4	1.9	2.4	3.5	3.0	1.04	2.67	4.41	2.5	4.6	3.5	2.7	3.8	3.3	2.78	2.78	2.75
					GH2585	Slate	S_1	2.36	4.52								1.04	2.46	4.70							2.78		
					GH2728	Slate	S_1	2.31	4.47								1.04	2.40	4.65							2.80		
					GH3072	Slate	S_1	2.27	4.52								1.04	2.36	4.70							2.76		
					GH3128	Slate	S_1	2.29	4.28								1.04	2.38	4.45							2.76		
			Silty slate	50	GLE-03	Silty slate	S_0	2.76	2.42	2.5	2.6	2.6	1.0				1.18	3.26	2.85	3.0	3.1	3.0				2.72	2.73	
					GLE-04	Silty slate	S_0	2.58	2.77								1.18	3.04	3.27							2.70		
					GLE-05	Silty slate	S_0	2.25	2.62								1.18	2.66	3.10							2.76		
	VEN	Rv3 + 4	Slate	30	VEN-04	Slate	S_1	1.97	2.60	2.3	4.1	3.2	1.8	4.4	4.9	4.7	1.23	2.42	3.20	2.4	4.4	3.4	4.9	5.5	5.2	2.70	2.76	2.72
					GH2386	Slate	S_1	2.56	4.24								1.04	2.67	4.41							2.78		
					GH2585	Slate	S_1	2.36	4.52								1.04	2.46	4.70							2.78		
					GH2728	Slate	S_1	2.31	4.47								1.04	2.40	4.65							2.80		
					GH3072	Slate	S_1	2.27	4.52								1.04	2.36	4.70							2.76		
					GH3128	Slate	S_1	2.29	4.28								1.04	2.38	4.45							2.76		
			Quartzite	70	GH2600	Quartzite	S_0	5.06	5.15	5.2	5.4	5.3	1.0				1.12	5.66	5.77	5.8	6.0	5.9				2.68	2.70	
					GH3216	Quartzite	S_0	5.35	5.63								1.12	5.99	6.31							2.71		
	WAN	Rv1 + 2	Slate	40	GH2386	Slate	S_1	2.56	4.24	2.4	4.4	3.4	1.9	3.3	4.3	3.8	1.04	2.67	4.41	2.5	4.6	3.5	4.0	5.0	4.5	2.78	2.78	2.75
					GH2585	Slate	S_1	2.36	4.52								1.04	2.46	4.70							2.78		
					GH2728	Slate	S_1	2.31	4.47								1.04	2.40	4.65							2.80		
					GH3072	Slate	S_1	2.27	4.52								1.04	2.36	4.70							2.76		
					GH3128	Slate	S_1	2.29	4.28								1.04	2.38	4.45							2.76		
			Silty slate	20	WAN-07	Silty slate	S_0	2.26	2.55	2.3	3.0	2.6	1.3				1.18	2.67	3.00	2.7	3.6	3.2				2.77	2.85	
					WAN-08	Slate	S_1	2.21	2.68								1.23	2.71	3.29							2.88		
					WAN-09	Slate	S_1	2.33	3.74								1.23	2.86	4.60							2.89		
			Quartzite	40	WAN-02	Quartzite	S_0	4.42	4.50	4.8	4.9	4.8	1.0				1.38	6.10	6.21	6.1	6.2	6.1				2.62	2.67	
					WAN-06	Quartzite	S_0	4.40	4.32								1.38	6.07	5.97							2.67		
					WAN-10	Quartzite	S_0	4.68	4.81								1.38	6.46	6.64							2.66		
					GH2600	Quartzite	S_0	5.06	5.15								1.12	5.66	5.77							2.68		
					GH3216	Quartzite	S_0	5.35	5.63								1.12	5.99	6.31							2.71		

Table A.4 continued

Group	Fm.	Mbr.	Lithology	Vol. [%]	Sample	Lithotype	λ_{dry} O	λ_{dry} ⊥ [W m^{-1}K^{-1}]	λ_{dry} // [W m^{-1}K^{-1}]	Litho. λ_{dry} ⊥ [W m^{-1}K^{-1}]	Litho. λ_{dry} // [W m^{-1}K^{-1}]	Litho. λ_{dry} AM [W m^{-1}K^{-1}]	Litho. λ_{dry} A [W m^{-1}K^{-1}]	Fm. λ_{dry} ⊥ [W m^{-1}K^{-1}]	Fm. λ_{dry} // [W m^{-1}K^{-1}]	Fm. λ_{dry} AM [W m^{-1}K^{-1}]	TF	λ_{sat} calc. ⊥ [W m^{-1}K^{-1}]	λ_{sat} calc. // [W m^{-1}K^{-1}]	Litho. λ_{sat} ⊥ [W m^{-1}K^{-1}]	Litho. λ_{sat} // [W m^{-1}K^{-1}]	Litho. λ_{sat} AM [W m^{-1}K^{-1}]	Fm. λ_{sat} ⊥ [W m^{-1}K^{-1}]	Fm. λ_{sat} // [W m^{-1}K^{-1}]	Fm. λ_{sat} AM [W m^{-1}K^{-1}]	Density Sample [10^3 kg m^{-3}]	Density Litho. [10^3 kg m^{-3}]	Density Fm. [10^3 kg m^{-3}]
DEVILLE	BEL		Slate/shale	50	BEL-01	Sandy shale	S_1	3.12	3.65	2.5	3.1	2.8	1.2	3.6	3.9	3.8	1.19	3.72	4.34	3.0	3.7	3.4	4.3	4.7	4.5	2.61	2.66	2.66
					BEL-02	Slate	S_1	1.98	2.81								1.23	2.44	3.45							2.67		
					BEL-03	Slate	S_1	2.42	2.74								1.23	2.98	3.37							2.69		
			Quartz. sst./ quartzite	50	BEL-06	Quartzitic sst.	S_0	4.63	4.83	4.6	4.8	4.7	1.0				1.19	5.50	5.75	5.5	5.7	5.6				2.66	2.66	
	HUR		Slate	45	GH516	Slate	S_1	2.15	2.54	2.4	3.2	2.8	1.3	3.6	4.0	3.8	1.04	2.24	2.64	2.5	3.3	2.9	4.3	4.6	4.5	2.81	2.79	2.70
					GH835	Slate	S_1	2.49	2.51								1.04	2.59	2.61							2.81		
					GH1453	Slate	S_1	2.34	4.32								1.04	2.43	4.49							2.79		
					GH2004	Slate	S_1	2.24	2.68								1.04	2.33	2.78							2.75		
					GH2008	Slate	S_1	2.35	2.62								1.04	2.45	2.72							2.77		
					GH2315	Slate	S_1	2.88	3.64								1.04	3.00	3.78							2.78		
					GH2331	Slate	S_1	2.51	3.87								1.04	2.61	4.03							2.82		
			Quartzite	55	GH350	Quartzite	S_0	5.57	5.60	4.6	4.7	4.6	1.0				1.12	6.24	6.27	5.7	5.8	5.8				2.63	2.63	
					GH2021	Quartzite	S_0	4.87	4.69								1.12	5.45	5.25							2.66		
					GH2355	Quartzitic sst.	S_0	3.48	4.17								1.12	3.90	4.67							2.73		
					HUR-03	Quartzite	S_0	4.82	5.15								1.38	6.65	7.11							2.65		
					HUR-05	Quartzite	S_0	4.62	4.49								1.38	6.37	6.19							2.64		
					HUR-06	Quartzitic sst.	S_0	4.29	4.33								1.19	5.11	5.15							2.60		
					HUR-12	Quartzite	S_0	4.41	4.44								1.38	6.08	6.12							2.51		

Table A.5: Details on samples used to compose the petrophysical properties of the Lower Devonian geological formations in the Belgian and Luxembourgish Ardennes.

Formation		Lithology	Vol.	Sample	Lithotype	λ_{dry}			Litho. λ_{dry}				Fm. λ_{dry}			TF	λ_{sat} calc.		Litho. λ_{sat}			Fm. λ_{sat}			Density		
Be	Lux		[%]			O	⊥	//	⊥	//	AM	A	⊥	//	AM		⊥	//	⊥	//	AM	⊥	//	AM	Sample	Litho.	Fm.
							[$Wm^{-1}K^{-1}$]		[$Wm^{-1}K^{-1}$]				[$Wm^{-1}K^{-1}$]				[$Wm^{-1}K^{-1}$]		[$Wm^{-1}K^{-1}$]			[$Wm^{-1}K^{-1}$]			[10^3 kg m^{-3}]		
	E3	Sandy shale	90	E3-001	Shale	S_1	2.28	1.94	2.1	1.8	1.9	0.9	2.2	2.0	2.1	1.19	2.71	2.31	2.5	2.2	2.3	2.6	2.4	2.5	2.66	2.60	2.62
				E3-002	Shale	S_1	1.87	1.83								1.19	2.22	2.18							2.55		
				E3-003	Shale	S_1	2.05	1.69								1.19	2.44	2.02							2.59		
			10	E3-005	Sandy shale	S_1	3.23	3.73	3.2	3.7	3.5	1.2				1.19	3.84	4.44	3.8	4.4	4.1				2.77	2.77	
	q	Quartzite	100	q-001	Quartzite	S_0	3.73	3.99	4.4	4.6	4.5	1.0	4.5	4.5	4.5	1.38	5.15	5.51	6.1	6.3	6.2	6.2	6.2	6.2	2.35	2.50	2.50
				q-002	Quartzite	S_0	*4.14*	4.14								1.38	5.71	5.71							2.55		
				q-003	Quartzite	S_0	5.31	5.56								1.38	7.33	7.67							2.59		
	E2	Shale/siltstone	70	E2-002	Siltstone	S_0	2.35	2.34	2.4	2.6	2.5	1.1	2.9	2.9	2.9	1.17	2.75	2.74	2.9	3.1	3.0	3.3	3.3	3.3	2.71	2.66	2.66
				E2-004	Siltstone	S_0	2.13	2.56								1.17	2.50	2.99							2.71		
				E2-007	Siltstone	S_0	2.84	3.15								1.17	3.32	3.68							2.70		
				E2-008	Siltstone	S_0	3.17	3.14								1.17	3.71	3.67							2.67		
				E2-010-1	Siltstone	S_0	2.32	2.61								1.17	2.71	3.06							2.51		
				E2-010-2	Siltstone	S_0	1.81	2.06								1.17	2.12	2.41							2.66		
		Sandstone	25	E1b-008	Sandstone	S_0	3.19	3.47	3.4	3.6	3.5	1.0				1.17	3.73	4.06	4.0	4.2	4.1				2.65	2.66	
				E1b-009	Sandstone	S_0	3.67	3.68								1.17	4.30	4.31							2.66		
		Quartzitic sst.	5	E2-001	Quartzitic sst.	S_0	3.96	4.30	4.0	4.3	4.1	1.1				1.17	4.63	5.03	4.6	5.0	4.8				2.66	2.66	
	E1b	Silty slate/siltstone	70	E1b-001	Siltstone	S_0	2.19	2.95	2.4	2.9	2.7	1.2	2.8	3.1	2.9	1.17	2.56	3.45	2.9	3.4	3.1	3.5	3.5	3.5	2.72	2.69	2.68
				E1b-003	Siltstone	S_0	2.35	2.40								1.17	2.75	2.80							2.68		
				E1b-004	Silty slate	S_0	2.70	3.54								1.19	3.21	4.21							2.71		
				E1b-006	Silty slate	S_0	1.97	2.26								1.19	2.34	2.69							2.74		
				E1b-007	Siltstone	S_0	2.81	3.29								1.17	3.29	3.85							2.66		
				E1b-010	Siltstone	S_0	2.54	3.01								1.17	2.98	3.52							2.65		
				E1b-012	Siltstone	S_0	2.50	2.63								1.17	2.92	3.07							2.67		
		Sandstone	20	E1b-008	Sandstone	S_0	3.19	3.47	3.4	3.6	3.5	1.0				1.17	3.73	4.06	4.0	4.2	4.1				2.65	2.66	
				E1b-009	Sandstone	S_0	3.67	3.68								1.17	4.30	4.31							2.66		
		Quarzitic sst.	10	E1b-002	Quartzitic sst.	S_0	4.01	4.25	3.7	4.0	3.8	1.1				1.17	4.69	4.97	4.3	4.7	4.5				2.68	2.66	
				E1b-005	Quartzitic sst.	S_0	3.38	3.72								1.17	3.95	4.35							2.64		

Be – Belgium, Lux – Luxembourg, Vol. – volume fraction, Litho. – lithotype, Fm. – formation, O – orientation, λ_{dry} and λ_{sat} – thermal conductivity under dry and saturated conditions, respectively, S_0 and S_1 – bedding and cleavage, respectively, ⊥ and // – thermal conductivity perpendicular and parallel to orientation, AM – arithmetic mean, A – anisotropy, TF – transformation factor, calc. – calculated, sst. – sandstone, congl. – conglomeratic. Composition of the individual formations is estimated after Dejonghe (2008) and Lucius (1950).

Table A.5 continued

Formation		Lithology	Vol.	Sample	Lithotype	λ_{dry}			Litho. λ_{dry}				Fm. λ_{dry}			TF	λ_{sat} calc.		Litho. λ_{sat}			Fm. λ_{sat}			Density		
Be	Lux		[%]			O	⊥	//	⊥	//	AM	A	⊥	//	AM		⊥	//	⊥	//	AM	⊥	//	AM	Sample	Litho.	Fm.
							[$Wm^{-1}K^{-1}$]		[$Wm^{-1}K^{-1}$]				[$Wm^{-1}K^{-1}$]				[$Wm^{-1}K^{-1}$]		[$Wm^{-1}K^{-1}$]			[$Wm^{-1}K^{-1}$]			[10^3 kg m^{-3}]		
	E1a	Sandy shale	94	E1a-003	Sandy shale	S_1	2.11	2.39	2.6	2.7	2.6	1.0	2.6	2.7	2.7	1.19	2.51	2.84	3.0	3.2	3.1	3.1	3.3	3.2	2.73	2.74	2.73
				E1a-004	Sandy shale	S_1	2.52	2.53								1.19	3.00	3.00							2.71		
				E1a-006	Sandy shale	S_1	3.21	2.95								1.19	3.82	3.51							2.75		
				E1a-007	Sandy shale	S_1	2.45	2.73								1.19	2.92	3.25							2.73		
				E1a-009	Sandy shale	S_1	2.56	2.41								1.19	3.04	2.86							2.75		
				E1a-010	Sandy shale	S_1	2.50	3.05								1.19	2.98	3.63							2.75		
		Quartzitic sst.	6	E1a-005	Sandstone	S_0	3.03	2.80	3.7	3.8	3.7	1.0				1.17	3.54	3.28	4.3	4.4	4.3				2.69	2.71	
				E1a-011	Quartzitic sst	S_0	4.08	4.39								1.17	4.78	5.14							2.71		
				E1a-013	Sandstone	S_0	3.86	4.10								1.17	4.51	4.80							2.72		
LAR	Sg3	Sandy shale	100	Sg3-001	Sandy shale	S_1	2.52	2.98	2.4	2.5	2.5	1.0	2.4	2.5	2.5	1.19	2.99	3.54	2.9	3.0	2.9	2.9	3.0	2.9	2.68	2.67	2.67
				Sg3-002	Sandy shale	S_1	2.30	2.58								1.19	2.74	3.07							2.67		
				Sg3-003	Sandy shale	S_1	2.52	2.45								1.19	3.00	2.91							2.69		
				Sg3-006	Sandy shale	S_1	2.21	2.24								1.19	2.63	2.67							2.59		
				Sg3-009	Sandy shale	S_1	1.95	1.95								1.19	2.32	2.32							2.63		
				Sg3-010	Sandy shale	S_1	2.06	2.32								1.19	2.46	2.75							2.67		
				Sg3-011	Sandy shale	S_1	2.52	2.30								1.19	3.00	2.74							2.65		
				Sg3-012	Sandy shale	S_1	3.13	3.48								1.19	3.72	4.14							2.75		
				Sg3-013	Sandy shale	S_1	2.55	2.33								1.19	3.03	2.77							2.71		
	Sg3a	Slate	100	Sg3a-1	Slate	S_1	2.50	2.71	2.4	2.9	2.6	1.2	2.4	2.9	2.6	1.23	3.07	3.34	2.9	3.5	3.2	2.9	3.5	3.2	2.75	2.73	2.73
				Sg3a-2	Slate	S_1	2.37	2.68								1.23	2.91	3.30							2.74		
				Sg3a-3	Slate	S_1	2.42	3.39								1.23	2.97	4.17							2.69		
				Sg3a-4	Slate	S_1	2.29	2.72								1.23	2.82	3.34							2.75		

Table A.5 continued

Formation		Lithology	Vol.	Sample	Lithotype	λ_{dry}			Litho. λ_{dry}				Fm. λ_{dry}			TF	λ_{sat} calc.		Litho. λ_{sat}			Fm. λ_{sat}			Density		
						O	⊥	//	⊥	//	AM	A	⊥	//	AM		⊥	//	⊥	//	AM	⊥	//	AM	Sample	Litho.	Fm.
Be	Lux		[%]				[$Wm^{-1}K^{-1}$]		[$Wm^{-1}K^{-1}$]				[$Wm^{-1}K^{-1}$]				[$Wm^{-1}K^{-1}$]		[$Wm^{-1}K^{-1}$]			[$Wm^{-1}K^{-1}$]			[10^3 kg m^{-3}]		
VIL	Sg2	Shale/siltstone	35	VIL-02	Shale	S_1	1.91	1.90	2.2	2.1	2.1	1.0	3.0	3.0	3.0	1.19	2.27	2.26	2.6	2.5	2.5	3.5	3.5	3.5	2.57	2.58	2.58
				VIL-05	Shale	S_1	2.05	2.28								1.19	2.44	2.71							2.57		
				VIL-06	Shale	S_1	2.27	2.11								1.19	2.70	2.52							2.56		
				VIL-09	Shale	S_1	1.93	1.88								1.19	2.29	2.24							2.61		
				VIL-11	Sandy shale	S_1	2.23	2.17								1.19	2.65	2.58							2.56		
				VIL-12	Sandy shale	S_1	2.75	2.29								1.19	3.27	2.73							2.61		
				VIL-14	Sandy shale	S_1	1.96	1.99								1.19	2.34	2.37							2.58		
		Siltstone + calc. sst/sandy limestone	65	VIL-04	Sandstone	S_0	4.42	4.17	3.5	3.5	3.5	1.0				1.17	5.17	4.88	4.1	4.1	4.1				2.56	2.59	
				VIL-08	Sandstone	S_0	3.18	3.39								1.17	3.73	3.96							2.63		
				VIL-10	Sandstone	S_0	*2.85*	2.85								1.17	3.33	3.33							2.57		
MIR	Sg1	Slate	80	Sg1-001	Slate	S_1	2.28	2.55	2.5	2.6	2.5	1.0	2.8	2.9	2.8	1.23	2.80	3.14	3.1	3.2	3.1	3.4	3.5	3.4	2.72	2.73	2.73
				Sg1-002	Slate	S_1	2.77	2.58								1.23	3.40	3.18							2.74		
				Sg1-003	Slate	S_1	2.42	2.69								1.23	2.98	3.31							2.73		
		Silty slate	5	Sg1-008	Silty slate	S_0	2.56	2.99	2.6	3.1	2.8	1.2				1.19	3.04	3.56	3.1	3.6	3.4				2.70	2.69	
				Sg1-010	Silty slate	S_0	2.14	2.79								1.19	2.55	3.32							2.73		
				Sg1-007	Silty slate	S_0	3.20	3.40								1.19	3.81	4.05							2.64		
		Quartz. sst./quartzite	15	Sg1-005	Quartzitic sst.	S_0	4.13	4.49	4.1	4.5	4.3	1.1				1.17	4.83	5.26	4.8	5.3	5.0				2.71	2.71	
STH		Shale/siltstone	80	STH-01	Shale	S_1	2.12	2.34	2.9	3.2	3.1	1.1	3.3	3.3	3.3	1.19	2.52	2.78	3.4	3.8	3.6	3.9	3.9	3.9	2.73	2.71	2.70
				STH-03	Shale	S_1	2.97	*2.97*								1.19	3.53	3.53							2.67		
				STH-04	Siltstone	S_0	2.90	3.30								1.17	3.39	3.86							2.72		
				STH-05	Siltstone	S_0	2.95	3.66								1.17	3.45	4.28							2.74		
				STH-10	Siltstone	S_0	3.39	3.38								1.17	3.96	3.95							2.74		
				STH-13	Sandy siltstone	S_0	3.25	3.62								1.17	3.80	4.23							2.67		
				STH-14	Siltstone	S_0	2.71	3.17								1.17	3.17	3.71							2.71		
		Sandstone	20	STH-07	Quartzitic sst.	S_0	4.00	4.04	4.3	4.4	4.4	1.0				1.17	4.68	4.73	5.1	5.2	5.1				2.71	2.67	
				STH-08	Quartzitic sst.	S_0	4.29	4.26								1.17	5.02	4.99							2.62		
				STH-09	Quartzitic sst.	S_0	4.92	5.08								1.17	5.76	5.94							2.66		
				STH-11	Sandstone	S_0	4.17	4.30								1.17	4.87	5.03							2.67		

Table A.5 continued

Formation		Lithology	Vol.	Sample	Lithotype	λ_{dry}			Litho. λ_{dry}				Fm. λ_{dry}			TF	λ_{sat} calc.		Litho. λ_{sat}			Fm. λ_{sat}			Density		
Be	Lux		[%]			O	⊥	//	⊥	//	AM	A	⊥	//	AM		⊥	//	⊥	//	AM	⊥	//	AM	Sample	Litho.	Fm.
							[$Wm^{-1}K^{-1}$]		[$Wm^{-1}K^{-1}$]				[$Wm^{-1}K^{-1}$]				[$Wm^{-1}K^{-1}$]		[$Wm^{-1}K^{-1}$]			[$Wm^{-1}K^{-1}$]			[10^3 kg m^{-3}]		
OIG		Siltstone	15	OIG-01	Siltstone	S_0	2.64	2.75	2.7	2.7	2.7	1.0	2.6	2.6	2.6	1.17	3.09	3.21	3.1	3.1	3.1	3.0	3.0	3.0	2.57	2.50	2.60
				OIG-05	Siltstone	S_0	2.70	2.63								1.17	3.16	3.08							2.43		
		Shale	60	OIG-10	Shale	S_1	2.00	2.15	2.2	2.2	2.2	1.0				1.19	2.38	2.56	2.6	2.6	2.6				2.66	2.61	
				OIG-12	Shale	S_1	2.18	2.13								1.19	2.59	2.53							2.43		
				OIG-13	Shale	S_1	2.48	2.38								1.19	2.95	2.84							2.74		
		Sandstone	25	OIG-04	Silty sandstone	S_0	3.31	3.17	3.3	3.3	3.3	1.0				1.17	3.87	3.71	3.9	3.9	3.9				2.63	2.62	
				OIG-07	Sandstone	S_0	2.80	2.90								1.17	3.27	3.40							2.57		
				OIG-08	Sandstone	S_0	3.99	4.15								1.17	4.66	4.85							2.57		
				OIG-09	Silty sandstone	S_0	3.10	3.11								1.17	3.63	3.64							2.70		
FEP		Shale/siltstone	50	FEP-05	Shale	S_1	3.24	*3.24*	2.8	2.9	2.9	1.0	3.7	3.7	3.7	1.19	3.85	3.85	3.4	3.5	3.4	4.3	4.4	4.3	2.70	2.70	2.67
				FEP-07	Shale	S_1	2.42	2.60								1.19	2.88	3.09							2.70		
		Sandstone	20	FEP-06	Sandstone	S_0	4.79	4.39	4.8	4.4	4.6	0.9				1.17	5.60	5.13	5.6	5.1	5.4				2.68	2.68	
		Congl. sandstone	30	FEP-01	Congl. sst.	S_0	3.99	3.72	4.4	4.4	4.4	1.0				1.17	4.66	4.35	5.2	5.1	5.2				2.63	2.62	
				FEP-02	Congl. sst.	S_0	4.43	4.60								1.17	5.19	5.39							2.63		
				FEP-03	Congl. sst.	S_0	4.88	4.74								1.17	5.71	5.54							2.61		
				FEP-04	Congl. sst.	S_0	4.43	4.45								1.17	5.18	5.21							2.60		

Table A.6: Details on samples used to compose the petrophysical properties of the Lower Devonian geological formations in the Eifel and Mosel Syncline/Hunsrück regions.

Formation	Lithology	Vol.	Sample	Lithotype	λ_{dry}			Litho. λ_{dry}				Fm. λ_{dry}			TF	λ_{sat} calc.		Litho. λ_{sat}			Fm. λ_{sat}			Density		
(Code)		[%]			O	⊥	//	⊥	//	AM	A	⊥	//	AM		⊥	//	⊥	//	AM	⊥	//	AM	Sample	Litho.	Fm.
					[W m^{-1} K^{-1}]			[W m^{-1} K^{-1}]				[W m^{-1} K^{-1}]				[W m^{-1} K^{-1}]		[W m^{-1} K^{-1}]			[W m^{-1} K^{-1}]			[10^{3} kg m^{-3}]		
Wissenbach-Schiefer	Shale	> 90	E3-001	Shale	S_1	2.28	1.94	2.4	2.3	2.3	1.0	2.5	2.5	2.5	1.19	2.71	2.31	2.8	2.7	2.8	3.0	2.9	3.0	2.66	2.64	2.64
(de/dzoWI)			E3-002	Shale	S_1	1.87	1.83								1.19	2.22	2.18							2.55		
			E3-003	Shale	S_1	2.05	1.69								1.19	2.44	2.02							2.59		
			E3-005	Sandy shale	S_1	3.23	3.73								1.19	3.84	4.44							2.77		
	Quartzitic sst.	< 10	E2-001	Quartzitic sst.	S_0	3.96	4.30	4.0	4.3	4.1	1.1				1.17	4.63	5.03	4.6	5.0	4.8				2.66	2.66	
Kieselgallenschiefer	Shale/shaly siltstone	> 90	E3-001	Shale	S_1	2.28	1.94	2.4	2.3	2.3	1.0	2.4	2.3	2.3	1.19	2.71	2.31	2.8	2.7	2.8	2.8	2.8	2.8	2.66	2.64	2.64
(dzo3KG)			E3-002	Shale	S_1	1.87	1.83								1.19	2.22	2.18							2.55		
			E3-003	Shale	S_1	2.05	1.69								1.19	2.44	2.02							2.59		
			E3-005	Sandy shale	S_1	3.23	3.73								1.19	3.84	4.44							2.77		
	Siltstone/ sandstone	< 10	E2-002	Siltstone	S_0	2.35	2.34	2.4	2.6	2.5	1.1				1.17	2.75	2.74	2.9	3.1	3.0				2.71	2.66	
			E2-004	Siltstone	S_0	2.13	2.56								1.17	2.50	2.99							2.71		
			E2-007	Siltstone	S_0	2.84	3.15								1.17	3.32	3.68							2.70		
			E2-008	Siltstone	S_0	3.17	3.14								1.17	3.71	3.67							2.67		
			E2-010-1	Siltstone	S_0	2.32	2.61								1.17	2.71	3.06							2.51		
			E2-010-2	Siltstone	S_0	1.81	2.06								1.17	2.12	2.41							2.66		
Sphärosideritschiefer	Shale/shaly siltstone	> 80	E3-001	Shale	S_1	2.28	1.94	2.4	2.3	2.3	1.0	2.6	2.5	2.6	1.19	2.71	2.31	2.8	2.7	2.8	3.1	3.0	3.0	2.66	2.64	2.65
(dzo3SS)			E3-002	Shale	S_1	1.87	1.83								1.19	2.22	2.18							2.55		
			E3-003	Shale	S_1	2.05	1.69								1.19	2.44	2.02							2.59		
			E3-005	Sandy shale	S_1	3.23	3.73								1.19	3.84	4.44							2.77		
	Sandstone	< 20	E1b-008	Sandstone	S_0	3.19	3.47	3.4	3.6	3.5	1.0				1.17	3.73	4.06	4.0	4.2	4.1				2.65	2.66	
			E1b-009	Sandstone	S_0	3.67	3.68								1.17	4.30	4.31							2.66		
Brauneisenstein	Sandstone	> 70	E1b-008	Sandstone	S_0	3.19	3.47	3.4	3.6	3.5	1.0	3.2	3.1	3.1	1.17	3.73	4.06	4.0	4.2	4.1	3.7	3.7	3.7	2.65	2.66	2.65
(dzo3BE)			E1b-009	Sandstone	S_0	3.67	3.68								1.17	4.30	4.31							2.66		
	Shale/shaly siltstone	< 30	E3-001	Shale	S_1	2.28	1.94	2.4	2.3	2.3	1.0				1.19	2.71	2.31	2.8	2.7	2.8				2.66	2.64	
			E3-002	Shale	S_1	1.87	1.83								1.19	2.22	2.18							2.55		
			E3-003	Shale	S_1	2.05	1.69								1.19	2.44	2.02							2.59		
			E3-005	Sandy shale	S_1	3.23	3.73								1.19	3.84	4.44							2.77		

Vol. – volume fraction, Litho. – lithotype, Fm. – formation, O – orientation, λ_{dry} and λ_{sat} – thermal conductivity under dry and saturated conditions, respectively, S_0 and S_1 – bedding and cleavage, respectively, ⊥ and // – thermal conductivity perpendicular and parallel to orientation, AM – arithmetic mean, A – anisotropy, TF – transformation factor, calc. – calculated, sst. – sandstone. Composition of the individual formations is taken from Häfner et al. (2007) and completed according to LGB (2005).

Table A.6 continued

Formation	Lithology	Vol.	Sample	Lithotype	λ_{dry}			Litho. λ_{dry}				Fm. λ_{dry}			TF	λ_{sat} calc.		Litho. λ_{sat}			Fm. λ_{sat}			Density		
(Code)		[%]			O	⊥	//	⊥	//	AM	A	⊥	//	AM		⊥	//	⊥	//	AM	⊥	//	AM	Sample	Litho.	Fm.
					[W m^{-1} K^{-1}]			[W m^{-1} K^{-1}]				[W m^{-1} K^{-1}]				[W m^{-1} K^{-1}]		[W m^{-1} K^{-1}]			[W m^{-1} K^{-1}]			[10^{3} kg m^{-3}]		
Rötelgallen-Schichten (dzo2RG)	Shale	50	E3-001	Shale	S_1	2.28	1.94	2.4	2.3	2.3	1.0	2.9	2.9	2.9	1.19	2.71	2.31	2.8	2.7	2.8	3.4	3.4	3.4	2.66	2.64	2.65
			E3-002	Shale	S_1	1.87	1.83								1.19	2.22	2.18							2.55		
			E3-003	Shale	S_1	2.05	1.69								1.19	2.44	2.02							2.59		
			E3-005	Sandy shale	S_1	3.23	3.73								1.19	3.84	4.44							2.77		
	Sandstone + limestone	50	E1b-008	Sandstone	S_0	3.19	3.47	3.4	3.6	3.5	1.0				1.17	3.73	4.06	4.0	4.2	4.1				2.65	2.66	
			E1b-009	Sandstone	S_0	3.67	3.68								1.17	4.30	4.31							2.66		
Höllenthal-Schichten (dzo2HÖ)	Shale	50	E3-001	Shale	S_1	2.28	1.94	2.4	2.3	2.3	1.0	2.9	2.9	2.9	1.19	2.71	2.31	2.8	2.7	2.8	3.4	3.4	3.4	2.66	2.64	2.65
			E3-002	Shale	S_1	1.87	1.83								1.19	2.22	2.18							2.55		
			E3-003	Shale	S_1	2.05	1.69								1.19	2.44	2.02							2.59		
			E3-005	Sandy shale	S_1	3.23	3.73								1.19	3.84	4.44							2.77		
	Sandstone	50	E1b-008	Sandstone	S_0	3.19	3.47	3.4	3.6	3.5	1.0				1.17	3.73	4.06	4.0	4.2	4.1				2.65	2.66	
			E1b-009	Sandstone	S_0	3.67	3.68								1.17	4.30	4.31							2.66		
Flußbach-Schichten (dzo1FL)	Shale/shaly siltstone	40	E3-001	Shale	S_1	2.28	1.94	2.4	2.3	2.3	1.0	3.4	3.4	3.4	1.19	2.71	2.31	2.8	2.7	2.8	3.6	3.6	3.6	2.66	2.64	2.65
			E3-002	Shale	S_1	1.87	1.83								1.19	2.22	2.18							2.55		
			E3-003	Shale	S_1	2.05	1.69								1.19	2.44	2.02							2.59		
			E3-005	Sandy shale	S_1	3.23	3.73								1.19	3.84	4.44							2.77		
	Quartzitic sst.	60	E2-001	Quartzitic sst.	S_0	3.96	4.30	4.0	4.3	4.1	1.1				1.17	4.63	5.03	4.0	4.3	4.1				2.66	2.66	
Emsquarzit (dzo1EQ)	Quartzitic sst./quartzite	> 90	q-001	Quartzite	S_0	3.73	3.99	4.4	4.6	4.5	1.0	4.3	4.3	4.3	1.38	5.15	5.51	6.1	6.3	6.2	5.8	5.8	5.8	2.35	2.50	2.51
			q-002	Quartzite	S_0	*4.14*	4.14								1.38	5.71	5.71							2.55		
			q-003	Quartzite	S_0	5.31	5.56								1.38	7.33	7.67							2.59		
	Shale	< 10	E3-001	Shale	S_1	2.28	1.94	2.4	2.3	2.3	1.0				1.19	2.71	2.31	2.8	2.7	2.8				2.66	2.64	
			E3-002	Shale	S_1	1.87	1.83								1.19	2.22	2.18							2.55		
			E3-003	Shale	S_1	2.05	1.69								1.19	2.44	2.02							2.59		
			E3-005	Sandy shale	S_1	3.23	3.73								1.19	3.84	4.44							2.77		

Table A.6 continued

Formation	Lithology	Vol.	Sample	Lithotype	λ_{dry}			Litho. λ_{dry}				Fm. λ_{dry}			TF	λ_{sat} calc.		Litho. λ_{sat}			Fm. λ_{sat}			Density		
(Code)		[%]			O	⊥	//	⊥	//	AM	A	⊥	//	AM		⊥	//	⊥	//	AM	⊥	//	AM	Sample	Litho.	Fm.
					[W m^{-1} K^{-1}]			[W m^{-1} K^{-1}]				[W m^{-1} K^{-1}]				[W m^{-1} K^{-1}]		[W m^{-1} K^{-1}]			[W m^{-1} K^{-1}]			[10^{3} kg m^{-3}]		
Klerf-Schichten	Shale/shaly siltstone	30	E2-002	Siltstone	S_0	2.35	2.34	2.4	2.6	2.5	1.1	3.4	3.4	3.4	1.17	2.75	2.74	2.9	3.1	3.0	3.9	3.9	3.9	2.71	2.66	2.66
(dzu3KL)			E2-004	Siltstone	S_0	2.13	2.56								1.17	2.50	2.99							2.71		
			E2-007	Siltstone	S_0	2.84	3.15								1.17	3.32	3.68							2.70		
			E2-008	Siltstone	S_0	3.17	3.14								1.17	3.71	3.67							2.67		
			E2-010-1	Siltstone	S_0	2.32	2.61								1.17	2.71	3.06							2.51		
			E2-010-2	Siltstone	S_0	1.81	2.06								1.17	2.12	2.41							2.66		
	Sandstone/ quartzite	70	E1b-008	Sandstone	S_0	3.19	3.47	3.6	3.8	3.7	1.1				1.17	3.73	4.06	4.2	4.5	4.3				2.65	2.66	
			E1b-009	Sandstone	S_0	3.67	3.68								1.17	4.30	4.31							2.66		
			E2-001	Quartzitic sst.	S_0	3.96	4.30								1.17	4.63	5.03							2.66		
Gladbach-Schichten	Shale	60	E1a-003	Sandy shale	S_1	2.11	2.39	2.6	2.7	2.6	1.0	2.8	2.9	2.8	1.19	2.51	2.84	3.0	3.2	3.1	3.3	3.4	3.4	2.73	2.74	2.72
(dzu3GL)			E1a-004	Sandy shale	S_1	2.52	2.53								1.19	3.00	3.00							2.71		
			E1a-006	Sandy shale	S_1	3.21	2.95								1.19	3.82	3.51							2.75		
			E1a-007	Sandy shale	S_1	2.45	2.73								1.19	2.92	3.25							2.73		
			E1a-009	Sandy shale	S_1	2.56	2.41								1.19	3.04	2.86							2.75		
			E1a-010	Sandy shale	S_1	2.50	3.05								1.19	2.98	3.63							2.75		
	Siltstone	20	E1b-001	Siltstone	S_0	2.19	2.95	2.4	2.9	2.7	1.2				1.17	2.56	3.45	2.9	3.4	3.1				2.72	2.69	
			E1b-003	Siltstone	S_0	2.35	2.40								1.17	2.75	2.80							2.68		
			E1b-004	Silty slate	S_0	2.70	3.54								1.19	3.21	4.21							2.71		
			E1b-006	Silty slate	S_0	1.97	2.26								1.19	2.34	2.69							2.74		
			E1b-007	Siltstone	S_0	2.81	3.29								1.17	3.29	3.85							2.66		
			E1b-010	Siltstone	S_0	2.54	3.01								1.17	2.98	3.52							2.65		
			E1b-012	Siltstone	S_0	2.50	2.63								1.17	2.92	3.07							2.67		
	Sandstone	20	E1b-008	Sandstone	S_0	3.19	3.47	3.6	3.8	3.7	1.0				1.17	3.73	4.06	4.2	4.4	4.3				2.65	2.68	
			E1b-009	Sandstone	S_0	3.67	3.68								1.17	4.30	4.31							2.66		
			E1b-002	Quartzitic sst.	S_0	4.01	4.25								1.17	4.69	4.97							2.68		
			E1b-005	Quartzitic sst.	S_0	3.38	3.72								1.17	3.95	4.35							2.64		
			E1a-005	Sandstone	S_0	3.03	2.80								1.17	3.54	3.28							2.69		
			E1a-011	Quartzitic sst	S_0	4.08	4.39								1.17	4.78	5.14							2.71		
			E1a-013	Sandstone	S_0	3.86	4.10								1.17	4.51	4.80							2.72		

Table A.6 continued

Formation	Lithology	Vol.	Sample	Lithotype	λ_{dry}			Litho. λ_{dry}				Fm. λ_{dry}			TF	λ_{sat} calc.		Litho. λ_{sat}			Fm. λ_{sat}			Density		
(Code)		[%]			O	⊥	//	⊥	//	AM	A	⊥	//	AM		⊥	//	⊥	//	AM	⊥	//	AM	Sample	Litho.	Fm.
					[W m^{-1} K^{-1}]			[W m^{-1} K^{-1}]				[W m^{-1} K^{-1}]				[W m^{-1} K^{-1}]		[W m^{-1} K^{-1}]			[W m^{-1} K^{-1}]			[10^3 kg m^{-3}]		
"Singhofen-Schichten" (old: dzS)	Shale/sandy shale	90	E1a-003	Sandy shale	S_1	2.11	2.39	2.6	2.7	2.6	1.0	2.7	2.8	2.7	1.19	2.51	2.84	3.0	3.2	3.1	3.2	3.3	3.2	2.73	2.74	2.73
			E1a-004	Sandy shale	S_1	2.52	2.53								1.19	3.00	3.00							2.71		
			E1a-006	Sandy shale	S_1	3.21	2.95								1.19	3.82	3.51							2.75		
			E1a-007	Sandy shale	S_1	2.45	2.73								1.19	2.92	3.25							2.73		
			E1a-009	Sandy shale	S_1	2.56	2.41								1.19	3.04	2.86							2.75		
			E1a-010	Sandy shale	S_1	2.50	3.05								1.19	2.98	3.63							2.75		
	Sandstone	10	E1b-008	Sandstone	S_0	3.19	3.47	3.6	3.8	3.7	1.0				1.17	3.73	4.06	4.2	4.4	4.3				2.65	2.68	
			E1b-009	Sandstone	S_0	3.67	3.68								1.17	4.30	4.31							2.66		
			E1b-002	Quartzitic sst.	S_0	4.01	4.25								1.17	4.69	4.97							2.68		
			E1b-005	Quartzitic sst.	S_0	3.38	3.72								1.17	3.95	4.35							2.64		
			E1a-005	Sandstone	S_0	3.03	2.80								1.17	3.54	3.28							2.69		
			E1a-011	Quartzitic sst	S_0	4.08	4.39								1.17	4.78	5.14							2.71		
			E1a-013	Sandstone	S_0	3.86	4.10								1.17	4.51	4.80							2.72		
Kaubschichten (Hunsrückschiefer) (dzu1KA)	Shale	85	Sg3-001	Sandy shale	S_1	2.52	2.98	2.4	2.5	2.5	1.0	2.4	2.6	2.5	1.19	2.99	3.54	2.9	3.0	2.9	2.9	3.1	3.0	2.68	2.67	2.67
			Sg3-002	Sandy shale	S_1	2.30	2.58								1.19	2.74	3.07							2.67		
			Sg3-003	Sandy shale	S_1	2.52	2.45								1.19	3.00	2.91							2.69		
			Sg3-006	Sandy shale	S_1	2.21	2.24								1.19	2.63	2.67							2.59		
			Sg3-009	Sandy shale	S_1	1.95	1.95								1.19	2.32	2.32							2.63		
			Sg3-010	Sandy shale	S_1	2.06	2.32								1.19	2.46	2.75							2.67		
			Sg3-011	Sandy shale	S_1	2.52	2.30								1.19	3.00	2.74							2.65		
			Sg3-012	Sandy shale	S_1	3.13	3.48								1.19	3.72	4.14							2.75		
			Sg3-013	Sandy shale	S_1	2.55	2.33								1.19	3.03	2.77							2.71		
	Slate	10	Sg3a-1	Slate	S_1	2.50	2.71	2.4	2.9	2.6	1.2				1.23	3.07	3.34	2.9	3.5	3.2				2.75	2.73	
			Sg3a-2	Slate	S_1	2.37	2.68								1.23	2.91	3.30							2.74		
			Sg3a-3	Slate	S_1	2.42	3.39								1.23	2.97	4.17							2.69		
			Sg3a-4	Slate	S_1	2.29	2.72								1.23	2.82	3.34							2.75		
	Quartzitic sst.	5	Sg3-008	Sandstone	S_0	3.08	3.03	3.0	2.9	2.9	1.0				1.17	3.60	3.54	3.5	3.4	3.4				2.61	2.62	
			Sg3-007	Sandstone	S_0	2.88	2.70								1.17	3.37	3.16							2.62		

Table A.6 continued

Formation	Lithology	Vol.	Sample	Lithotype	λ_{dry}			Litho. λ_{dry}				Fm. λ_{dry}			TF	λ_{sat} calc.		Litho. λ_{sat}			Fm. λ_{sat}			Density		
(Code)		[%]			O	⊥	//	⊥	//	AM	A	⊥	//	AM		⊥	//	⊥	//	AM	⊥	//	AM	Sample	Litho.	Fm.
					[W m^{-1} K^{-1}]			[W m^{-1} K^{-1}]				[W m^{-1} K^{-1}]				[W m^{-1} K^{-1}]		[W m^{-1} K^{-1}]			[W m^{-1} K^{-1}]			[10^{3} kg m^{-3}]		
Zerf-Schichten	Sandy shale	75	Sg3-001	Sandy shale	S_1	2.52	2.98	2.4	2.5	2.5	1.0	2.9	3.0	2.9	1.19	2.99	3.54	2.9	3.0	2.9	3.4	3.5	3.5	2.68	2.67	2.68
(dzu1ZE)			Sg3-002	Sandy shale	S_1	2.30	2.58								1.19	2.74	3.07							2.67		
			Sg3-003	Sandy shale	S_1	2.52	2.45								1.19	3.00	2.91							2.69		
			Sg3-006	Sandy shale	S_1	2.21	2.24								1.19	2.63	2.67							2.59		
			Sg3-009	Sandy shale	S_1	1.95	1.95								1.19	2.32	2.32							2.63		
			Sg3-010	Sandy shale	S_1	2.06	2.32								1.19	2.46	2.75							2.67		
			Sg3-011	Sandy shale	S_1	2.52	2.30								1.19	3.00	2.74							2.65		
			Sg3-012	Sandy shale	S_1	3.13	3.48								1.19	3.72	4.14							2.75		
			Sg3-013	Sandy shale	S_1	2.55	2.33								1.19	3.03	2.77							2.71		
	Quartzitic sst./	25	Sg1-005	Quartzitic sst.	S_0	4.13	4.49	4.1	4.5	4.3	1.1				1.17	4.83	5.26	4.8	5.3	5.0				2.71	2.71	
Dhrontal-Schichten	Sandy shale	70	Sg3-001	Sandy shale	S_1	2.52	2.98	2.4	2.5	2.5	1.0	3.0	3.1	3.0	1.19	2.99	3.54	2.9	3.0	2.9	3.6	3.6	3.6	2.68	2.67	2.67
(ds3DR)			Sg3-002	Sandy shale	S_1	2.30	2.58								1.19	2.74	3.07							2.67		
			Sg3-003	Sandy shale	S_1	2.52	2.45								1.19	3.00	2.91							2.69		
			Sg3-006	Sandy shale	S_1	2.21	2.24								1.19	2.63	2.67							2.59		
			Sg3-009	Sandy shale	S_1	1.95	1.95								1.19	2.32	2.32							2.63		
			Sg3-010	Sandy shale	S_1	2.06	2.32								1.19	2.46	2.75							2.67		
			Sg3-011	Sandy shale	S_1	2.52	2.30								1.19	3.00	2.74							2.65		
			Sg3-012	Sandy shale	S_1	3.13	3.48								1.19	3.72	4.14							2.75		
			Sg3-013	Sandy shale	S_1	2.55	2.33								1.19	3.03	2.77							2.71		
	Quartzitic sst./ quartzite	30	STH-07	Quartzitic sst.	S_0	4.00	4.04	4.3	4.4	4.4	1.0				1.17	4.68	4.73	5.1	5.2	5.1				2.71	2.67	
			STH-08	Quartzitic sst.	S_0	4.29	4.26								1.17	5.02	4.99							2.62		
			STH-09	Quartzitic sst.	S_0	4.92	5.08								1.17	5.76	5.94							2.66		
			STH-11	Sandstone	S_0	4.17	4.30								1.17	4.87	5.03							2.67		

Table A.6 continued

Formation	Lithology	Vol.	Sample	Lithotype	λ_{dry}			Litho. λ_{dry}				Fm. λ_{dry}			TF	λ_{sat} calc.		Litho. λ_{sat}			Fm. λ_{sat}			Density		
(Code)		[%]			O	⊥	//	⊥	//	AM	A	⊥	//	AM		⊥	//	⊥	//	AM	⊥	//	AM	Sample	Litho.	Fm.
					[W m^{-1} K^{-1}]			[W m^{-1} K^{-1}]				[W m^{-1} K^{-1}]				[W m^{-1} K^{-1}]		[W m^{-1} K^{-1}]			[W m^{-1} K^{-1}]			[10^{3} kg m^{-3}]		
Taunusquarzit	Shale	5	OIG-10	Shale	S_1	2.00	2.15	2.2	2.2	2.2	1.0	4.3	4.3	4.3	1.19	2.38	2.56	2.6	2.6	2.6	5.0	5.0	5.0	2.66	2.61	2.66
(ds2TQ)			OIG-12	Shale	S_1	2.18	2.13								1.19	2.59	2.53							2.43		
			OIG-13	Shale	S_1	2.48	2.38								1.19	2.95	2.84							2.74		
	Quartzitic sst./quartzite	95	STH-07	Quartzitic sst.	S_0	4.00	4.04	4.3	4.4	4.4	1.0				1.17	4.68	4.73	5.1	5.2	5.1				2.71	2.67	
			STH-08	Quartzitic sst.	S_0	4.29	4.26								1.17	5.02	4.99							2.62		
			STH-09	Quartzitic sst.	S_0	4.92	5.08								1.17	5.76	5.94							2.66		
			STH-11	Sandstone	S_0	4.17	4.30								1.17	4.87	5.03							2.67		
Hermeskeil-Schichten	Shale	50	OIG-10	Shale	S_1	2.00	2.15	2.2	2.2	2.2	1.0	3.3	3.3	3.3	1.19	2.38	2.56	2.6	2.6	2.6	3.9	3.9	3.9	2.66	2.61	2.64
(ds1HE)			OIG-12	Shale	S_1	2.18	2.13								1.19	2.59	2.53							2.43		
			OIG-13	Shale	S_1	2.48	2.38								1.19	2.95	2.84							2.74		
	Quartzitic sst.	50	STH-07	Quartzitic sst.	S_0	4.00	4.04	4.3	4.4	4.4	1.0				1.17	4.68	4.73	5.1	5.2	5.1				2.71	2.67	
			STH-08	Quartzitic sst.	S_0	4.29	4.26								1.17	5.02	4.99							2.62		
			STH-09	Quartzitic sst.	S_0	4.92	5.08								1.17	5.76	5.94							2.66		
			STH-11	Sandstone	S_0	4.17	4.30								1.17	4.87	5.03							2.67		
Züsch-Schiefer	Shale	80	gd-01	Slate	S_1	2.26	2.37	2.7	2.8	2.8	1.0	3.1	3.2	3.1	1.23	2.78	2.91	3.3	3.4	3.3	3.9	4.0	3.9	2.69	2.72	2.70
(gd)			gd-02	Sandy shale	S_1	3.16	3.29								1.19	3.76	3.92							2.74		
	Quartzitic sst.	20	gd-06	Quartzite	S_0	4.49	4.53	4.5	4.5	4.5	1.0				1.38	6.20	6.25	6.2	6.2	6.2				2.66	2.66	

Table A.7: Details on samples used to compose the thermal conductivity of the Mesozoic geological formations (basin facies) of the Trier–Luxembourg Basin.

						$\lambda_{\perp}$						$\lambda_{//}$						A	
						Sample		Litho.		Unit		Sample		Litho.		Unit		Litho.	
Strat. unit	Lithology	Vol.	Sample	Unit	Lithotype	Dry	Sat	Dry	Sat	Dry	Sat	Dry	Sat	Dry	Sat	Dry	Sat	Dry	Sat
		[%]				[W m^{-1}K^{-1}]						[W m^{-1}K^{-1}]							
dom4b	Sandy marlstone	100	Ru2	dom4b	Calcareous marlstone	2.14	2.54	2.14	2.54	2.1	2.5	2.11	2.47	2.11	2.47	2.1	2.5	1.0	1.0
dom4a	Limestone	80	Ru6	dom4a	Limestone	1.55	2.16	1.55	2.16	1.7	2.3	1.50	2.13	1.50	2.13	1.7	2.3	1.0	1.0
	Reef limestone (corals)	20	Ru4	dom4a	Limestone	2.40	2.68	2.40	2.68			2.65	2.85	2.65	2.85			1.1	1.1
dom3	Sandy limestone	100	M9	dom3	Limestone	2.11	2.49	2.11	2.49	2.1	2.5	2.09	2.48	2.09	2.48	2.1	2.5	1.0	1.0
dom2	Limestone	70	M9	dom3	Limestone	2.11	2.49	2.11	2.49	2.1	2.5	2.09	2.48	2.09	2.48	2.1	2.5	1.0	1.0
	Marlstone	30	M8	dom1	Calcareous marlstone	2.03	2.44	2.03	2.44			1.99	2.39	1.99	2.39			1.0	1.0
dom1	Marlstone	10	M8	dom1	Calcareous marlstone	2.03	2.44	2.03	2.44	1.5	2.3	1.99	2.39	1.99	2.39	1.6	2.5	1.0	1.0
	Marl	90	Bv4	lo4	Silty marl	1.40	2.27	1.40	2.27			1.54	2.49	1.54	2.49			1.1	1.1
lo6-7 + dou	Iron-rich limestone + calcareous sandstone	50	M3	dou	Limestone	1.82	2.31	1.92	2.31	1.5	2.2	1.89	2.33	2.02	2.40	1.6	2.2	1.1	1.0
			M6	dou	Limestone	2.01	2.30					2.14	2.46						
	Iron-rich + marly sst.	50	M5	dou	Iron-rich limestone	1.08	2.02	1.08	2.02			1.23	2.09	1.23	2.09			1.1	1.0
lo5	Marl	100	Bv4	lo4	Silty marl	1.40	2.27	1.40	2.27	1.4	2.3	1.54	2.49	1.54	2.49	1.5	2.5	1.1	1.1
lo4	Sandstone	50	Bv2	lo4	Marly siltstone	1.17	2.80	1.17	2.80	1.3	2.5	1.28	3.00	1.28	3.00	1.4	2.7	1.1	1.1
	Sandy marl	50	Bv4	lo4	Silty marl	1.40	2.27	1.40	2.27			1.54	2.49	1.54	2.49			1.1	1.1
lo3	Marl	83	Bv11	lo3	Claystone	0.93	1.71	0.93	1.71	1.0	1.9	1.56	2.82	1.56	2.82	1.6	2.8	1.7	1.6
	Sandy marl	17	Bv12	lo3	Silty marl	1.41	2.74	1.41	2.74			1.51	2.90	1.51	2.90			1.1	1.1
lo2	Marly claystone	100	Bv14	lo2	Claystone	1.06	1.87	1.08	1.82	1.1	1.8	1.21	2.11	1.26	2.10	1.3	2.1	1.2	1.2
			Bv16	lo1	Claystone	1.09	1.77					1.30	2.09						
lo1	Marly claystone	100	Bv14	lo2	Claystone	1.06	1.87	1.08	1.82	1.1	1.8	1.21	2.11	1.26	2.10	1.3	2.1	1.2	1.2
			Bv16	lo1	Claystone	1.09	1.77					1.30	2.09						
lm3b	Marly sandstone	19	Rb34	lm3a	Silty sandstone	2.43	2.69	2.43	2.69	1.3	1.9	2.18	2.64	2.18	2.64	1.3	2.1	0.9	1.0
	Sandy claystone	81	Rb40	lm3b	Clayey siltstone	0.99	1.73	0.99	1.73			1.12	1.95	1.12	1.95			1.1	1.1
lm3a	Clayey sandstone	2	Rb34	lm3a	Silty sandstone	2.43	2.69	2.43	2.69	1.2	2.1	2.18	2.64	2.18	2.64	1.7	2.8	0.9	1.0
	Silty marl	98	Rb35	lm2	Marl	1.17	2.03	1.23	2.09			1.61	2.75	1.64	2.81			1.3	1.3
			Rb36	lm2	Marl	1.28	2.15					1.67	2.87						

Strat. unit – stratigraphic unit, Vol. – volume fraction, $\lambda_{\perp}$ and $\lambda_{//}$ – thermal conductivity perpendicular and parallel to bedding, Dry and Sat – dry and saturated conditions, respectively, Litho. – lithotype, sst. – sandstone, marlst. – marlstone, calc. – calcareous, fibr. – fibrous. Composition of individual units is estimated from different borehole sections located in the basin facies of the Trier–Luxembourg Basin.

Table A.7 continued

						$\lambda_{\perp}$						$\lambda_{//}$						A	
						Sample		Litho.		Unit		Sample		Litho.		Unit		Litho.	
Strat. unit	Lithology	Vol.	Sample	Unit	Lithotype	Dry	Sat	Dry	Sat	Dry	Sat	Dry	Sat	Dry	Sat	Dry	Sat	Dry	Sat
		[%]				[W m^{-1}K^{-1}]						[W m^{-1}K^{-1}]							
lm3	Clayey sandstone	11	Rb34	lm3a	Silty sandstone	2.43	2.69	2.43	2.69	1.3	2.0	2.18	2.64	2.18	2.64	1.5	2.5	0.9	1.0
	Silty marl	89	Rb35	lm2	Marl	1.17	2.03	1.15	1.97			1.61	2.75	1.47	2.52			1.3	1.3
			Rb36	lm2	Marl	1.28	2.15					1.67	2.87						
			Rb40	lm3b	Clayey siltstone	0.99	1.73					1.12	1.95						
lm2	Clayey marl	100	Rb35	lm2	Marl	1.17	2.03	1.23	2.09	1.2	2.1	1.61	2.75	1.64	2.81	1.6	2.8	1.3	1.3
			Rb36	lm2	Marl	1.28	2.15					1.67	2.87						
lm1	Limestone	23	Rb39	li3	Marly limestone	1.94	2.17	1.94	2.17	1.39	2.1	2.10	2.19	2.10	2.19	1.7	2.7	1.1	1.0
	Marl	77	Rb35	lm2	Marl	1.17	2.03	1.23	2.09			1.61	2.75	1.64	2.81			1.3	1.3
			Rb36	lm2	Marl	1.28	2.15					1.67	2.87						
li4	Clayey, silty marl	87	Rb38	li4	Marly siltstone	1.64	2.29	1.64	2.29	1.7	2.3	1.93	2.63	1.93	2.63	2.0	2.6	1.2	1.1
		13	Rb39	li3	Marly limestone	1.94	2.17	1.94	2.17			2.10	2.19	2.10	2.19			1.1	1.0
li3	Marlstone	59	Rw13	li1	Marlstone	1.28	1.50	1.28	1.50	1.6	1.8	1.88	2.24	1.88	2.24	2.0	2.2	1.5	1.5
	Limestone	41	Rb39	li3	Marly limestone	1.94	2.17	1.94	2.17			2.10	2.19	2.10	2.19			1.1	1.0
li2	Sandstone	45	Rw10	li2	Sandstone	1.77	3.87	1.77	3.87	2.3	3.6	1.71	3.73	1.71	3.73	2.3	3.6	1.0	1.0
	Calcareous sandstone	55	Kb2	li2	Calcareous sandstone	2.83	3.38	2.77	3.43			2.71	3.38	2.81	3.48			1.0	1.0
			Rw2	li2	Marly, calc. sandstone	2.70	3.48					2.90	3.57						
li1	Marlstone	46	Rw13	li1	Marlstone	1.28	1.50	1.28	1.50	1.5	1.8	1.88	2.24	1.88	2.24	1.9	2.3	1.5	1.5
	Sandy marlstone	30	Gr6	li1	Sandy marlstone	1.36	2.08	1.36	2.08			1.70	2.56	1.70	2.56			1.3	1.2
	Limestone	24	Rb39	li3	Marly limestone	1.94	2.17	1.94	2.17			2.10	2.19	2.10	2.19			1.1	1.0
ko	Clayey marl	25	Rb5	km3	Clayey marl	2.30	2.69	2.02	2.47	1.6	2.1	2.50	3.02	2.39	2.97	2.1	2.8	1.2	1.2
			Rb9	km2	Marl	1.73	2.25					2.27	2.92						
	Sandstone + conglomerate	33	Gr7	ko1	Marly sandstone	1.70	2.69	1.70	2.69			2.08	3.27	2.08	3.27			1.2	1.2
	Claystone	42	Rw13	li1	Marlstone	1.28	1.50	1.28	1.50			1.88	2.24	1.88	2.24			1.5	1.5
km3	Dolomitic marlstone	45	Gr11	km3	Dolomitic marlstone	1.57	2.19	1.57	2.19	2.0	2.4	1.67	2.32	1.67	2.32	2.1	2.6	1.1	1.1
	Marl	39	Rb5	km3	Clayey marl	2.30	2.69	2.30	2.69			2.50	3.02	2.50	3.02			1.1	1.1
	Anhydrite + gypsum	11	Rb16	km3	Anhydrite + fibr. gypsum	1.95	1.96	1.95	1.96			1.98	1.94	1.98	1.94			1.0	1.0
	Dolomite	5	Rb17	km1	Dolomite	3.20	3.39	3.20	3.39			3.39	3.37	3.39	3.37			1.1	1.0

Table A.7 continued

						$\lambda_{\perp}$						$\lambda_{//}$						A	
						Sample		Litho.		Unit		Sample		Litho.		Unit		Litho.	
Strat. unit	Lithology	Vol.	Sample	Unit	Lithotype	Dry	Sat	Dry	Sat	Dry	Sat	Dry	Sat	Dry	Sat	Dry	Sat	Dry	Sat
		[%]				[W m^{-1}K^{-1}]						[W m^{-1}K^{-1}]							
km2	Clayey marl	89	Rb9	km2	Marl	1.73	2.25	1.73	2.25	1.8	2.3	2.27	2.92	2.27	2.92	2.4	3.0	1.3	1.3
	Gypsum	0	Rb16	km3	Anhydrite + fibr. gypsum	1.95	1.96	1.95	1.96			1.98	1.94	1.98	1.94			1.0	1.0
	Sandstone	11	Rb8	km2	Dolomitic sandstone	2.68	3.04	2.68	3.04			3.03	3.20	3.03	3.20			1.1	1.1
km2S	Sandstone	90	Ki5	km2S	Silty, micaceous sst.	0.91	1.91	0.91	1.91	1.0	1.9	0.95	2.04	0.95	2.04	1.1	2.1	1.0	1.1
	Claystone	10	Rb9	km2	Marl	1.73	2.25	1.73	2.25			2.27	2.92	2.27	2.92			1.3	1.3
km1	Clayey marl	4	Wb1	km1	Clayey marl	1.29	2.04	1.29	2.04	1.6	2.2	1.45	2.31	1.45	2.31	1.9	2.6	1.1	1.1
	Marl	30	Rb13	km1	Silty marl	1.83	2.66	1.83	2.66			2.12	3.04	2.12	3.04			1.2	1.1
	Sandstone	6	Rb10	km1	Dolomitic sandstone	2.65	3.45	2.65	3.45			2.25	2.91	2.25	2.91			0.8	0.8
	Dolomitic marlstone	60	Wb7	ku	Silty, dolomitic marlstone	1.35	1.81	1.35	1.81			1.82	2.39	1.82	2.39			1.3	1.3
ku	Dolomite	7	Rb17	km1	Dolomite	3.20	3.39	3.20	3.39	1.5	2.0	3.39	3.37	3.39	3.37	1.8	2.4	1.1	1.0
	Marl	39	Wb1	km1	Clayey marl	1.29	2.04	1.29	2.04			1.45	2.31	1.45	2.31			1.1	1.1
	Marlstone	54	Wb7	ku	Silty, dolomitic marlstone	1.35	1.81	1.35	1.81			1.82	2.39	1.82	2.39			1.3	1.3
mos	Dolomitic sandstone	100	Id1	mos	Dolomitic sandstone	3.75	4.82	3.75	4.82	3.8	4.8	3.78	5.02	3.78	5.02	3.8	5.0	1.0	1.0
mo2	Marlstone	5	Wb15	mm1	Marlstone	2.60	2.77	2.60	2.77	3.6	3.7	3.14	3.45	3.14	3.45	3.8	3.8	1.2	1.2
	Dolomite	23	Wb8	mo1	Dolomite	4.17	4.36	4.23	4.32			4.21	4.34	4.27	4.33			1.0	1.0
			Wb12	mo1	Dolomite	4.28	4.28					4.32	4.32						
	Dolomitic siltstone/marlstone	13	Wb9	mo1	Dolomitic siltstone	2.60	3.07	2.76	3.09			2.77	3.16	2.80	3.12			1.0	1.0
			Wb10	mo1	Dolomitic marlstone	2.91	3.10					2.82	3.08						
	Marly dolomite	59	Wb11	mo1	Marly dolomite	3.68	3.80	3.61	3.65			3.83	3.82	3.83	3.83			1.1	1.0
			Wb13	mo1	Marly dolomite	3.53	3.50					3.83	3.83						
mo1	Marlstone	0	Wb15	mm1	Marlstone	2.60	2.77	2.60	2.77	3.9	4.0	3.14	3.45	3.14	3.45	4.0	4.1	1.2	1.2
	Dolomite	52	Wb8	mo1	Dolomite	4.17	4.36	4.23	4.32			4.21	4.34	4.27	4.33			1.0	1.0
			Wb12	mo1	Dolomite	4.28	4.28					4.32	4.32						
	Dolomitic siltstone/marlstone	3	Wb9	mo1	Dolomitic siltstone	2.60	3.07	2.76	3.09			2.77	3.16	2.80	3.12			1.0	1.0
			Wb10	mo1	Dolomitic marlstone	2.91	3.10					2.82	3.08						
	Marly dolomite	45	Wb11	mo1	Marly dolomite	3.68	3.80	3.61	3.65			3.83	3.82	3.83	3.83			1.1	1.0
			Wb13	mo1	Marly dolomite	3.53	3.50					3.83	3.83						

Table A.7 continued

						$\lambda_{\perp}$						$\lambda_{//}$						A	
						Sample		Litho.		Unit		Sample		Litho.		Unit		Litho.	
Strat. unit	Lithology	Vol.	Sample	Unit	Lithotype	Dry	Sat	Dry	Sat	Dry	Sat	Dry	Sat	Dry	Sat	Dry	Sat	Dry	Sat
		[%]				[W m^{-1}K^{-1}]						[W m^{-1}K^{-1}]							
mm2	Marlstone	67	Wb15	mm1	Marlstone	2.60	2.77	2.36	2.72	3.0	3.3	3.14	3.45	2.75	3.19	3.2	3.6	1.2	1.2
			Me2	mm1	Silty, dolomitic marlstone	2.32	2.84					2.61	3.12						
			Me6	mm1	Dolomitic marlstone	2.17	2.56					2.49	3.00						
	Dolomite	33	Wb8	mo1	Dolomite	4.17	4.36	4.23	4.32			4.21	4.34	4.27	4.33			1.0	1.0
			Wb12	mo1	Dolomite	4.28	4.28					4.32	4.32						
mm1	Marl (gypsum-rich)	45	Me12	mm1	Silty marl	1.73	1.94	1.52	1.85	2.4	2.7	1.94	2.15	1.95	2.37	2.7	3.1	1.3	1.3
			Me13	mm1	Silty marl	1.55	1.94					1.96	2.42						
			Me14	mm1	Silty marl	1.29	1.76					2.00	2.65						
			Me15	mm1	Silty marl	1.49	1.77					1.89	2.25						
	Dolomitic marlstone	27	Me2	mm1	Silty, dolomitic marlstone	2.32	2.84	2.36	2.72			2.61	3.12	2.75	3.19			1.2	1.2
			Me6	mm1	Dolomitic marlstone	2.17	2.56					2.49	3.00						
			Wb15	mm1	Marlstone	2.60	2.77					3.14	3.45						
	Dolomite	3	Wb8	mo1	Dolomite	4.17	4.36	4.23	4.32			4.21	4.34	4.27	4.33			1.0	1.0
			Wb12	mo1	Dolomite	4.28	4.28					4.32	4.32						
	Sandstone	13	Me7	mm1	Silty sandstone	3.02	3.61	3.02	3.61			3.12	3.78	3.12	3.78			1.0	1.0
	Anhydrite	12	Me8	mm1	Anhydrite	4.53	4.51	4.53	4.51			4.62	4.52	4.62	4.52			1.0	1.0
mu2	Dolomite	20	Rd18	mu	Marly dolomite	3.36	3.68	3.36	3.68	2.1	2.6	3.45	3.82	3.45	3.82	2.3	2.8	1.0	1.0
	Marlstone	55	Rd17	mu	Dolomitic marlstone	1.82	2.22	1.82	2.22			2.00	2.44	2.00	2.44			1.1	1.1
	Sandy marlstone	25	Rd14	mu	Dolomitic, sandy marlstone	1.66	2.42	1.66	2.42			1.95	2.67	1.95	2.67			1.2	1.1
mu1	Dolomite	2	Rd18	mu	Marly dolomite	3.36	3.68	3.36	3.68	1.7	2.4	3.45	3.82	3.45	3.82	2.0	2.6	1.0	1.0
	Marlstone	31	Rd17	mu	Dolomitic marlstone	1.82	2.22	1.82	2.22			2.00	2.44	2.00	2.44			1.1	1.1
	Sandy marlstone	67	Rd14	mu	Dolomitic, sandy marlst.	1.66	2.42	1.66	2.42			1.95	2.67	1.95	2.67			1.2	1.1
so2	Sandstone	46	Rd1	so1	Dolomitic sandstone	1.75	2.84	1.71	2.99	1.7	2.7	1.83	3.09	1.77	3.19	2.0	3.2	1.0	1.1
			Rd4	so1	Dolomitic sandstone	1.67	3.14					1.71	3.29						
	Claystone	54	Rd12	so1	Silty claystone	1.64	2.38	1.64	2.38			2.22	3.25	2.22	3.25			1.4	1.4
so1	Dolomitic sandstone	71	Rd1	so1	Dolomitic sandstone	1.75	2.84	1.71	2.99	1.7	2.8	1.83	3.09	1.77	3.19	1.9	3.2	1.0	1.1
			Rd4	so1	Dolomitic sandstone	1.67	3.14					1.71	3.29						
	Clayey sst./sandy claystone	29	Rd12	so1	Silty claystone	1.64	2.38	1.64	2.38			2.22	3.25	2.22	3.25			1.4	1.4

Table A.7 continued

						$\lambda_{\perp}$						$\lambda_{//}$						A	
						Sample		Litho.		Unit		Sample		Litho.		Unit		Litho.	
Strat. unit	Lithology	Vol.	Sample	Unit	Lithotype	Dry	Sat	Dry	Sat	Dry	Sat	Dry	Sat	Dry	Sat	Dry	Sat	Dry	Sat
		[%]				[W m^{-1}K^{-1}]						[W m^{-1}K^{-1}]							
sm (+ su)	Sandstone	81	Bi2	sm	Sandstone (soft)	1.77	2.95	1.77	2.95	1.9	3.0	1.84	3.10	1.84	3.10	2.0	3.2	1.0	1.1
	Sandstone (conglomeratic)	12	Bi5	sm	Sandstone (coarse, gravel)	2.86	3.83	2.86	3.83			2.77	3.79	2.77	3.79			1.0	1.0
	Claystone	7	Rd12	so1	Silty claystone	1.64	2.38	1.64	2.38			2.22	3.25	2.22	3.25			1.4	1.4

Table A.8: Details on samples used to compose the thermal conductivity of Mesozoic geological formations (margin facies) of the Trier–Luxembourg Basin.

						$\lambda_{\perp}$						$\lambda_{//}$						A	
						Sample		Litho.		Unit		Sample		Litho.		Unit		Litho.	
Strat. unit	Lithology	Vol.	Sample	Unit	Lithotype	Dry	Sat	Dry	Sat	Dry	Sat	Dry	Sat	Dry	Sat	Dry	Sat	Dry	Sat
		[%]				[W m^{-1} K^{-1}]						[W m^{-1} K^{-1}]							
km2	Sandy marlstone	47	Rb12	km1	Sandy marlstone	2.26	2.46	2.23	2.86	2.2	2.9	2.10	2.50	2.30	3.00	2.3	3.0	1.0	1.0
+ km2S			Rb11	km1	Marly sandstone	2.67	3.17					2.72	3.29						
			El3	km1	Clayey sandstone	2.16	3.15					2.15	3.17						
	Sandy marl	35	Rb13	km1	Silty marl	1.83	2.66	1.83	2.66			2.22	3.04	2.22	3.04			1.2	1.1
	Dolomitic sandstone	18	Rb10	km1	Dolomitic sandstone	2.65	3.45	2.67	3.25			2.25	2.91	2.64	3.06			1.0	0.9
			Rb8	km2	Dolomitic sandstone	2.68	3.04					3.03	3.20						
km1	Sandy marlstone	51	Rb12	km1	Sandy marlstone	2.26	2.46	2.36	2.93	2.6	3.3	2.10	2.50	2.32	2.99	2.5	3.2	1.0	1.0
			Rb11	km1	Marly sandstone	2.67	3.17					2.72	3.29						
			El3	km1	Clayey sandstone	2.16	3.15					2.15	3.17						
	Conglomeratic dolomite	2	Rb17	km1	Dolomite (marly)	3.20	3.39	3.20	3.39			3.39	3.37	3.39	3.37			1.1	1.0
	Dolomitic + sandy congl.	14	Rb19	km1	Sandy, dolomitic congl.	4.11	4.48	4.11	4.48			3.96	4.30	3.96	4.30			1.0	1.0
	Marly sandstone	24	Rb10	km1	Dolomitic sandstone	2.65	3.45	2.65	3.45			2.25	2.91	2.25	2.91			0.8	0.8
	Marl	9	Rb13	km1	Silty marl	1.83	2.66	1.83	2.66			2.22	3.04	2.22	3.04			1.2	1.1
ku	Siltstone	21	Rb21	ku	Silty marlstone	2.84	3.49	2.84	3.49	2.4	3.1	3.59	4.42	3.59	4.42	2.6	3.4	1.3	1.3
	Marl + claystone	23	Ev1	ku	Sandy, dolomitic marlst.	2.09	3.61	1.80	3.15			2.07	3.65	1.92	3.41			1.1	1.1
			Ev3	ku	Sandy, dolomitic marl	1.50	2.69					1.76	3.17						
	Sandstone	48	Rb12	km1	Sandy marlstone	2.26	2.46	2.36	2.93			2.10	2.50	2.32	2.99			1.0	1.0
			Rb11	km1	Marly sandstone	2.67	3.17					2.72	3.29						
			El3	km1	Clayey sandstone	2.16	3.15					2.15	3.17						
	Sandy dolomite	8	Rb17	km1	Dolomite (marly)	3.20	3.39	3.20	3.39			3.39	3.37	3.39	3.37			1.1	1.0

Strat. unit – stratigraphic unit, Vol. – volume fraction, $\lambda_{\perp}$ and $\lambda_{//}$ – thermal conductivity perpendicular and parallel to bedding, Dry and Sat – dry and saturated conditions, respectively, Litho. – lithotype, congl. – conglomerate, marlst. – marlstone. Composition of individual units is estimated from different borehole sections located in the margin facies of the Trier–Luxembourg Basin.

Table A.8 continued

						$\lambda_{\perp}$						$\lambda_{//}$						A	
						Sample		Litho.		Unit		Sample		Litho.		Unit		Litho.	
Strat. unit	Lithology	Vol.	Sample	Unit	Lithotype	Dry	Sat	Dry	Sat	Dry	Sat	Dry	Sat	Dry	Sat	Dry	Sat	Dry	Sat
		[%]				[W m^{-1} K^{-1}]						[W m^{-1} K^{-1}]							
mo(s)	Marly, sandy dolomite	24	Rb24	mo	Marly dolomite	3.50	4.09	3.50	4.09	3.0	3.9	3.54	3.83	3.54	3.83	3.0	3.9	1.0	0.9
(Rebierg +		15	Rb25	mo	Marly, sandy dolomite	4.47	4.58	4.47	4.58			4.09	4.15	4.09	4.15			0.9	0.9
Everlange)	Dolomitic sandstone	23	Ev5	mo	Dolomitic sandstone	2.66	4.11	2.66	4.11			2.70	4.20	2.70	4.20			1.0	1.0
		11	Id1	mos	Dolomitic sandstone	3.75	4.82	3.75	4.82			3.78	5.02	3.78	5.02			1.0	1.0
	Sandstone + siltstone	11	Ev9	mg	Sandstone	1.39	3.05	1.39	3.05			1.48	3.21	1.48	3.21			1.1	1.1
		6	Ev11	mg	Sandy siltstone	1.64	2.76	1.64	2.76			1.81	3.28	1.81	3.28			1.1	1.2
		10	Me11	mm1	Silty sandstone	2.32	2.98	2.32	2.98			2.57	3.30	2.57	3.30			1.1	1.1
mo(s)	Dolomitic sandstone	11	Id1	mos	Dolomitic sandstone	3.75	4.82	3.75	4.82	3.2	3.6	3.78	5.02	3.78	5.02	3.3	3.7	1.0	1.0
(Bissen +	Marlstone	5	Wb15	mm1	Marlstone	2.6	2.77	2.60	2.77			3.14	3.45	3.14	3.45			1.2	1.2
Mersch)	Dolomite	19	Wb8	mo1	Dolomite	4.17	4.36	4.23	4.32			4.21	4.34	4.27	4.33			1.0	1.0
			Wb12	mo1	Dolomite	4.28	4.28					4.32	4.32						
	Dolomitic siltstone/marlstone	54	Wb9	mo1	Dolomitic siltstone	2.60	3.07	2.76	3.09			2.77	3.16	2.80	3.12			1.0	1.0
			Wb10	mo1	Dolomitic marlstone	2.91	3.10					2.82	3.08						
	Marly dolomite	11	Wb11	mo1	Marly dolomite	3.68	3.80	3.61	3.65			3.83	3.82	3.83	3.83			1.1	1.0
			Wb13	mo1	Marly dolomite	3.53	3.50					3.83	3.83						
mg	Sandstone/conglomerate	27	Ev9	mg	Sandstone	1.39	3.05	1.39	3.05	1.7	2.5	1.48	3.21	1.48	3.21	1.9	2.9	1.1	1.1
(Rebierg +	Siltstone	11	Ev11	mg	Sandy siltstone	1.64	2.76	1.64	2.76			1.81	3.28	1.81	3.28			1.1	1.2
Everlange)		12	Me11	mm1	Silty sandstone	2.32	2.98	2.32	2.98			2.57	3.30	2.57	3.30			1.1	1.1
	Dolomite	4	Rd18	mu	Marly dolomite	3.36	3.68	3.36	3.68			3.45	3.82	3.45	3.82			1.0	1.0
	Clay-/marlstone	46	Me12	mm1	Silty marl	1.73	1.94	1.52	1.85			1.94	2.15	1.95	2.37			1.3	1.3
			Me13	mm1	Silty marl	1.55	1.94					1.96	2.42						
			Me14	mm1	Silty marl	1.29	1.76					2.00	2.65						
			Me15	mm1	Silty marl	1.49	1.77					1.89	2.25						

Table A.8 continued

						$\lambda_{\perp}$						$\lambda_{//}$						A	
						Sample		Litho.		Unit		Sample		Litho.		Unit		Litho.	
Strat. unit	Lithology	Vol. [%]	Sample	Unit	Lithotype	Dry	Sat	Dry	Sat	Dry	Sat	Dry	Sat	Dry	Sat	Dry	Sat	Dry	Sat
						[W m^{-1} K^{-1}]						[W m^{-1} K^{-1}]							
mm	Marl (gypsum-rich)	70	Me12	mm1	Silty marl	1.73	1.94	1.52	1.85	2.0	2.3	1.94	2.15	1.95	2.37	2.3	2.7	1.3	1.3
(Mersch)			Me13	mm1	Silty marl	1.55	1.94					1.96	2.42						
			Me14	mm1	Silty marl	1.29	1.76					2.00	2.65						
			Me15	mm1	Silty marl	1.49	1.77					1.89	2.25						
	Dolomite	5	Wb8	mo1	Dolomite	4.17	4.36	4.23	4.32			4.21	4.34	4.27	4.33			1.0	1.0
			Wb12	mo1	Dolomite	4.28	4.28					4.32	4.32						
	Dolomitic marlstone	21	Me2	mm1	Silty, dolomitic marlstone	2.32	2.84	2.50	3.00			2.61	3.12	2.69	3.30			1.1	1.1
			Me6	mm1	Dolomitic marlstone	2.17	2.56					2.23	3.00						
			Me7	mm1	Silty sandstone	3.02	3.61					3.22	3.78						
	Anhydrite	4	Me8	mm1	Anhydrite	4.53	4.51	4.53	4.51			4.62	4.52	4.62	4.52			1.0	1.0
mu	Sandy/marly dolomite	3	Rd18	mu	Marly dolomite	3.36	3.68	3.36	3.68	1.7	2.5	3.45	3.82	3.45	3.82	2.1	3.2	1.0	1.0
	Sandstone	6	Ev13	mu	Dolomitic sandstone	1.65	3.04	1.65	3.04			1.70	3.07	1.70	3.07			1.0	1.0
	Sandy marlstone	3	Rd14	mu	Dolomitic, sandy marlst.	1.66	2.42	1.66	2.42			1.95	2.67	1.95	2.67			1.2	1.1
	Dolomitic marlstone	11	Rd17	mu	Dolomitic marlstone	1.82	2.22	1.82	2.22			2.00	2.44	2.00	2.44			1.1	1.1
	Claystone	51	Rd12	so1	Silty claystone	1.64	2.38	1.64	2.38			2.22	3.25	2.22	3.25			1.4	1.4
	Siltstone	26	Ev11	mg	Sandy siltstone	1.64	2.76	1.64	2.76			1.81	3.28	1.81	3.28			1.1	1.2
so2	Dolomitic sandstone	22	Rd1	so1	Dolomitic sandstone	1.75	2.84	1.71	2.99	1.6	2.6	1.83	3.09	1.77	3.19	2.0	3.2	1.0	1.1
			Rd4	so1	Dolomitic sandstone	1.67	3.14					1.71	3.29						
	Sandstone	24	Ev19	so	Marly sandstone	1.53	2.75	1.53	2.75			1.70	2.99	1.70	2.99			1.1	1.1
	Claystone + (sandy) siltstone	54	Rd12	so1	Silty claystone	1.64	2.38	1.64	2.38			2.22	3.25	2.22	3.25			1.4	1.4
so1	Conglomerate	25	Ev25	so	Sandy, dolomitic congl.	2.81	3.42	2.81	3.42	1.9	2.9	2.87	3.58	2.87	3.58	2.1	3.2	1.0	1.0
	Conglomeratic sandstone	43	Ev24	so	Sandstone (conglomeratic)	1.42	2.84	1.61	2.94			1.59	2.88	1.71	3.09			1.1	1.0
			Rd1	so1	Sandstone (dolomitic)	1.75	2.84					1.83	3.09						
			Rd4	so1	Sandstone (dolomitic)	1.67	3.14					1.71	3.29						
	Marly sandstone	17	Ev19	so	Marly sandstone	1.53	2.75	1.53	2.75			1.70	2.99	1.70	2.99			1.1	1.1
	Claystone + siltstone	15	Rd12	so1	Silty claystone	1.64	2.38	1.64	2.38			2.22	3.25	2.22	3.25			1.4	1.4

Table A.9: Summary of petrophysical properties of the Cambrian and Ordovician groups, geological formations and their members in the Lower Paleozoic Stavelot Massif.

Stratigraphy	Group	Formation	Code	Mbr.	Lithology	Vol.	Fm. λ_{dry}			Fm. λ_{sat}				Error	Formation		Thickness range				
							⊥	//	AM	⊥	//	AM	A		d	H	Min.	Ref.		Max.	Ref.
						[%]	[W m^{-1} K^{-1}]			[W m^{-1} K^{-1}]			[-]	[%]	[10^{3} kg m^{-3}]	[10^{-6} W m^{-3}]	[m]			[m]	
Ordovician	SALM	Bihain	BIH		Silty slate (includes slate 65% and minor sandstone 15 %)	100	2.0	2.4	2.2	2.3	2.8	2.6	1.2	10	2.78	2.1	200	a	–	300	a
		Ottré	OTT	COL	Slate	100	2.2	2.6	2.4	2.7	3.2	3.0	1.2	10	2.87	2.3	50	c	–	100	a
				PLA	Slate	100	1.9	2.7	2.3	2.4	3.3	2.8	1.4	15	2.89	1.9	30	c	–	50	a
				MEU	Silty slate	90	2.4	2.9	2.6	2.9	3.4	3.1	1.2	15	2.91	1.8	70	c	–	150	a
					Sandstone	10															
		Jalhay	JAL	LIE	Silty slate	80	2.6	2.8	2.7	3.1	3.3	3.2	1.1	10	2.69	1.9	80	c	–	100	a
					Sandstone	20															
				SPA	Silty slate	40	3.3	3.5	3.4	3.9	4.1	4.0	1.1	15	2.69	1.5	200	a		200	a
					Quartzitic sst.	60															
				SLW	Slate	20	3.2	3.7	3.4	3.7	4.2	3.9	1.1	15	2.72	2.0	60	c	–	250	a
					Silty slate	50															
					Quartzite	30															
Cambrian	REVIN	La Gleize	GLE	Rv5	Slate	50	2.4	3.5	3.0	2.7	3.8	3.3	1.4	5	2.75	2.5	> 300	a	>	300	a
(Upper)					Silty slate	50															
		La Venne	VEN	Rv3 + 4	Slate	30	4.4	4.9	4.7	4.9	5.5	5.2	1.1	5	2.72	1.7	500	c	>	500	a
					Quartzite	70															
		Wanne	WAN	Rv1 + 2	Slate	40	3.3	4.3	3.8	4.0	5.0	4.5	1.3	5	2.75	2.1	200	a	–	650	c
					Silty slate	20															
					Quartzite	40															
(Lower)	DEVILLE	Bellevaux	BEL		Slate/shale	45	3.6	3.9	3.8	4.3	4.7	4.5	1.1	10	2.66	1.3	150	a, c	–	250	a
					Quartz. sst./quartzite	55															
		Hour	HUR		Slate	40	3.6	4.0	3.8	4.3	4.6	4.5	1.1	15	2.70	1.2	> 150	a, c	>	1200	b
					Quartzite	60															
Total thickness																	1990		>	4050	

Mbr. – Member, Vol. – volume fraction, Fm. – formation, λ_{dry} and λ_{sat} – thermal conductivity under dry and saturated conditions, respectively, ⊥ and // – thermal conductivity perpendicular and parallel to cleavage, AM – arithmetic mean, A – anisotropy, d – density, H – radiogenic heat production, Ref. – literature reference, Quartz. – quartzitic, sst. – sandstone. Thickness range of the individual formations after a) Geukens (2008), b) Hollmann (1997) and c) Verniers et al. (2001). Lithological composition is estimated after Geukens (2008) and Verniers et al. (2001).

Table A.10: Summary of petrophysical properties of the Lower Devonian geological formations in the Belgian and Luxembourgish Ardennes.

Stratigraphy	Formation	Code		Lithology	Vol.	Fm. λ_{dry}			Fm. λ_{sat}				Error	Fm.		Thickness range							
						⊥	//	AM	⊥	//	AM	A		d	H	Min.	Ref.		Max.	Ref.		Max.	Ref.
		Be	Lux		[%]	[$Wm^{-1}K^{-1}$]			[$Wm^{-1}K^{-1}$]			[-]	[%]	[10^3 kg m^{-3}]	[10^{-6} W m^{-3}]	[m]			[m]			[m]	
Emsian	Wiltz		E3	Sandy shale	100	2.2	2.0	2.1	2.6	2.4	2.5	0.9	10	2.62	2.0	250	g	>	1200	e			
	Berlé		q	Quartzite	100	4.5	4.5	4.5	6.2	6.2	6.2	1.0	20	2.50	0.6	0	g	–	15	g			
	Clervaux		E2	Shale/siltstone	70	2.9	2.9	2.9	3.3	3.3	3.3	1.0	15	2.66	1.5	200	g	–	660	e	–	1400	d
				Sandstone	25																		
				Quartzitic sst.	5																		
	Schuttbourg		E1b	Silty slate/siltstone	70	2.8	3.1	2.9	3.5	3.5	3.5	1.0	15	2.68	1.5	750	g	–	1200	e	>	3500	f
				Sandstone	20																		
				Quarzitic sst.	10																		
	Stolzembourg		E1a	Sandy shale	94	2.6	2.7	2.7	3.1	3.3	3.2	1.0	15	2.73	2.0	700	c	–	900	e			
				Quartzitic sst.	6																		
Siegenian	La Roche	LAR	Sg3	Sandy shale	100	2.4	2.5	2.5	2.9	3.0	2.9	1.0	15	2.67	2.0	> 1400	e	–	1500	b			
(~Praguian)			Sg3a	Slate	100	2.4	2.9	2.6	2.9	3.5	3.2	1.2	10	2.73	2.0				400	b			
	Villé	VIL	Sg2	Shale/siltstone	35	3.0	3.0	3.0	3.5	3.5	3.5	1.0	15	2.58	1.5	250	a, c	–	550	c			
				Siltstone + calc. sst/ sandy limestone	65																		
	Mirwart	MIR	Sg1	Slate	80	2.8	2.9	2.8	3.4	3.5	3.4	1.0	10	2.73	1.8	700	a	–	1050	c			
				Silty slate	5																		
				Quartz. sst./quartzite	15																		

Be – Belgium, Lux – Luxembourg, Vol. – volume fraction, Fm. – formation, λ_{dry} and λ_{sat} – thermal conductivity under dry and saturated conditions, respectively, ⊥ and // – thermal conductivity perpendicular and parallel to cleavage, AM – arithmetic mean, A – anisotropy, d – density, H – radiogenic heat production, Ref. – literature reference, sst. – sandstone, calc. – calcareous, Quartz. – quartzitic, Congl. – conglomeratic. Composition of the individual formations is estimated after Dejonghe (2008) and Lucius (1950). The highly variable thickness estimates or ranges are retrieved from a) Bultynck & Dejonghe (2001), b) Colbach & Maquil (2003), c) Dejonghe (2008), d) Furtak (1965), e) Hollmann (1997) and f) Konrad & Wachsmut (1973) and g) Lucius (1950).

Table A.10 continued

Stratigraphy	Formation	Code		Lithology	Vol.	Fm. λ_{dry}			Fm. λ_{sat}				Error	Fm.		Thickness range						
		Be	Lux			⊥	//	AM	⊥	//	AM	A		d	H	Min.	Ref.		Max.	Ref.	Max.	Ref.
					[%]	[$Wm^{-1}K^{-1}$]			[$Wm^{-1}K^{-1}$]			[-]	[%]	[10^3 kg m^{-3}]	[10^{-6} W m^{-3}]	[m]			[m]		[m]	
Lochkovian	Saint-Hubert	STH		Shale/siltstone	80	3.3	3.3	3.3	3.9	3.9	3.9	1.0	15	2.70	1.8	550	a, c	–	700	a, c		
				Sandstone	20																	
	Oignies	OIG		Siltstone	15	2.6	2.6	2.6	3.0	3.0	3.0	1.0	10	2.60	1.7	700	c	–	1200	c		
				Shale	60																	
				Sandstone	25																	
	Fépin	FEP		Shale/siltstone	50	3.7	3.7	3.7	4.3	4.4	4.3	1.0	15	2.67	1.4	20	a, c	>	300	a		
				Sandstone	20																	
				Congl. sst.	30																	
Total thickness																5520		>	9675		> 12715	

Table A.11: Summary of petrophysical properties of the Lower Devonian and Proterozoic geological formations in the Eifel and Mosel Syncline/Hunsrück regions.

Region	Stratigraphy	Formation	Code	Lithology	Vol.	Fm. λ_{dry}			Fm. λ_{sat}				Error	Fm.		Thickness range				
						⊥	//	AM	⊥	//	AM	A		d	H	Min.	Ref.		Max.	Ref.
					[%]	[W m^{-1} K^{-1}]			[W m^{-1} K^{-1}]			[-]	[%]	[10^{3} kg m^{-3}]	[10^{-6} W m^{-3}]	[m]			[m]	
Eifel/ Mosel Syncline	Eifelian	Wissenbach-Schiefer	de/dzoWI	Shale	> 90	2.5	2.5	2.5	3.0	2.9	3.0	1.0	15	2.64	1.9	400	a	–	450	a
				Quartzitic sst.	< 10															
	Emsian	Kieselgallenschiefer	dzo3KG	Shale/shaly siltstone	> 90	2.4	2.3	2.3	2.8	2.8	2.8	1.0	15	2.64	2.0	50	a	–	500	a
	(Upper)			Siltstone/sandstone	< 10															
		Sphärosideritschiefer	dzo3SS	Shale/shaly siltstone	> 80	2.6	2.5	2.6	3.1	3.0	3.0	1.0	15	2.65	1.9	100	a	–	250	a
				Sandstone	< 20															
		Brauneisenstein	dzo3BE	Sandstone	> 70	3.2	3.1	3.1	3.7	3.7	3.7	1.0	15	2.65	1.2	30	a	–	40	a
				Shale/shaly siltstone	< 30															
		Rötelgallen-Schichten	dzo2RG	Shale	50	2.9	2.9	2.9	3.4	3.4	3.4	1.0	15	2.65	1.5	30	a	–	40	a
				Sandstone + limestone	50															
		Höllenthal-Schichten	dzo2HÖ	Shale	50	2.9	2.9	2.9	3.4	3.4	3.4	1.0	15	2.65	1.5	60	a	–	130	a
				Sandstone	50															
		Flußbach-Schichten	dzo1FL	Shale/shaly siltstone	40	3.4	3.4	3.4	3.6	3.6	3.6	1.0	15	2.65	1.4	20	a	–	200	a, b
				Quartzitic sst.	60															
		Emsquarzit	dzo1EQ	Quartzitic sst./quartzite	> 90	4.3	4.3	4.3	5.8	5.8	5.8	1.0	20	2.51	0.7	15	a	–	200	a
				Shale	< 10															
	(Lower)	Klerf-Schichten	dzu3KL	Shale/shaly siltstone	30	3.4	3.4	3.4	3.9	3.9	3.9	1.0	15	2.67	1.2	500	b	–	1200	b
				Sandstone/quartzite	70															
		Gladbach-Schichten	dzu3GL	Shale	50–70	2.8	2.9	2.8	3.3	3.4	3.4	1.0	10	2.72	1.9	3000	b	–	3000	b
				Siltstone/sandstone	30–50															
		"Singhofen-Schichten"	dzS	Shale/sandy shale	90	2.7	2.8	2.7	3.2	3.3	3.2	1.0	15	2.73	1.9	0		>	1000	b
				Sandstone	10															

Vol. – volume fraction, Fm. – formation, λ_{dry} and λ_{sat} – thermal conductivity under dry and saturated conditions, respectively, ⊥ and // – thermal conductivity perpendicular and parallel to cleavage, AM – arithmetic mean, A – anisotropy, d – density, H – radiogenic heat production, Ref. – literature reference, sst. – sandstone. Composition of the individual formations is taken from Häfner et al. (2007) and completed by LGB (2005). The regional thickness estimates are retrieved from a) Häfner et al. (2007), b) LGB (2005), c) Wildberger (1992) and d) own completing estimates.

Table A.11 continued

Region	Stratigraphy	Formation	Code	Lithology	Vol.	Fm. λ_{dry}			Fm. λ_{sat}				Error	Fm.		Thickness range				
						⊥	//	AM	⊥	//	AM	A		d	H	Min.	Ref.		Max.	Ref.
					[%]	[W m^{-1} K^{-1}]			[W m^{-1} K^{-1}]			[-]	[%]	[10^{3} kg m^{-3}]	[10^{-6} W m^{-3}]	[m]			[m]	
Hunsrück		Kaubschichten	dzu1KA	Shale	85	2.4	2.6	2.5	2.9	3.1	3.0	1.1	15	2.67	2.0	> 1500	c	>	1700	b
				Quartzitic sst.	15															
		Zerf-Schichten	dzu1ZE	Sandy shale	75	2.9	3.0	2.9	3.4	3.5	3.5	1.0	15	2.68	1.8	500	d	–	1000	d
				Quartzitic sst./quarzite	25															
	Siegenian (~Praguian)	Dhrontal-Schichten	ds3DR	Sandy shale	70	3.0	3.1	3.0	3.6	3.6	3.6	1.0	10	2.66	1.7	700	d	–	1000	c
				Quartzitic sst./quartzite	30															
		Taunusquarzit	ds2TQ	Quartzitic sst./quartzite	> 95	4.3	4.3	4.3	5.0	5.0	5.0	1.0	10	2.66	0.6	> 800	c	–	1200	c
		Hermeskeil-Schichten	ds1HE	Shale	50	3.3	3.3	3.3	3.9	3.9	3.9	1.0	10	2.64	1.5	150	b	–	600	b
				Quartzitic sst.	50															
	Gedinnian (~Loch-kovian)	Züsch-Schiefer	gd	Shale	80	3.1	3.2	3.1	3.9	4.0	3.9	1.0	20	2.70	1.8	> 1100	c	–	2000	b
				Quartzitic sst.	20															
	Neo-proterozoic	Wartenstein Gneiss	War	Gneiss	85			3.0			3.6			2.64	1.3	?			?	
				Quartzitic sst.	5															
				Quartzite	5															
				Micaschist	5															
Total thickness																> 8955		>	14510	

Table A.12: Summary of petrophysical properties of the Mesozoic geological formations (basin facies) of the Trier–Luxembourg Basin.

				Formation									Thickness range	
				$\lambda_{\perp}$		$\lambda_{//}$				d		ϕ	Unit	
Stratigraphy	Stratigraphic unit	Unit	Lithology	Vol.	Dry	Sat	Dry	Sat	A	Error	Dry	Sat	Min.	Max.
				[%]	[W $m^{-1}K^{-1}$]		[W $m^{-1}K^{-1}$]			[%]	[10^3 kg m^{-3}]		[%]	[m]	
Dogger	Marnes sableuses d'Audun-le-Tiche	dom4b	Sandy marlstone	100	2.1	2.5	2.1	2.5	1.0	15	2.35	2.48	13.4	15	15
	Calcaires d'Audun-le-Tiche	dom4a	Limestone	80	1.7	2.3	1.7	2.3	1.0	15	2.09	2.31	22.4	20	20
			Reef limestone (corals)	20											
	Calcaire de Haut-Pont	dom3	Sandy limestone	100	2.1	2.5	2.1	2.5	1.0	10	2.51	2.59	8.2	15	25
	Calcaire d'Ottange	dom2	Limestone	70	2.1	2.5	2.1	2.5	1.0	15	2.50	2.59	8.4	12	20
			Marlstone	30											
	Marnes micacées	dom1	Marlstone	10	1.5	2.3	1.6	2.5	1.1	15	2.10	2.26	15.7	8	12
			Marl	90											
Liassic + Aalenian	Minette	lo6-7 + dou	Iron-rich limestone + calc. sst.	50	1.5	2.2	1.6	2.2	1.0	15	2.25	2.43	18.2	11	68
			Iron-rich + marly sst.	50											
	C. à P. fallaciosum	lo5	Marl	100	1.4	2.3	1.5	2.5	1.1	15	2.06	2.22	16.5	10	10
	C. à G. striatulum	lo4	Sandstone	50	1.3	2.5	1.4	2.7	1.1	10	2.01	2.23	21.7	15	25
			Sandy marl	50											
	Marnes à A. voltzi	lo3	Marl	83	1.0	1.9	1.6	2.8	1.5	10	2.06	2.27	20.8	15	23
			Sandy marl	17											
	C. à H. bifrons	lo2	Marly claystone	100	1.1	1.8	1.3	2.1	1.2	5	2.12	2.31	19.5	20	30
	C. à H. falciferum	lo1	Marly claystone	100	1.1	1.8	1.3	2.1	1.2	5	2.12	2.31	19.5	25	35
	Macigno	lm3b	Marly sandstone	19	1.3	1.9	1.3	2.1	1.1	15	2.09	2.27	16.7	20	45
			Sandy claystone	81											
	Faciès sablo-marneux	lm3a	Clayey sandstone	2	1.2	2.1	1.7	2.8	1.3	15	2.16	2.35	19.2	15	35
			Silty marl	98											
	C. à P. spinatum	lm3	Clayey sandstone	11	1.3	2.0	1.5	2.5	1.2	15	2.14	2.32	18.0	25	35
			Silty marl	89											
	C. à A. margaritatus	lm2	Clayey marl	100	1.2	2.1	1.6	2.8	1.3	5	2.16	2.35	19.4	80	90
	Calcaire ocreux	lm1	Limestone	23	1.4	2.1	1.7	2.7	1.3	15	2.26	2.42	15.8	4	15
			Marl (calcareous)	77											

Vol. – volume fraction, $\lambda_{\perp}$ and $\lambda_{//}$ – thermal conductivity perpendicular and parallel to bedding, Dry and Sat – dry and saturated conditions, respectively, A – anisotropy, d – density, ϕ – porosity, C. – couches, calc. – calcareous, sst. – sandstone. Composition of individual units is an average of different borehole sections located in the basin facies of the Trier–Luxembourg Basin. Indicative thickness ranges are retrieved from the geological maps 1: 25,000 and completed after Schintgen & Förster (2013).

Table A.12 continued

					Formation									Thickness range	
					$\lambda_{\perp}$		$\lambda_{//}$				d		ϕ	Unit	
Stratigraphy	Stratigraphic unit	Unit	Lithology	Vol.	Dry	Sat	Dry	Sat	A	Error	Dry	Sat		Min.	Max.
				[%]	[W m^{-1}K^{-1}]		[W m^{-1}K^{-1}]			[%]	[10^{3} kg m^{-3}]		[%]	[m]	
	Marnes pauvres en fossiles	li4	Clayey, silty marl	87	1.7	2.3	2.0	2.6	1.1	10	2.30	2.39	9.1	30	40
			Limestone	13											
	Marnes et calcaires de Strassen	li3	Marlstone	59	1.6	1.8	2.0	2.2	1.3	10	2.44	2.49	5.5	8	10
			Limestone	41											
	Grès de Luxembourg	li2	Sandstone	45	2.3	3.6	2.3	3.6	1.0	5	2.21	2.38	16.9	10	105
			Calcareous sandstone	55											
	Marnes d'Elvange	li1	Marlstone	46	1.5	1.8	1.9	2.3	1.3	10	2.35	2.43	7.5	0	30
			Sandy marlstone	30											
			Limestone	24											
Keuper	Rhät	ko	Clayey marl	25	1.6	2.1	2.1	2.8	1.3	15	2.30	2.40	9.3	0	17
			Sandstone + conglomerate	33											
			Claystone	42											
	Steinmergelkeuper	km3	Dolomitic marlstone	45	2.0	2.4	2.1	2.6	1.1	10	2.39	2.47	7.9	50	75
			Marl	39											
			Anhydrite + gypsum	11											
			Dolomite	5											
	Rote Gipsmergel	km2	Clayey marl	89	1.8	2.3	2.4	3.0	1.3	15	2.34	2.43	8.8	15	30
			Gypsum	0											
			Sandstone	11											
	Schilfsandstein	km2S	Sandstone	90	1.0	1.9	1.1	2.1	1.1	15	1.90	2.18	28.1	0	50
			Claystone	10											
	Pseudomorphosen-keuper	km1	Clayey marl	4	1.6	2.2	1.9	2.6	1.2	15	2.32	2.43	10.9	50	100
			Marl	30											
			Sandstone	6											
			Dolomitic marlstone	60											
	Lettenkeuper	ku	Dolomite	7	1.5	2.0	1.8	2.4	1.2	15	2.30	2.43	12.0	15	28
			Marl	39											
			Marlstone	54											

Table A.12 continued

					Formation									Thickness range	
					$\lambda_{\perp}$		$\lambda_{//}$				d		ϕ	Unit	
Stratigraphy	Stratigraphic unit	Unit	Lithology	Vol.	Dry	Sat	Dry	Sat	A	Error	Dry	Sat		Min.	Max.
				[%]	[W m^{-1}K^{-1}]		[W m^{-1}K^{-1}]			[%]	[10^{3} kg m^{-3}]		[%]	[m]	
Muschelkalk	Gilsdorfer Sandstein	mos	Dolomitic sandstone	100	3.8	4.8	3.8	5.0	1.0	10	2.60	2.66	6.4	0	10
	Ceratitenschichten	mo2	Marl	5	3.6	3.7	3.8	3.8	1.0	10	2.74	2.77	2.3	20	30
			Dolomite	23											
			Dolomitic siltstone/marlstone	13											
			Marly dolomite	59											
	Trochitenschichten	mo1	Dolomite	52	3.9	4.0	4.0	4.1	1.0	10	2.78	2.80	1.6	20	34
			Dolomitic siltstone/marlstone	3											
			Marly dolomite	45											
	Linguladolomit	mm2	Marlstone	67	3.0	3.3	3.2	3.6	1.1	10	2.56	2.59	3.5	0	7
			Dolomite	33											
	Gipsmergel	mm1	Marl (gypsum-rich)	45	2.4	2.7	2.7	3.1	1.1	15	2.43	2.48	5.3	50	108
			Dolomitic marlstone	27											
			Dolomite	3											
			Sandstone	13											
			Anhydrite	12											
	Orbicularisschichten	mu2	Dolomite	20	2.1	2.6	2.3	2.8	1.1	15	2.46	2.54	7.6	0	7
			Marlstone	55											
			Sandy marlstone	25											
	Muschelsandstein	mu1	Dolomite	2	1.7	2.4	2.0	2.6	1.1	15	2.39	2.50	10.2	25	45
			Marlstone	31											
			Sandy marlstone	67											

Table A.12 continued

					Formation									Thickness range	
					$\lambda_{\perp}$		$\lambda_{//}$				d		ϕ	Unit	
Stratigraphy	Stratigraphic unit	Unit	Lithology	Vol.	Dry	Sat	Dry	Sat	A	Error	Dry	Sat		Min.	Max.
				[%]	[W m^{-1}K^{-1}]		[W m^{-1}K^{-1}]			[%]	[10^{3} kg m^{-3}]		[%]	[m]	
Buntsandstein	Voltziensandstein	so2	Sandstone	46	1.7	2.7	2.0	3.2	1.2	10	2.23	2.38	15.0	12	15
			Claystone	54											
	Zwischenschichten	so1	Dolomitic sandstone	71	1.7	2.8	1.9	3.2	1.1	10	2.20	2.37	16.7	75	150
			Clayey sst./sandy claystone	29											
	Vogesensandstein	sm (+ su)	Sandstone	81	1.9	3.0	2.0	3.2	1.1	15	2.08	2.29	20.6	15	340
			Sandstone (conglomeratic)	12											
			Claystone	7											

Table A.13: Summary of petrophysical properties of Mesozoic geological formations (margin facies) of the Trier–Luxembourg Basin.

					Formation									Thickness range	
					$\lambda_{\perp}$		$\lambda_{//}$				d		ϕ	Unit	
Stratigraphy	Stratigraphic unit	Unit	Lithology	Vol.	Dry	Sat	Dry	Sat	A	Error	Dry	Sat		Min.	Max.
				[%]	[W m^{-1}K^{-1}]		[W m^{-1}K^{-1}]			[%]	[10^{3} kg m^{-3}]		[%]	[m]	
Keuper	Rote Gipsmergel + Schilfsandstein	km2 + km2S	Sandy marlstone	47	2.2	2.9	2.3	3.0	1.1	15	2.34	2.43	9.8	2.5	19
			Sandy marl	35											
			Dolomitic sandstone	18											
	Pseudomorphosen-keuper	km1	Sandy marlstone	51	2.6	3.3	2.5	3.2	1.0	15	2.40	2.48	8.3	5	50
			Conglomeratic dolomite	2											
			Dolomitic + sandy conglomerate	14											
			Marly sandstone	24											
			Marl	9											
	Lettenkeuper	ku	Siltstone	21	2.4	3.1	2.6	3.4	1.1	15	2.39	2.49	9.7	6	15
			Marl + claystone	23											
			Sandstone	48											
			Sandy dolomite	8											
Muschelkalk	Gilsdorfer Sandstein	mo(s)	Marly, sandy dolomite	24	3.0	3.9	3.0	3.9	1.0	20	2.50	2.59	9.4	4	30
	+ Ceratitenschichten	(Rebierg +		15											
	+ Trochitenschichten	Everlange)	Dolomitic sandstone	23											
				11											
			Sandstone + siltstone	11											
				6											
				10											
		mo(s)	Dolomitic sandstone	11	3.2	3.6	3.3	3.7	1.0	20	2.67	2.71	4.4		
		(Bissen +	Marlstone	5											
		Mersch)	Dolomite	19											
			Dolomitic siltstone/marlstone	54											
			Marly dolomite	11											

Vol. – volume fraction, $\lambda_{\perp}$ and $\lambda_{//}$ – thermal conductivity perpendicular and parallel to bedding, Dry and Sat – dry and saturated conditions, respectively, A – anisotropy, d – density, ϕ – porosity. Composition of individual units is an average of different borehole sections located in margin facies of the Trier–Luxembourg Basin. Indicative thickness ranges are retrieved from the geological maps 1: 25,000.

Table A.13 continued

Stratigraphy	Stratigraphic unit	Unit	Lithology	Vol.	Formation $\lambda_{\perp}$ Dry	$\lambda_{\perp}$ Sat	$\lambda_{//}$ Dry	$\lambda_{//}$ Sat	A	Error	d Dry	d Sat	ϕ	Thickness range Unit Min.	Max.
				[%]	[W m^{-1}K^{-1}]		[W m^{-1}K^{-1}]			[%]	[10^{3} kg m^{-3}]		[%]	[m]	
	Grobklastischer Muschelkalk	mg	Sandstone/ conglomerate	27	1.7	2.5	1.9	2.9	1.2	20	2.24	2.38	13.5	5	50
		(Rebierg +	Siltstone	11											
		Everlange)		12											
			Dolomite	4											
			Clay-/marlstone	46											
	Gipsmergel	mm	Marl (gypsum-rich)	70	2.0	2.3	2.3	2.7	1.2	20	2.37	2.43	6.3		
		(Mersch)	Dolomite	5											
			Dolomitic marlstone	21											
			Anhydrite	4											
	Muschelsandstein	mu	Sandy/marly dolomite	3	1.7	2.5	2.1	3.2	1.2	20	2.28	2.42	13.3	0	25
			Sandstone	6											
			Sandy marlstone	3											
			Dolomitic marlstone	11											
			Claystone	51											
			Siltstone	26											
Buntsandstein	Voltziensandstein	so2	Dolomitic sandstone	22	1.6	2.6	2.0	3.2	1.2	15	2.22	2.36	14.5	0	12
			Sandstone	24											
			Claystone + (sandy) siltstone	54											
	Zwischenschichten	so1	Conglomerate	25	1.9	2.9	2.1	3.2	1.1	15	2.23	2.38	15.3	15	75
			Conglomeratic sandstone	43											
			Marly sandstone	17											
			Claystone + siltstone	15											

Table A.14: Details on samples used to compose the radiogenic heat production of the Cambrian and Ordovician groups, geological formations and their members in the Lower Paleozoic Stavelot Massif.

Group	Fm.	Mbr.	Lithology	Vol. [%]	Sample	Lithotype	H Sample [10^{-6} W m^{-3}]	H Litho. [10^{-6} W m^{-3}]	H Fm. [10^{-6} W m^{-3}]
SALM	BIH		Silty slate (includes slate 65% and minor sandstone 15 %)	100	BIH-06	Silty slate	2.09	2.1	2.1
	OTT	COL	Slate	100	COL-05	Slate	2.34	2.3	2.3
		PLA	Slate	100	PLA-01	Slate	1.89	1.9	1.9
		MEU	Silty slate	90	PLA-01	Slate	1.89	1.9	1.8
			Sandstone	10	Sg1-07	Quartzitic sst.	1.18	1.2	
	JAL	LIE	Silty slate	80	SPA-02	Silty slate	2.04	2.0	1.9
			Sandstone	20	Sg1-07	Quartzitic sst.	1.18	1.2	
		SPA	Silty slate	40	SPA-02	Silty slate	2.04	2.0	1.5
			Quartzitic sst.	60	Sg1-07	Quartzitic sst.	1.18	1.2	
		SLW	Slate	20	SLW-10	Slate	2.95	3.0	2.0
			Silty slate	50	SPA-02	Silty slate	2.04	2.0	
			Quartzite	30	GH3216	Quartzite	1.20	1.2	
REVIN	GLE	Rv5	Slate	50	GH3128	Slate	2.96	3.0	2.5
			Silty slate	50	SPA-02	Silty slate	2.04	2.0	
	VEN	Rv3 + 4	Slate	30	GH3128	Slate	2.96	3.0	1.7
			Quartzite	70	GH3216	Quartzite	1.20	1.2	
	WAN	Rv1 + 2	Slate	40	GH3128	Slate	2.96	3.0	2.1
			Silty slate	20	SPA-02	Silty slate	2.04	2.0	
			Quartzite	40	GH3216	Quartzite	1.20	1.2	
DEVILLE	BEL		Slate/shale	50	GH2331	Slate	1.94	1.9	1.3
			Quartz. sst./quartzite	50	GH350	Quartzite	0.59	0.6	
	HUR		Slate	45	GH2331	Slate	1.94	1.9	1.2
			Quartzite	55	GH350	Quartzite	0.59	0.6	
	War		Gneiss/mica shist	10	War-01	Gneiss	1.12	1.1	1.4
				80	War-03	Gneiss	1.55	1.6	
			Quartzitic sst./quartzite	10	GH350	Quartzite	0.59	0.6	

Fm. – formation, Mbr. – Member, Vol. – volume fraction, Litho. – lithotype, sst. – sandstone. Lithological composition is estimated after Geukens (2008) and Verniers et al. (2001).

Table A.15: Details on samples used to compose the radiogenic heat production of the Lower Devonian geological formations in the Belgian and Luxembourgish Ardennes.

Formation		Lithology	Vol.	Sample	Lithotype	H		
						Sample	Litho.	Fm.
Be	Lux		[%]			[10^{-6} W m^{-3}]		
	E3	Sandy shale	100	E1a-004	Sandy shale	1.99	2.0	2.0
				E1a-009	Sandy shale	2.15		
				Sg3-003	Sandy shale	1.96		
	q	Quartzite	100	GH350	Quartzite	0.59	0.6	0.6
	E2	Shale/siltstone	70	E1b-007	Siltstone	1.68	1.7	1.5
		Sandstone	25	E1a-011	Quartzitic sst.	0.96	1.0	
		Quartzitic sst.	5	E1a-011	Quartzitic sst.	0.96	1.0	
	E1b	Silty slate/siltstone	70	E1b-007	Siltstone	1.68	1.7	1.5
		Sandstone	20	E1a-011	Quartzitic sst.	0.96	1.0	
		Quarzitic sst.	10	E1a-011	Quartzitic sst.	0.96	1.0	
	E1a	Sandy shale	94	E1a-004	Sandy shale	1.99	2.0	2.0
				E1a-009	Sandy shale	2.15		
				Sg3-003	Sandy shale	1.96		
		Quartzitic sst.	6	E1a-011	Quartzitic sst.	0.96	1.0	
LAR	Sg3	Sandy shale	100	E1a-004	Sandy shale	1.99	2.0	2.0
				E1a-009	Sandy shale	2.15		
				Sg3-003	Sandy shale	1.96		
	Sg3a	Slate	100	Sg1-003	Slate	1.98	2.0	2.0
VIL	Sg2	Shale/siltstone	35	E1a-004	Sandy shale	1.99	2.0	1.5
				E1a-009	Sandy shale	2.15		
				Sg3-003	Sandy shale	1.96		
		Siltstone + calc. sst.	65	Sg1-07	Silty slate	1.18	1.2	
MIR	Sg1	Slate	80	Sg1-003	Slate	1.98	2.0	1.8
		Silty slate	5	Sg1-07	Silty slate	1.18	1.2	
		Quartz. sst./quartzite	15	E1a-011	Quartzitic sst.	0.96	1.0	
STH		Shale/siltstone	80	OIG-13	Shale	2.26	2.0	1.8
				FEP-07	Shale	1.73		
		Sandstone	20	E1a-011	Quartzitic sst.	0.96	1.0	
OIG		Siltstone	15	OIG-13	Shale	2.26	2.0	1.7
				FEP-07	Shale	1.73		
		Shale	60	OIG-13	Shale	2.26	2.0	
				FEP-07	Shale	1.73		
		Sandstone	25	E1a-011	Quartzitic sst.	0.96	1.0	
FEP		Shale/siltstone	50	OIG-13	Shale	2.26	2.0	1.4
				FEP-07	Shale	1.73		
		Sandstone	20	E1a-011	Quartzitic sst.	0.96	1.0	
		Congl. sandstone	30	GH350	Quartzite	0.59	0.6	

Be – Belgium, Lux – Luxembourg, Vol. – volume fraction, Litho. – lithotype, Fm. – formation, sst. – sandstone, calc. – calcareous, congl. – conglomeratic. Composition of the individual formations is estimated after Dejonghe (2008) and Lucius (1950).

Table A.16: Details on samples used to compose the radiogenic heat production of the Lower Devonian and Proterozoic geological formations in the Eifel and Mosel Syncline/Hunsrück regions.

Formation	Code	Lithology	Vol. [%]	Sample	Lithotype	H Sample [10^{-6} W m^{-3}]	H Litho. [10^{-6} W m^{-3}]	H Fm. [10^{-6} W m^{-3}]
Wissenbach-Schiefer	de/dzoWI	Shale	> 90	Sg3-003	Sandy shale	1.96	2.0	1.9
		Quartzitic sst.	< 10	E1a-011	Quartzitic sst.	0.96	1.0	
Kieselgallenschiefer	dzo3KG	Shale/shaly siltstone	> 90	E1a-004	Sandy shale	1.99	2.0	2.0
				E1a-009	Sandy shale	2.15		
				Sg3-003	Sandy shale	1.96		
		Siltstone/sandstone	< 10	E1b-007	Siltstone	1.68	1.7	
Sphärosideritschiefer	dzo3SS	Shale/shaly siltstone	> 80	E1a-004	Sandy shale	1.99	2.0	1.9
				E1a-009	Sandy shale	2.15		
				Sg3-003	Sandy shale	1.96		
		Sandstone	< 20	E1a-011	Quartzitic sst.	0.96	1.0	
Brauneisenstein	dzo3BE	Sandstone	> 70	E1a-011	Quartzitic sst.	0.96	1.0	1.2
		Shale/shaly siltstone	< 30	E1a-004	Sandy shale	1.99	2.0	
				E1a-009	Sandy shale	2.15		
				Sg3-003	Sandy shale	1.96		
Rötelgallen-Schichten	dzo2RG	Shale	50	E1a-004	Sandy shale	1.99	2.0	1.5
				E1a-009	Sandy shale	2.15		
				Sg3-003	Sandy shale	1.96		
		Sandstone + limestone	50	E1a-011	Quartzitic sst.	0.96	1.0	
Höllenthal-Schichten	dzo2HÖ	Shale	50	E1a-004	Sandy shale	1.99	2.0	1.5
				E1a-009	Sandy shale	2.15		
				Sg3-003	Sandy shale	1.96		
		Sandstone	50	E1a-011	Quartzitic sst.	0.96	1.0	
Flußbach-Schichten	dzo1FL	Shale/shaly siltstone	40	E1a-004	Sandy shale	1.99	2.0	1.4
				E1a-009	Sandy shale	2.15		
				Sg3-003	Sandy shale	1.96		
		Quartzitic sst.	60	E1a-011	Quartzitic sst.	0.96	1.0	
Emsquarzit	dzo1EQ	Quartzitic sst./quartzite	> 90	GH350	Quartzite	0.59	0.6	0.7
		Shale	< 10	E1a-004	Sandy shale	1.99	2.0	
				E1a-009	Sandy shale	2.15		
				Sg3-003	Sandy shale	1.96		
Klerf-Schichten	dzu3KL	Shale/shaly siltstone	30	E1b-007	Siltstone	1.68	1.7	1.2
		Sandstone/quartzite	70	E1a-011	Quartzitic sst.	0.96	1.0	
Gladbach-Schichten	dzu3GL	Shale	50–70	E1a-004	Sandy shale	1.99	2.0	1.9
				E1a-009	Sandy shale	2.15		
				Sg3-003	Sandy shale	1.96		
		Siltstone/sandstone	30–50	E1b-007	Siltstone	1.68	1.7	
"Singhofen-Schichten"	dzS	Shale/sandy shale	90	E1a-004	Sandy shale	1.99	2.0	1.9
				E1a-009	Sandy shale	2.15		
				Sg3-003	Sandy shale	1.96		
		Sandstone	10	E1a-011	Quartzitic sst.	0.96	1.0	

Vol. – volume fraction, Litho. – lithotype, Fm. – formation, sst. – sandstone. Composition of the individual formations is taken from Häfner et al. (2007) and completed according to LGB (2005).

Table A.16 continued

Formation	Code	Lithology	Vol. [%]	Sample	Lithotype	H Sample [10^{-6} W m^{-3}]	H Litho. [10^{-6} W m^{-3}]	H Fm. [10^{-6} W m^{-3}]
Kaubschichten	dzu1KA	Shale	85	E1a-004	Sandy shale	1.99	2.0	2.0
				E1a-009	Sandy shale	2.15		
				Sg3-003	Sandy shale	1.96		
		Slate	10	Sg1-003	Slate	1.98	2.0	
		Quartzitic sst.	5	E1a-011	Quartzitic sst.	0.96	1.0	
Zerf-Schichten	dzu1ZE	Sandy shale	75	E1a-004	Sandy shale	1.99	2.0	1.8
				E1a-009	Sandy shale	2.15		
				Sg3-003	Sandy shale	1.96		
		Quartzitic sst./quarzite	25	E1a-011	Quartzitic sst.	0.96	1.0	
Dhrontal-Schichten	ds3DR	Sandy shale	70	E1a-004	Sandy shale	1.99	2.0	1.7
				E1a-009	Sandy shale	2.15		
				Sg3-003	Sandy shale	1.96		
		Quartzitic sst./quartzite	30	E1a-011	Quartzitic sst.	0.96	1.0	
Taunusquarzit	ds2TQ	Quartzitic sst./quartzite	> 95	GH350	Quartzite	0.59	0.6	0.6
Hermeskeil-Schichten	ds1HE	Shale	50	OIG-13	Shale	2.26	2.0	1.5
				FEP-07	Shale	1.73		
		Quartzitic sst.	50	E1a-011	Quartzitic sst.	0.96	1.0	
Züsch-Schiefer	gd	Shale	80	OIG-13	Shale	2.26	2.0	1.8
				FEP-07	Shale	1.73		
		Quartzitic sst.	20	E1a-011	Quartzitic sst.	0.96	1.0	
Wartenstein Gneiss	War	Gneiss/mica schist	90	War-01	Gneiss	1.12	1.3	1.3
				War-03	Gneiss	1.55		
		Quartzite	10	GH350	Quartzite	0.59	0.6	

Table A.17: Geochemical data of representative rock samples.

Region	Ardennes									Stavelot Massif					SE Hunsrück		Grand-Halleux borehole			
Sample	E1b-07	E1a-04	E1a-09	E1a-11	Sg3-03	Sg1-03	Sg1-07	OIG-13	FEP-07	BIH-06	COL-05	PLA-01	SPA-02	SLW-10	War-01	War-03	GH350	GH2331	GH3128	GH3216
Lithotype	Stst	Sh	Sh	Sst	Sh	Sl	Sst	Sh	Sh	Ssl	Sl	Sl	Ssl	Sl	Gn	Gn	Q	Sl	Sl	Q
SiO_2 (wt%)	73.0	61.7	60.1	75.0	59.6	59.2	70.4	68.4	67.4	55.0	53.9	49.4	63.9	50.7	72.7	65.2	94.4	58.2	56.1	79.3
TiO_2	0.76	0.92	0.93	0.49	0.90	0.96	0.67	1.05	0.88	0.98	0.98	0.90	0.90	1.37	0.49	0.83	0.25	0.92	1.07	0.72
Al_2O_3	11.9	18.5	18.9	7.48	18.0	18.9	11.5	17.2	15.4	22.0	23.0	20.4	17.7	26.3	13.2	15.5	2.63	19.9	21.6	6.21
Fe_2O_3	5.32	6.29	6.82	8.11	6.62	7.92	8.91	4.68	6.88	9.53	9.62	15.47	5.60	6.00	3.84	6.36	0.76	7.99	7.38	6.40
MnO	0.02	0.07	0.13	0.15	0.10	0.14	0.15	<0.01	<0.01	0.34	0.82	1.61	0.14	0.06	0.05	0.08	<0.01	0.04	0.05	0.09
MgO	1.87	2.17	2.47	2.29	2.78	2.97	3.18	0.68	1.41	2.10	1.74	2.38	1.57	1.58	1.33	2.15	0.19	1.89	2.01	1.47
CaO	0.17	0.57	0.36	0.78	0.89	0.27	0.11	0.04	0.04	0.32	0.16	0.34	0.38	0.06	0.15	0.27	0.07	0.11	0.13	0.12
Na_2O	1.52	1.02	0.98	0.77	1.03	1.20	0.98	0.94	0.35	0.81	1.24	0.97	1.87	0.24	2.70	2.14	0.67	1.19	0.75	0.64
K_2O	1.88	3.82	3.90	0.31	3.62	3.16	0.89	3.40	2.88	3.38	3.63	3.17	3.90	6.76	2.82	3.36	0.39	5.26	4.47	0.68
Cr_2O_3	0.022	0.022	0.020	0.015	0.025	0.022	0.017	0.019	0.027	0.015	0.017	0.015	0.014	0.020	0.007	0.009	0.009	0.013	0.016	0.011
P_2O_5	0.10	0.14	0.16	0.23	0.13	0.17	0.08	0.07	0.07	0.26	0.13	0.24	0.10	0.09	0.08	0.19	0.02	0.07	0.06	0.03
LOI	3.36	4.66	5.01	3.62	6.01	4.57	3.65	3.11	3.57	4.77	4.03	4.14	3.48	5.99	2.35	3.39	0.57	3.63	6.08	3.49
Total	99.9	99.9	99.8	99.3	99.7	99.5	100.5	99.6	99.3	99.6	99.3	99.2	99.6	99.3	99.8	99.6	99.9	99.3	99.7	99.2
TOT/C	0.05	0.39	0.51	0.28	0.82	0.20	0.06	0.02	0.02	0.08	<0.02	<0.02	0.08	0.48	0.02	0.06	0.03	<0.02	1.39	0.44
TOT/S	<0.02	<0.02	0.05	<0.02	0.08	<0.02	<0.02	<0.02	0.07	<0.02	<0.02	<0.02	<0.02	<0.02	<0.02	<0.02	<0.02	<0.02	1.64	1.84
Ba (ppm)	319	495	541	54	480	608	171	638	3440	641	841	1360	844	1250	419	697	76	955	568	91
Be	2	3	3	<1	5	3	1	3	3	6	6	5	5	7	2	2	<1	6	6	1
Co	14.9	19.3	27.4	18.0	21.5	17.9	21.4	8.5	13.5	8.0	36.2	109	15.2	6.4	8.3	12.3	2.5	21.1	19.6	12.2
Cs	2.9	6.2	7.2	1.1	6.3	6.4	1.6	4.5	7.5	5.9	7.7	6.9	5.5	9.6	3.7	4.0	0.7	8.9	10.0	0.8
Ga	15.9	24.8	25.2	8.9	24.4	26.2	15.0	22.9	20.9	30.2	31.1	29.5	24.5	36.1	14.1	20.2	1.5	26.7	29.9	6.5
Hf	9.0	6.2	5.2	9.1	5.3	5.9	5.0	8.2	8.8	4.6	4.0	3.8	7.1	7.1	4.6	5.7	11.1	4.8	5.5	11.3
Nb	14.8	17.6	18.3	10.3	16.3	17.6	11.3	18.7	15.6	18.5	20.1	17.3	17.8	24.8	8.3	12.3	4.9	18.5	21.4	14.0
Rb	78	171	177	12	170	145	37	168	141	161	172	150	170	264	102	121	14	220	201	29
Sn	2	4	5	1	3	4	2	3	3	5	4	3	4	5	2	3	<1	3	4	1
Sr	67	108	108	119	117	110	51	136	171	158	321	295	136	77	42	47	31	125	114	24
Ta	1.2	1.1	1.3	0.6	1.1	1.2	0.9	1.4	1.2	1.5	1.5	1.1	1.4	1.9	0.6	0.8	0.4	1.3	1.6	1.0
Th	11.0	13.6	14.3	7.6	13.6	13.2	9.0	15.3	12.5	16.5	16.9	14.7	14.6	20.1	7.0	9.9	4.2	14.2	17.1	8.4
U	3.1	2.9	3.2	1.6	2.9	3.1	2.0	3.5	2.5	2.4	2.9	1.8	2.7	3.7	1.7	2.4	1.1	1.8	5.3	2.2
V	90	163	168	70	149	153	93	141	115	131	133	119	105	161	72	126	11	121	208	42
W	1.5	2.2	2.4	1.1	2.0	1.9	1.3	2.9	2.0	2.3	3.2	4.2	2.1	3.3	1.8	1.2	0.7	2.3	3.2	1.9
Zr	341	213	196	362	200	193	205	314	331	180	146	143	268	239	181	209	444	180	198	441

LOI – loss on ignition, TOT/C – total carbon, TOT/S – total sulfur, Stst – siltstone, Sh – shale, Sst – sandstone, Sl – Slate, Ssl – silty slate, Gn – gneiss, Q – quartzite.

Table A.17 continued

Region	Ardennes									Stavelot Massif					SE Hunsrück		Grand-Halleux borehole			
Sample	E1b-07	E1a-04	E1a-09	E1a-11	Sg3-03	Sg1-03	Sg1-07	OIG-13	FEP-07	BIH-06	COL-05	PLA-01	SPA-02	SLW-10	War-01	War-03	GH350	GH2331	GH3128	GH3216
Lithotype	Stst	Sh	Sh	Sst	Sh	Sl	Sst	Sh	Sh	Ssl	Sl	Sl	Ssl	Sl	Gn	Gn	Q	Sl	Sl	Q
Y	28.9	32.7	35.7	25.1	29.6	37.2	27.6	41.0	36.3	38.2	37.4	38.9	33.2	42.8	14.9	30.0	11.0	28.4	41.7	31.4
La	37.6	56.0	51.4	24.9	45.0	38.9	24.2	48.8	36.9	54.8	57.7	58.1	49.3	72.3	26.3	31.7	12.7	42.3	57.5	23.1
Ce	75.7	95.6	101	53.3	92.3	62.3	58.0	101	79.8	116	117	147	103	143	50.5	66.4	27.3	88.8	118	48.2
Pr	9.50	11.1	12.2	6.64	11.0	9.09	6.43	12.1	9.55	13.3	13.3	13.6	11.8	17.8	5.80	7.93	3.38	10.1	14.5	5.68
Nd	36.8	44.0	48.7	27.0	42.4	35.1	25.4	46.7	36.9	47.9	53.7	55.4	46.8	66.2	24.0	29.8	12.7	37.7	54.6	24.2
Sm	6.63	7.76	8.01	5.35	7.40	6.55	4.90	8.73	6.78	9.90	9.07	9.23	8.07	11.5	3.89	6.09	2.49	6.84	10.1	4.45
Eu	1.25	1.66	1.79	1.25	1.57	1.50	1.01	1.76	1.46	2.10	1.92	1.76	1.77	2.44	0.84	1.18	0.48	1.38	2.28	0.99
Gd	5.78	7.14	7.30	5.40	6.52	6.61	4.98	7.75	6.08	8.59	8.47	8.13	7.27	8.81	3.63	5.61	2.07	5.59	8.75	4.51
Tb	0.86	1.00	1.06	0.77	0.91	1.00	0.78	1.17	0.97	1.20	1.19	1.26	1.01	1.23	0.48	0.82	0.29	0.85	1.29	0.76
Dy	5.60	6.07	6.72	4.32	6.21	6.66	5.11	8.00	6.12	7.26	7.23	8.41	6.46	7.93	2.69	5.28	1.67	5.35	8.38	5.53
Ho	1.04	1.15	1.13	0.85	1.07	1.22	0.95	1.46	1.19	1.20	1.33	1.40	1.18	1.52	0.54	1.00	0.36	0.89	1.55	1.13
Er	3.05	3.42	3.42	2.62	3.30	3.58	2.59	4.22	3.51	3.50	3.82	4.07	3.39	4.57	1.54	2.98	1.15	2.88	4.19	3.30
Tm	0.46	0.51	0.53	0.34	0.47	0.52	0.39	0.61	0.54	0.50	0.53	0.55	0.48	0.67	0.25	0.44	0.17	0.40	0.64	0.51
Yb	2.97	3.25	3.59	2.43	3.07	3.31	2.56	4.55	3.27	3.03	3.26	3.70	3.32	4.39	1.67	3.05	1.29	3.13	4.33	3.35
Lu	0.44	0.50	0.48	0.34	0.47	0.51	0.38	0.61	0.54	0.45	0.50	0.51	0.48	0.64	0.25	0.42	0.18	0.43	0.62	0.52
Mo	<0.1	0.1	0.3	0.1	0.1	<0.1	<0.1	<0.1	<0.1	<0.1	<0.1	0.8	<0.1	0.3	<0.1	0.2	<0.1	0.1	3.2	0.3
Cu	12	12	43	9.9	26	26	26	5.1	2.2	20	17	8.1	24	32	8.3	40	3.1	41	52	18
Pb	7.3	9.9	2.5	8.7	21.7	9.3	6.0	4.9	4.8	9.4	6.7	7.9	11.6	23.9	10.6	14.9	1.1	2.4	8.4	19.9
Zn	66	74	66	67	91	102	112	35	63	128	76	116	82	92	37	85	10	80	93	54
Ag	<0.1	<0.1	<0.1	<0.1	<0.1	<0.1	<0.1	<0.1	<0.1	<0.1	<0.1	<0.1	<0.1	<0.1	<0.1	<0.1	<0.1	<0.1	0.2	<0.1
Ni	62.9	65.4	63.4	39.9	78.5	82.2	66.7	37.0	58.0	50.6	56.4	71.3	32.1	34.2	13.1	28.8	3.8	35.6	32.5	13.3
As	<0.5	3.0	16.0	3.9	10.4	10.3	0.6	<0.5	<0.5	22.2	2.6	17.3	1.4	36.5	2.8	12.8	<0.5	<0.5	<0.5	19.8
Cd	<0.1	<0.1	<0.1	<0.1	<0.1	<0.1	<0.1	<0.1	<0.1	<0.1	<0.1	<0.1	<0.1	<0.1	<0.1	<0.1	<0.1	<0.1	0.1	<0.1
Sb	<0.1	0.1	<0.1	0.4	<0.1	<0.1	<0.1	<0.1	<0.1	<0.1	<0.1	<0.1	<0.1	<0.1	<0.1	<0.1	<0.1	<0.1	0.2	0.3
Bi	0.1	0.2	0.3	<0.1	0.2	0.1	0.1	0.2	0.2	0.2	0.3	0.5	<0.1	0.1	<0.1	<0.1	<0.1	<0.1	0.3	0.3
Hg	0.02	<0.01	0.03	0.13	0.04	0.05	<0.01	0.05	0.03	<0.01	<0.01	<0.01	<0.01	<0.01	0.13	0.14	<0.01	<0.01	0.05	0.01
Tl	<0.1	<0.1	<0.1	<0.1	<0.1	<0.1	<0.1	0.1	<0.1	<0.1	<0.1	<0.1	0.1	<0.1	0.1	0.1	<0.1	<0.1	<0.1	<0.1
Se	0.5	<0.5	<0.5	0.6	<0.5	<0.5	<0.5	<0.5	<0.5	0.5	<0.5	0.6	<0.5	<0.5	<0.5	<0.5	<0.5	<0.5	<0.5	<0.5
Au (ppb)	<0.5	<0.5	<0.5	<0.5	<0.5	<0.5	<0.5	0.7	1.0	<0.5	<0.5	0.6	<0.5	<0.5	0.9	0.6	<0.5	<0.5	<0.5	0.9

References

Bultynck, P., Dejonghe, L. (2001). Devonian lithostratigraphic units (Belgium). In: Bultynck, P., Dejonghe, L. (Eds.), Guide to a Revised Lithostratigraphic Scale of Belgium, vol. 4 (1–2). Geologica Belgica, Brussels, pp. 39–69.

Colbach, R., Maquil, R. (2003). Carte géologique du Luxembourg 1:25000, feuille 7 Rédange. Serv. Géol. Luxemb., Luxembourg.

Dejonghe, L. (2008). Carte géologique de Wallonie 1/25.000, feuille 55/5–6 Hotton–Dochamps, notice explicative. Région Wallonne, Namur, 88 pp.

Furtak, H., (1965). Die Tektonik der underdevonischen Gesteinsfolge im deutsch–belgisch–luxemburgischen Grenzgebiet. Geol. Mitt. 4, 273–332.

Geukens, F. (2008). Carte géologique de Wallonie 1/25.000, feuille 55/3–4 Bra–Lierneux, notice explicative. Région Wallonne, Namur, 40 pp.

Graulich, J. M. (1980). Le sondage de Grand-Halleux. In: Professional Paper 175, Administration des Mines. Service géologique de Belgique, Brussels, 78 pp.

Häfner, F., Kött, A., Spindeldreher, J., Rein, B., Grubert, A. (2007). Nutzung von oberflächennaher Erdwärme für die Gebäudeheizung in Rheinland-Pfalz. Landesamt für Geologie und Bergbau Rheinland-Pfalz, Mainz, 97 pp., unpublished report.

Hollmann, E.G. (1997). Der variszische Vorlandüberschiebungsgürtel der Ostbelgischen Ardennen – Ein bilanziertes Modell. Aachener Geowiss. Beitr. 25, 235 pp.

Konrad, H.J., Wachsmut, W. (1973). Zur Lithologie und Tektonik des Unterdevons im südlichen Oesling Luxemburgs. Publ. Serv. Géol. Luxemb. 5, 1–20.

LGB (Landesamt für Geologie und Bergbau Rheinland-Pfalz) (Ed.) (2005). Geologie von Rheinland-Pfalz. Schweizerbart, Stuttgart, 400 pp.

Lucius, M. (1950). Das Oesling – Erläuterungen zu der geologischen Spezialkarte Luxemburgs. Publ. Serv. Géol. Luxemb., vol. 6. Luxembourg, 174 pp.

Meyer, W., Stets, J. (1980). Zur Paläogeographie von Unter- und Mitteldevon im westlichen und zentralen Rheinischen Schiefergebirge. Z. Dt. Geol. Ges. 131, 725–751.

Meyer, W., Stets, J. (1996). Das Rheintal zwischen Bingen und Bonn. In: Sammlung geol. Führer 89. Borntraeger, Berlin, Stuttgart, 386 pp.

Schintgen, T., Förster, A. (2013). Geology and basin structure of the Trier–Luxembourg Basin – implications for the existence of a buried Rotliegend graben. Z. Dt. Ges. Geowiss. 164 (4), 615–637.

Stets, J., Schäfer, A. (2002). Depositional environments in the Lower Devonian siliciclastics of the Rhenohercynian Basin (Rheinisches Schiefergebirge, W-Germany) – Case studies and a model. Contr. Sed. Geol. 22, 77 pp.

Verniers, J., Herbosch, A., Vanguestaine, M., Geukens, F., Delcambre, B., Pingot J.-L., Belanger, I., Hennebert, M., Debacker, T., Sintubin, M., De Vos, W. (2001). Cambrian–Ordovician–Silurian lithostratigraphic units (Belgium). In: Bultynck, P., Dejonghe, L. (Eds.), Guide to a Revised Lithostratigraphic Scale of Belgium, vol. 4 (1–2). Geologica Belgica, Brussels, pp. 5–38.

Wildberger, J. (1992). Zur tektonischen Entwicklung des südwestlichen Hunsrücks (SW-Deutschland). Mitt. Pollichia 79, 5–119.